2020

Volcanic Impact on Stratospheric Chlorine Chemistry and Perchlorate Formation: Evidence from Ice Cores

Joshua Andrew Kennedy
South Dakota State University

VOLCANIC IMPACT ON STRATOSPHERIC CHLORINE CHEMISTRY AND PERCHLORATE FORMATION: EVIDENCE FROM ICE CORES

BY

JOSHUA ANDREW KENNEDY

A dissertation submitted in partial fulfillment of the requirements for the

Doctor of Philosophy

Major in Chemistry

South Dakota State University

2020

DISSERTATION ACCEPTANCE PAGE

Joshua Andrew Kennedy

This dissertation is approved as a creditable and independent investigation by a candidate for the Doctor of Philosophy degree and is acceptable for meeting the dissertation requirements for this degree. Acceptance of this does not imply that the conclusions reached by the candidate are necessarily the conclusions of the major department.

Jihong Cole-Dai
Advisor Date

Douglas Raynie
Department Head Date

Dean, Graduate School Date

ACKNOWLEDGEMENTS

I would like to thank all those that helped me through the last several years of graduate school. Foremost, thanks to my wife, Vanessa, for all of her encouragement and support, making this possible. My daughters, Gwenyth and Zoë, thanks you for giving me inspiration to succeed and someone to make proud. I want to thank all of my family for enduring the last ten years alongside me, and for propping me up through difficult times. To my advisor, Jihong Cole-Dai, thank you for providing mentorship, guidance, end encouragement throughout my graduate studies. I also would like to send my appreciation the members of my committee, Drs. Brian Logue, Matt Miller, and Keith Underwood, for their service and feedback. For inspiring me to study areas of chemistry, geology, and Earth science, I thank Drs. Tom Jempty and Bruce Darling at Austin Community College. Last, my thanks go out to all those present and past members of the group that contributed to my sanity, research, and good times over the last couple years; Carleigh Larrick, Tommy Cox, Joe Gibson, Amanda Shea, Kari Peterson, and of course, Dave Ferris.

As I write this, the number of COVID-19 cases and deaths during this pandemic is peaking across the world and shows no signs of slowing. The university is closed, all classes have moved online, and all work is being done remotely. Unemployment is at an all-time high in the US, and the economy is at record lows. I cannot help but be reminded of Isaac Newton, who devised many of his theories on optics, physics, and calculus during a break from his own university studies during an outbreak of bubonic plague. Times such

as these may be exceptional, but also show how we can overcome tremendous adversity and serve as testament to the tenacity of mankind.

Tigger. Buddy. I knew you weren't making it out of South Dakota.

CONTENTS

LIST OF TABLES

LIST OF FIGURES

ABSTRACT

VOLCANIC IMPACT ON STRATOSPHERIC CHLORINE CHEMISTRY AND PERCHLORATE FORMATION: EVIDENCE FROM ICE CORES

JOSHUA KENNEDY

2020

Perchlorate, suspected to be chemically formed in both the troposphere and stratosphere, has been recently measured in Arctic snow and ice cores. These comprise both discontinuous snow and ice cores from the Canadian Arctic and a continuous record of perchlorate was compiled from an analysis of Greenland ice cores. While the background perchlorate concentration typically is very low, a few spikes in concentration coinciding with deposition of volcanic sulfate were observed in the Greenland record, suggesting that perchlorate levels in the atmosphere may be impacted by volcanic eruptions. As of yet, no work has been done to investigate the connection between volcanic eruptions and perchlorate formation. It was not known 1) whether the volcanic perchlorate response is limited to samples collected in Greenland, 2) if the volcanic perchlorate response is just limited to certain eruptions, 3) what factors influence the magnitude of the response, and 4) what chemistry drives the volcanic perchlorate response.

In this work, detailed analysis and careful examination of the data collected from Antarctic, Alaskan, and Greenland ice cores show no seasonal oscillation during nonvolcanic periods prior to the 1980s, indicating a relatively small role for stratospheric

photochemical production pathways in the Arctic during these times. The development of a strong seasonal oscillation in perchlorate concentration in snow since 1980 corresponds with a drastic increase in stratospheric organic chlorine throughout the late 20th century, indicating that the relative contribution of stratospheric photochemical processes to the perchlorate deposition in the Arctic has increased as a result of increased stratospheric organic chlorine. Correlation of annual perchlorate flux with mean annual ozone abundance in recent decades suggests that the abundance of both ozone and perchlorate are influenced by stratospheric chlorine.

The analysis of ice cores from the South Pole containing the sulfate fallout from several large volcanoes revealed that volcanic perchlorate response is not restricted to the Arctic and occurs in the Antarctic as well. The large flux of perchlorate deposition during periods perturbed by volcanic eruptions relative to background levels in snow during nonvolcanic periods indicate volcanism is a significant source of perchlorate in the environment. Perchlorate formation and deposition in response to some eruptions easily exceed decades of perchlorate deposition during nonvolcanic periods.

The flux of sulfate is highly correlated with the flux of perchlorate during volcanically perturbed periods in the stratosphere, indicating that the impact of volcanic aerosol on stratospheric chlorine chemistry results in increased formation of perchlorate. Examination of proposed perchlorate chemistry and formation mechanisms leads to the conclusion that chlorine activation is likely the key process. Volcanic eruptions enhance perchlorate formation through injections of aerosol-forming sulfur, promoting formation of chlorine radicals and other important perchlorate intermediates.

Unlike sulfate, perchlorate in snow experiences post-depositional change. The main characteristic of that change is probably diffusion in the firn column. The perchlorate response in ice cores exhibits what appears to be high effective diffusivity relative to sulfate. The diffusivity for perchlorate is modeled based upon the perchlorate response of the 1912 eruption of Katmai and estimated to be about 10^{-5} m^2 yr^{-1}. Comparison of volcanic perchlorate response signals in ice cores from multiple time periods and sampling locations support diffusion in the firn layer.

1.0 Introduction

1.1 Volcanic Eruptions and the Environment

Earth is home to a staggering array of intertwined physical and chemical processes that have interacted for eons, changing the air, water, and surface to give rise to the planet we know today. Wind, water, and gravity weather massive landforms and sculpt the landscape on shorter timescales, while tectonic movement of plates dramatically reshapes the surface over long periods of time. These physical processes change weather patterns on the surface and contribute to long and intense periods of climate variation. Other processes, such as the dissolution of limestone or formation of an oxygenated atmosphere are chemical in nature, rather than physical, but nonetheless are just as important in shaping Earth, and supporting life. Some natural events on Earth have far-reaching physical and chemical impacts, however, and few can match volcanic eruptions in either the scale or intensity of their impacts upon the environment.

The physical impacts of volcanic eruptions are diverse and vary in terms of scale and environmental impact. In the local vicinity of the eruption, lahars and pyroclastic flows decimate all life forms in their wake and can result in massive deforestation and redirection of river basins. Ash fall can form thick deposits many miles from the vent and can remain thick across vast continental regions, rapidly changing entire ecosystems. The fine ash that is injected into the stratosphere after major eruptions scatters solar radiation, reducing the amount reaching the surface, and may result in multi-year cooling and sea ice expansion. In addition, these physical impacts of eruptions can displace

populations, cause crops to fail, and change the biosphere for many years (Cole-Dai, 2010; Ayris and Delmelle, 2012).

Volcanic eruptions do not just cause physical disruption of the environment, but also may have significant impact upon the chemical processes that occur in nature. Eruptions may emit high amounts of acid halides, leading to deaths from respiratory distress in many living things. The sulfur dioxide emitted from volcanic eruptions is converted to sulfuric acid in the atmosphere, leading both to the buildup of the aforementioned stratospheric aerosol, and precipitating long distances from the vicinity of the volcano with rain, along with much of the emitted halogen halides. The chemical impact of eruptions on the environment, however, is quite complex and poorly understood. The study of the impacts that eruptions have upon chemistry in the environment benefits from the construction of records of explosive volcanism. These records may be constructed from various sources of information and environmental measurements, such as written or oral accounts, tree-ring analysis, geologic evidence, and ice core chemical measurements and tephra analysis.

Of course, detailed and well-dated written histories from direct observation of the eruptions would be most valuable, but records such as these are largely limited to the last few centuries, and then are highly constrained in both accuracy and quality by the technological advancement of the observing civilization. Fortunately, both physical and chemical evidence of volcanic eruptions are preserved in various media on the Earth's surface, and these records may be used to construct longer timelines of volcanic activity and impact. While both types of evidence may be found in the lithosphere, and very long

records of volcanic eruptions may be constructed, the absolute dating and time resolution of geologic records is quite poor, and in many cases the uncertainty of an eruption date may be thousands of years or more. Ice cores though, strike a good balance between length of the record, resolution of events, completeness of the record, and precision is assigning dates to the signals.

Multiple types of artifacts have been observed in ice cores pertaining to volcanic eruptions, such as pieces of tephra and strata of high concentrations of sulfuric acid. However, what ice cores gain in those regards, they lose in the ability to confidently assign an actual volcano to the observed signal. While tephra may help in this regard, usually the samples collected for analysis are quite small and few in number, leading to some uncertainties in their interpretation. Sulfate on the other hand, leaves no signature of its emission source. Few other reliable chemical signals exist, but some recent work has shown that perchlorate levels in ice cores become elevated following some eruptions, showing promise for its use in discerning details about the chemical impact of large eruptions on the environment.

1.2 Perchlorate in the Environment

Perchlorate, ClO_4^-, is a water-soluble anion with tetrahedral geometry where the chlorine atom is in its most oxidized state, +7. Owing to its somewhat high activation energy required for reduction and relative stability in an aqueous matrix (Urbansky, 1998; Urbansky, 2002; Brown and Gu, 2006; Gu and Coates, 2006), perchlorate persists for long periods in groundwater (Sturchio *et al.*, 2014). Due to the readily soluble nature of

perchlorate, groundwater constitutes one of the primary reservoirs of environmental perchlorate. Low levels of perchlorate occur across the planet other matrices, however. Not only has perchlorate been detected in subsurface waters and groundwater totally isolated from possible human sources of pollution, but it has also been found in certain hyper arid environments as well. These arid areas include the Atacama Desert, Antarctic Dry Valleys, High Plains of Texas and New Mexico in the US, and the deserts of the American Southwest (Urbansky, 2002; Plummer *et al.*, 2006; Rajagopalan *et al.*, 2006; Rao *et al.*, 2007; Catling *et al.*, 2010; Kounaves *et al.*, 2010; Lybrand *et al.*, 2013), where soils can possess high levels of perchlorate salts, spared from dissolution by precipitation. Some mineral deposits with high nitrate content from Chile also contain high levels of perchlorate, which has been detected in products using this nitrate source, such as fertilizer and projectile propellants (Urbansky *et al.*, 2001), though the release of perchlorate to the environment from these sources is not significant.

Perchlorate has negative health effects in humans. Exposure to perchlorate can impair thyroid function in humans by interfering with normal iodine uptake (Kirk, 2006; Sijimol *et al.*, 2015; Knight *et al.*, 2017). This leads to a wide array of health issues, including symptoms of hyperthyroidism or hypothyroxinemia, and low birth weights of infants born to women exposed to perchlorate (Rubin *et al.*, 2017). Some populations, such as those living in Nanchang, China, experience much higher exposure levels than most of the sampled population of China (Zhang *et al.*, 2010). Routes of perchlorate exposure also comprise milk, where in some cases, perchlorate concentrations in human breast milk have been measured to be much higher than animal milk (Kirk *et al.*, 2005).

Perchlorate may also be taken up into agricultural crops in areas experiencing perchlorate contamination in soil or water, increasing human exposure in some cases (Lawrence *et al.*, 2000; Dasgupta *et al.*, 2006; Sijimol *et al.*, 2015; Steinmaus, 2016).

1.3 Sources of Environmental Perchlorate

Sources of environmental perchlorate may be either anthropogenic in nature or the result of natural chemical reactions (discussed in section below). Recently, interest has focused on perchlorate as an emerging contaminant, though very high perchlorate levels in the environment tend to be localized areas of pollution, such as the lower Colorado River in the southwestern United States (Urbansky, 2002; Kumarathilaka *et al.*, 2016). Anthropogenic sources may comprise both release during normal use and production of perchlorate containing chemicals, and large pollution events, such as the 1988 explosion at the PEPCON chemical plant in Henderson, Nevada. Formed through electrolysis of saturated aqueous sodium chloride solutions, perchlorate pollution associated with production has been a recurring issue in the southwestern United States (Steinmaus, 2016).

Products which may release perchlorate to the environment through normal use include flares, fireworks, and certain rocket fuels (Motzer, 2001; Silva, 2003; Dasgupta *et al.*, 2006), though the contribution from these sources is thought to be small. Disposal, recycling, and demilitarizing of munitions also pose risks to the environment in terms of perchlorate pollution (Trumpolt *et al.*, 2005). Perchlorate has been measured at many US government facilities at a wide range of concentrations, but cleanup activities and

remediation actions are both slow and ongoing (Stephenson, 2011). To adequately quantify how much perchlorate naturally occurs in the environment, and to establish some regulatory threshold for exposure, records of environmental perchlorate are needed.

Records of perchlorate in the environment are sparse. Largely, measurements obtained on isolated and discontinuous samples provide only limited information as to how perchlorate in the environment has varied through time. Continuous records are of critical importance, however, for purposes of evaluating typical background levels in the environment, identifying short- or long-term deviations from background levels, and identifying causes for departures from said background.

A record of perchlorate in wet deposition across the United States and Puerto Rico was constructed that covered the time period from October 2004 to October 2007 from 16 sampling locations (Rajagopalan *et al.*, 2009). The average concentration was determined to be 14.1 ± 13.5 ppt, with the maximum concentrations reaching above 100 ppt. Though this study was of limited duration, a slight seasonality was detected with perchlorate concentration reaching a maximum in the summer, but only for two years of the study. A key shortcoming of liquid precipitation measurements, however, is that an archive is not generated; samples may only be collected at time of deposition. Clearly, some long-lasting archive of environmental perchlorate would be useful, and ice core records have proved to be valuable in this regard.

A record of perchlorate in Arctic snow from 1996 CE to 2005 CE was obtained from snow pit samples from the Devon Island ice cap in Nunavut, Canada (75° 20N, 82° 40W at 1797 masl) in the spring of 2006 (Furdui and Tomassini, 2010). The snow pit was 6.8 meters in depth, with sample resolution of 20 to 25 cm. The mean perchlorate concentration reported in this study was 5.5 ± 3.9 ppt, far lower than that reported by Rajagopalan, et al. (2009), and ranged from <1 to about 8 ppt, with the highest values in the years 1996 and 1997. Though the temporal resolution of this record was quite low in terms of samples per year, several key observations were made. First, the researchers speculate that the high flux of perchlorate in 1996 and 1997 is due to lingering stratospheric aerosol from the eruption of Mt. Pinatubo in 1991. The role of volcanic activity as a supplier of chlorine to the atmosphere was later considered by Dasgupta et al. (2005). Since the abundance of perchlorate-laden deposits in arid regions cannot be explained over geologic time frames by the normal abundance of chlorine in the atmosphere, it was suggested that at some point in the Earth's history additional sources of chlorine to the atmosphere were needed, such as volcanic emission (Dasgupta *et al.*, 2005). Second, similar summertime high seasonality was observed here as that reported by Rajagopalan et al. (2009). The authors postulated this is due to reliance upon photochemical reactions for at least one pathway of perchlorate formation, though the low number of samples per year in this study limits confidence in the exact timing of maximum concentration during the year. Finally, correlations were observed for both chloride (R^2 = 0.8494) in samples with high perchlorate concentrations, and for ozone (R^2 = 0.6153) when peaks in perchlorate concentrations were removed. Here, the authors

speculate that this may be the result of two formation pathways, one proceeding from a chloride radical and involving ozone, and another from oxidation of a chloride ion.

Results from ice cores from the Upper Fremont Glacier (UFG) in the Wind River Range, Wyoming (43°07′ N, 109°37′ W, elevation 4100 masl) and the Eclipse Icefield, Yukon Territory, Canada (60.51° N, 139.47° W, elevation 3017 masl), were used to construct records spanning the pre- and post-Industrial Revolution periods (Rao *et al.*, 2012). It was not a continuous record though, with only selected time periods analyzed in the Eclipse core, and a discontinuous series of samples representing annual layers in the UFG core. Here, consistent seasonal variation such as that observed in the study by Furdui and Tomassini (2010) was not seen in the Eclipse core and could not be evaluated in the UFG core due to low resolution. Concentrations of perchlorate, however, were broadly consistent with the Devon Island core. In the Eclipse core, overall concentrations ranged from less than 0.2 ppt to 8.8 ppt. The average perchlorate concentrations for the years 1970 to 1973 CE was 0.6 ± 0.3 ppt, from 1982 to 1986 CE the average concentration was 2.3 ± 1.7 ppt, and from 1999 to 2002 CE was 2.2 ± 2.0 ppt. Higher variance was observed post-1980 in the Eclipse core. In the UFG core the concentrations ranged from less than 0.2 ppt to 2.6 ppt, with a post-1980 average of 1.8 ± 0.7 ppt. In contrast to the results reported by Furdui and Tomassini (2010), there was no correlation between chloride and perchlorate for any time period at either sampling location, though correlation with nitrate and sulfate was observed post-1980.

A detailed ice core record of perchlorate covering the years 1950 to 2007 CE and 1701 to 1753 CE was constructed from a Summit, Greenland ice core (Peterson *et al.*,

2015b). This study provided relatively high resolution, with typically 9 to 12 samples per year measured for perchlorate, and as with the measurements from the Upper Fremont Glacier by Rao et al. (2012), the record was used to compare preindustrial perchlorate with that of modern years from the same sampling location. Here, it was found that perchlorate concentrations at Summit, Greenland varied from between 0.1 and 11.9 ppt during the time periods covered by the core. As with prior studies (Furdui and Tomassini, 2010; Rao *et al.*, 2012), an increase of perchlorate post-1980 was observed, from a pre-1980 average concentration of 0.8 ± 2.6 ppt to an average of 2.7 ± 2.1 ppt. Importantly, however, a correlation between increased sulfate deposition and elevated levels of perchlorate following the 1991 eruption of Mt. Pinatubo was observed here, similar to that found in the Devon Island core (Furdui and Tomassini, 2010). Further, a seasonal pattern, similar that recorded at Devon Island, was observed.

A record of perchlorate in Antarctic snow was later generated (Jiang *et al.*, 2016) from three locations; from a 15 m firn core taken from the South Pole (Ferris *et al.*, 2011), a 2.8 m deep snow pit dug near the West Antarctic Ice Sheet (WAIS) Divide ice core site (79°28'S, 112°05'W, elevation 1766 masl), and from a 3 m deep snow pit dug at Dome A (80°22'S, 77°22'E, elevation 4093 masl) on the East Antarctic Plateau (Jiang *et al.*, 2012). As with the work by Furdui and Tomassini, (2010), the number of samples per year in all three locations is quite low, about 2 years per sample at Dome A, 2 samples per year at South Pole, and about 7 samples per year at WAIS Divide. At Dome A and South Pole, no information about seasonality of the perchlorate signal could be deduced, but clear seasonality was observed at WAIS Divide. Due to the high resolution at that site, the exact

timing of the peak could be better deduced, appearing to peak in late-summer or autumn. The authors indicate that the seasonality is related to stratospheric ozone concentration, but that would require that perchlorate produced in the stratosphere to be immediately removed to the troposphere and deposited with snow (Jiang *et al.*, 2016). Though a mechanism such as that cannot technically be ruled out, such rapid removal of molecules from the stratosphere has not been observed, and in all cases, ozone exists far in excess of any stratospheric chlorine species. Regardless, this work shows that a clear and widespread increase in perchlorate seemingly in concert with increased stratospheric chlorine occurs in the last few decades in Antarctica similar to that observed in Greenland (Peterson *et al.*, 2015b), and that pronounced seasonality exists for the perchlorate signal in snow at WAIS Divide.

The repository of ice core records of environmental perchlorate was expanded with a continuous record spanning the years 1936 to 2007 CE from an ice core collected from the Agassiz Ice Cap (80.7°N, 73.1°W, elevation 1670 masl) located in Nunavut, Canada (Furdui *et al.*, 2017). While the annual resolution was quite low (3-5 samples per year) in this study, it further confirmed the post-1980 increase in perchlorate deposited to the Arctic, and the seasonality of the perchlorate signal. However, the authors found that volcanic eruptions did not influence perchlorate deposition here, calling into question the hypothesis of volcanically enhanced perchlorate production following the eruption of Mt. Pinatubo seen in earlier work (Furdui and Tomassini, 2010; Peterson *et al.*, 2015b), and that aerosol had no impact upon perchlorate levels at this sampling location and in fact they assert that the presence of aerosol suppresses perchlorate

formation in the stratosphere after 1979. Further, this study indicates that the dominant pre-1980 process for perchlorate formation at this site is tropospheric formation by lightning.

The most comprehensive and detailed record of perchlorate in the environment was generated (Cole-Dai *et al.*, 2018) upon completion of the analysis of the Summit, Greenland core started in earlier work (Peterson *et al.*, 2015b). This record spans over three centuries (1700-2007) at very high resolution (9-12 samples per year). Three key findings emerged: 1) that the onset of the industrial revolution did not impact perchlorate levels though large quantities of pollutants were released; 2) that the post-1980 increase in perchlorate is likely due to the release of organic chlorine to the atmosphere, and subsequent atmospheric formation of perchlorate; and that 3) some explosive volcanic eruptions appear to increase perchlorate concentrations in ice cores.

1.4 Overview of Ice Core Chemistry

To understand how perchlorate in the environment is formed, and to constrain the variables that govern its production, it would be useful to measure perchlorate and related chemical species in the atmosphere. Many factors such as the low levels speculated to exist in air and limitations in atmospheric measurement equipment render this either impossible or impractical. For example, measurements in a volcanic plume pose issues for the operation of analytical platforms, and the intermittent nature of eruptions makes prepositioning of measurement devices difficult. In other cases, analyte concentrations in the stratosphere may be far too low to measure reliably.

Ice cores provide a means to obtain data that may be extrapolated to atmospheric chemistry. As precipitation droplet sizes grow, chemicals in the atmosphere become trapped inside. When this precipitation falls to Earth as rain or snow, these atmospheric components are then brought to the surface; in the case of snow, which is well-preserved in polar regions, this is called air-snow transfer. This transfer of impurities from the air to the ice sheet then allows for reconstruction of atmospheric composition and studying of both chemical and physical atmospheric processes.

Ice cores provide long records of climate variation, which may be caused by a multitude of forcings. These forcings include large amounts of sulfate aerosol which can be generated by explosive volcanic eruptions. The eruption can then be detected in ice cores as layers with increased sulfate concentration, where the forcing can be evaluated. In contrast to these chemical measurements of forcings in ice cores are environmental archives such as tree rings. Narrow tree rings are also a response to climate forcing, i.e. cold periods. However, the cause of forcing in this example (volcanic eruption) and the effect of the event (narrow rings) are not independent of each other. This property makes interpretation of tree ring width problematic when used to investigate a relationship between climate forcing and the resultant change in climate, whereas in ice cores, the forcing (chemical measurement of sulfate) and the response (change in isotopic composition of water due to temperature change) are completely independent. Ice cores in this fashion, allow detailed study of both the forcings and climate effect without interference.

One of the most useful characteristics of ice cores is that with careful site selection, the chronological order of precipitation is preserved in the ice stratigraphy. This extremely helpful property allows for assignment of a date to any layer in the ice core. The accuracy of assignment of dates to layers of ice is affected by accumulation rate. In places where there is very high accumulation, ice core records of a given depth may be shorter in length of time covered, but the ability to discern each year is very good, leading to extremely high confidence in date assignment. In places with low accumulation the length of the records can be very long, while confidence in annual layer assignment may be lower.

Lastly, certain locations of ice collection may capture some chemical or physical processes better than others. For example, Greenland is an excellent choice for analyzing for human impact on the atmosphere, while Antarctic ice cores are relatively free of human influence, as the majority of human activities impacting the environment take place in the Northern Hemisphere. Therefore, we may use site selection for ice core retrieval to tune the objectives of record length, annual resolution, and which processes (chemical and physical) are captured in the snow.

1.5 Research Objectives

This work comprises the following objectives: 1) Investigate how proposed perchlorate formation pathways contribute to background perchlorate concentrations in snow, 2) Investigate the extent of occurrence of and conditions under which atmospheric formation of perchlorate occurs in response to volcanic eruptions, 3) Evaluate the

magnitude and specific features of the perchlorate concentration in snow as a response to volcanic eruptions such as timing and post-depositional change, and 4) Investigate how major perchlorate formation pathways are perturbed after volcanic eruptions.

2.0 Methods

2.1 Sample Collection

Several shallow ice cores were drilled during June and July, 2007 near Summit Station, Greenland (73.6° N, 38.5° W). The top 97.98 meters of one core (SM07C2, 211 m) was analyzed for perchlorate and major ions, except for a few short intervals (19.29-20.28, 27.405-28.42, 67.45-69.48, 76.49-76.84, 83.35-84.32, and 86.19-87.14 m) where ice had been consumed for other purposes. A section (95.665 to 124.365 m) of another Summit, Greenland core (SM07C4) from the same location as SM07C2 was also analyzed for major ions, and the section from 120.350 to 124.365 m depth was analyzed for perchlorate. All ice core sections were wrapped in clean plastic lay-flat tubings and kept frozen during transport from the field to the laboratory, where they were maintained at or below –20° C until chemical analysis.

The South Pole Ice Core (SPICEcore) project yielded a 1750 m ice core collected from a location about 2 km (89.99° S, 98.16° W, elevation 2835 masl) from the South Pole Station over the years 2014 to 2016. As part of the SPICE project, several shallow cores were drilled in addition to the main core, and two short sections (29.630 to 32.635 m, and 66.530 to 69.288 m depth) from one of these cores were used in this study. Cores were kept frozen until analysis, where each sample was measured for major ions and perchlorate.

In January 2013, a 2.6m deep snow pit was dug by hand near the West Antarctic Ice Sheet (WAIS) Divide ice core location (112.085°W, 79.467°S). Samples were taken

from the wall of the snow pit at 0.03 m intervals. Samples were transported frozen to South Dakota State University where each sample was measured for major ions and perchlorate. Exact sampling procedures are discussed elsewhere (Crawford *et al.*, 2017).

The Denali ice core (DIC) data is derived from two ice cores (DIC1 and DIC2, each 208 m long) collected from the Mt. Hunter summit plateau (62°56'N, 151°5'W, 3900 masl) in Denali National Park, Alaska (Winski *et al.*, 2017). A section from DIC1 (117.699 to 121.456 m depth) was measured for major ions and perchlorate.

2.2 Sample Preparation

Samples were prepared for both perchlorate and major ion measurement in the same way, and detailed procedures can be found elsewhere (Peterson *et al.*, 2015a). Briefly, for the SM07 cores, each sample was cut individually from a length of ice core using an electric bandsaw in a cold room (freezer) and samples below 57 m were decontaminated by washing away the outer portion of each sample with 18.2 MΩ ultrapure water until approximately 50% volume reduction was achieved. These samples were then melted and prepared in sample cups and vials washed with ultrapure water.

Firn samples (Summit samples above 57 m, and South Pole samples) were prepared by cutting away the outer surfaces of each sample with a clean bandsaw in a freezer. The Denali ice core samples were decontaminated by scraping the outer surfaces with a ceramic blade. Decontaminated samples were then placed into clean sample cups that had been washed with ultrapure water and air-dried in a clean bench, then capped and left to melt. Once melted, an aliquot of sample was decanted into test vials for

analysis that had been cleaned with ultrapure water and air-dried in a hood on a clean bench.

2.3 Analytical Methods

2.3.1 Ion Chromatography/Conductivity Detection

Samples were analyzed for major anions (Cl^-, NO_3^-, and SO_4^{2-}) and cations (Na^+, K^+, Mg^{2+}, and Ca^{2+}) using ion chromatography. Stock 1000 ppm solutions were prepared for each major ion from pure reagents and 18.2 MΩ ultrapure water. Reagents used to prepare stock solutions were K_2SO_4 (F.W. = 174.259), $NaNO_3$ (F.W. = 84.995), NaCl (F.W. = 58.44, Certified ACS, Fisher Chemical), $MgCl_2 \cdot 6\ H_2O$ (F.W. = 203.31, Acros Organics), Na_2CO_3 (F.W. = 105.99, HPLC Grade, Fisher Chemical), KCl (F.W. = 74.56, Certified ACS, Fisher Chemicals), and $CaCl_2 \cdot 2\ H_2O$ (F.W. = 147.01, Acros Organics). Intermediate

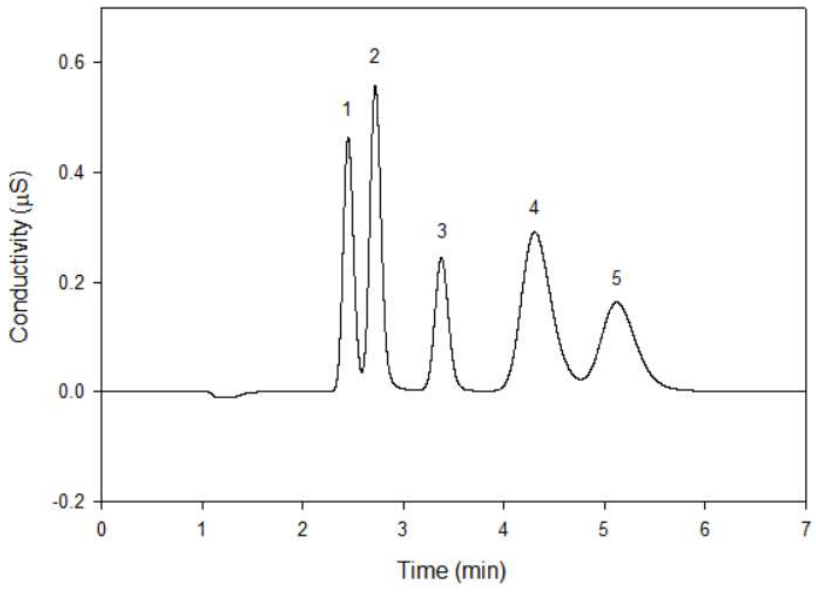

Figure 1. Chromatogram of 25 µg kg^{-1} cation calibration standard, CS12 analytical column (2mm x 250mm), 12 mM H_2SO_4, 0.5 mL min^{-1}. (1) Na^+, 2.45 min; (2) NH_4^+, 2.72 min; (3) K^+, 3.38 min; (4) Mg^{2+}, 4.31 min; (5) Ca^{2+}, 5.13 min.

solutions, typically between 1 and 10 ppm, containing either all of the major cations or anions were diluted from stock solutions, and daily calibration standards were prepared from the intermediates.

The analytical apparatus comprised two Thermo-Fisher (Dionex) ICS-1500 Ion Chromatography Systems, and a Dionex AS-AP Autosampler. The anion system used an IonPac AS11 (2mm x 250mm, Dionex) ion-exchange column, and sodium hydroxide mobile phase. This system was equipped with an ASRS 300 2mm electrolyte suppressor column using about 5 mA of current, which was tuned for the exact eluent concentration. The cation system used an IonPac CS12A (2mm x 250mm, Dionex) ion-exchange column, and isocratic elution with a sulfuric acid mobile phase. This system was equipped with CSRS 300 2mm electrolyte suppressor column using about 36 mA current. Both IC systems used a 125 µL injection loop. The AS-AP autosampler was configured with a 5.0

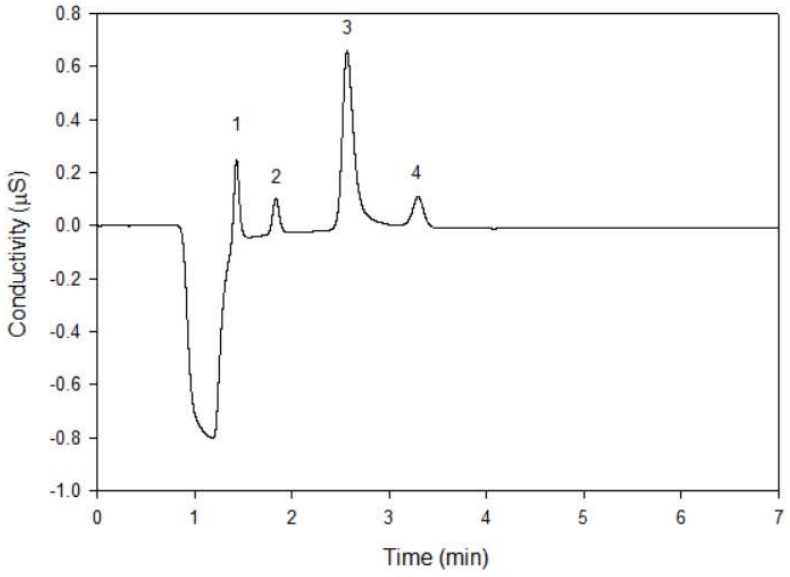

Figure 2. Chromatogram of 25 µg kg-1 anion calibration standard, AS11 analytical column (2mm x 250 mm), 3.8 mM NaOH, 0.5 mL min-1. (1) Cl-, 1.43 min; (2) NO3-, 1.83 min; (3) CO32-, 2.57 min; (4) SO42-, 3.29 min.

mL syringe to allow one-pull filling of the 1.2 mL injection buffer loop, and to simultaneously inject the sample to both IC systems. The typical run time for the ion analysis was 7.0 minutes but was varied by ±1 minute to accommodate variations in eluent strength. Typical chromatograms for cations and anions are shown in Figure 1 and Figure 2, respectively.

The chromatographic data (retention time, peak identification, peak size, peak area, calibration curves, etc.) was collected and processed using Chromelion 7.2 (Thermo-Fisher). All peak assignments, calibration curves, and peak integrations were performed using user-programmed processing methods in the software.

2.3.2 Ion Chromatography/Tandem Mass Spectroscopy

Perchlorate concentrations in polar snow and ice were found to be extremely low; less than 1 μg kg^{-1} (Furdui and Tomassini, 2010; Crawford *et al.*, 2017; Cole-Dai *et al.*, 2018). The low concentration and necessary chromatographic conditions for perchlorate analysis make the measurement of perchlorate in ice cores difficult with ion chromatography.

The procedures to prepare decontaminated Greenland ice core samples for measurement of perchlorate and other species have been described by Peterson et al. (2015a). Samples and procedural blanks were analyzed for perchlorate using ion chromatography-tandem mass spectrometry with electrospray ionization (IC-ESI-MS/MS) as described previously (Peterson *et al.*, 2015a). Perchlorate was eluted from a Dionex IonPac® AS16 (2 x 250 mm) analytical column with 60 mM NaOH at 0.3 mL min^{-1}. The

effluent from the ion chromatograph was mixed with an acetonitrile/water solution (90/10% v/v at 0.3 mL min^{-1}). This mixture was delivered to the ionization/nebulization inlet of an AB SCIEX QTRAP 5500 triple quadrupole mass spectrometer. Negative ion mode was used to detect $^{35}ClO_4^-$ and $^{37}ClO_4^-$ using multiple reaction monitoring of the *m/z* 99.0 to 83.0 and *m/z* 101.0 to 85.0 transitions, respectively. Quantification was performed using the $^{35}ClO_4^-$ peak area with external calibration. The limit of detection and lower limit of quantification of the method were 0.1 and 0.3 ng kg^{-1}, respectively (Peterson *et al.*, 2015a).

2.4 Ice Core Dating

2.4.1 Annual Layer Counting

Determining the age of ice at a given depth in an ice core, or the development of the depth-age relationship, is a crucial step in studies of ice cores. Several methods exist to determine dates in an ice core. They utilize annual layer counting (ALC), modelling, dated reference horizons, or exploit changes in insolation. Selection of an appropriate method is governed by required accuracy, snow accumulation rate at the coring site, and the time period under consideration. The ice cores used for this study were dated using the technique of ALC.

The amount, or concentration in snow, of some chemical species is different at various times of a year; an annual cycle is formed when the concentration proceeds through a maximum and a minimum in a year. As a result of this annual cycling, the distance (depth) between two peaks or troughs indicates a complete year (Legrand and

Mayewski, 1997). The species used for annual layer identification and counting in this study are discussed in detail below. ALC also yields the length, or thickness, of each year (annual cycle), which is equal to the accumulation rate (in ice) of that year. The method requires a minimum of about 6 samples in a year-long period to accurately discern the annual cycle in concentration. Ideally, an annual layer should comprise 10 or more samples per year. At 6 or fewer samples per year, however, significant risk of counting errors is present. Establishing an age scale based upon mean accumulation rate may be necessary if ALC is not possible due to lack of temporal resolution in the ice core, when the number of samples per year is insufficient to resolve annual cycles. The mean-annual-accumulation-rate method has the advantage of being usable with poorly resolved annual signals, but the mean accumulation rate is inaccurate in years when the annual accumulation is significantly different than the average. At a given ice coring site, the accumulation rate can easily deviate from the mean accumulation by 50% or more. While over a long period of time, tens or hundreds of years, the assignment of date does not incur large cumulative error due to the normal distribution of accumulation rates, a specific year can easily have a 1-2 year uncertainty in age assignment. Additional uncertainty may arise when using average accumulation rate to assign age if accumulation is higher or lower for a period of several consecutive years.

When a chemical concentration or physical property of an ice core varies in an annual cycle as described previously, these cycles may be used to count the number of years beginning from a layer with known year. The ALC methodology began in the 1960s using oxygen isotopes in water (Dansgaard, 1964). It was realized there that the isotopic

composition of water was dependent upon temperature, thereby allowing summer and winter seasons to be discerned. Other chemical species with regular annual concentration cycles such as nitrate, sulfate, calcium, sodium, and hydrogen peroxide may be used to differentiate years as well in various instances. In addition to chemical signatures of seasonal change, some physical properties change throughout the year. Ice density, hoar layers, and bubble density all have characteristic patterns attributable to seasonal change (Gow, 1965) and, therefore, may be useful as ALC markers.

In this study three chemical signals were used for ALC: the ratio of Cl^-/Na^+, and the concentrations of both NO_3^- and Ca^{2+}. The first signal used to resolve annual layers is the mass ratio of chloride to sodium. The dominant source of both chloride and sodium in ice cores is sea-salt aerosol (Blanchard and Woodcock, 1980; Legrand and Mayewski, 1997). This aerosol is produced from bursting bubbles generated from ocean surface by wind. As water evaporates from the droplets, the brine and aerosol particles are left in the air and carried to other locations by wind. The ratio in un-altered marine aerosol is close to 1.8, that of bulk seawater (Buat-Menard *et al.*, 1974), but work has revealed that the ratio in snow can deviate significantly (Martens *et al.*, 1973; Hitchcock *et al.*, 1980; Kritz and Rancher, 1980; Song and Carmichael, 1999). Other observations have identified HCl in the marine atmosphere (Duce *et al.*, 1965; Duce, 1969; Kritz and Rancher, 1980).

Legrand and Delmas sought to explain their observations of highly variable Cl/Na ratios in Antarctic snow in this context (Delmas *et al.*, 1982; Legrand and Delmas, 1984; Legrand and Delmas, 1985). It was determined that the ratio varies in response to two main factors: distance from the coast, and the age of the air mass (Legrand and Delmas,

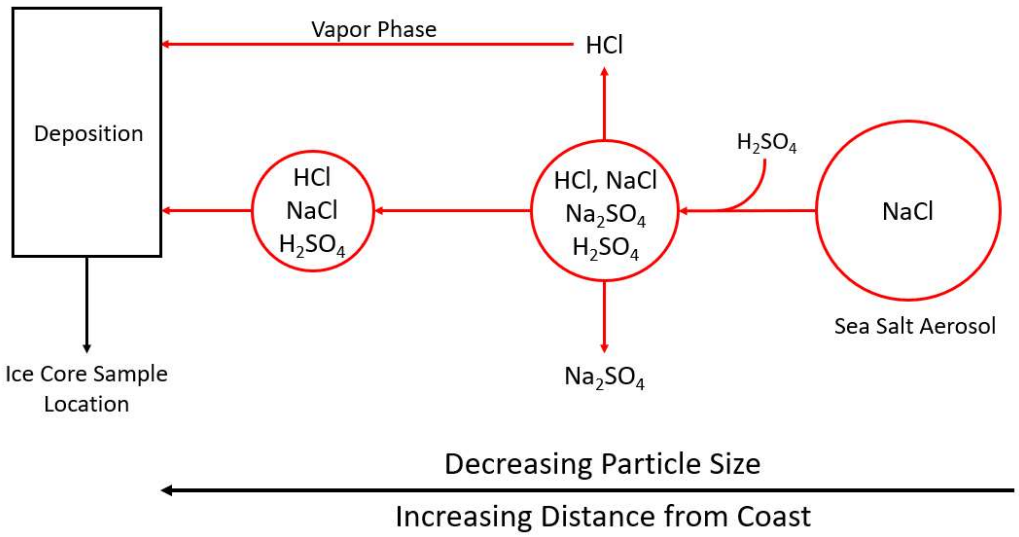

Figure 3. Schematic representation of sea salt aerosol fractionation. Mean particle size decreases and the ratio of chloride to sodium increases as the aerosol moves away from the coast.

1988). Changes in aerosol mass and chemical composition take place, as air mass containing sea salt aerosols move from the ocean into the ice sheet. A schematic representation is shown in Figure 3 to illustrate the changes.

As aerosol particles move further from the coast, HCl is volatilized to the gas phase by reaction of sulfuric acid with NaCl in sea salt. A schematic representation is shown in Figure 3. The heavy particles fall near the coast, containing more sodium relative to chloride compared with the composition in the original sea salt aerosols. As the air mass continues to move inland, the loss of sodium continues, and chloride is enriched in the remaining aerosol mass. Sodium is said to be fractionated or lost in relation to chloride, resulting in an excess of HCl, and an increase in the chloride/sodium ratio occurs (Mulvaney *et al.*, 1993). Since sulfuric acid is more abundant in the summer months, the

fractionation is more pronounced in summer resulting in higher chloride/sodium ratio, while in the winter where the mass ratio is close to 1.8, that of seawater, indicating little or no fractionation (Legrand and Mayewski, 1997). This yields an effective ALC proxy, as seen in Figure 4, along with nitrate and calcium concentrations.

As seen in Figure 4, ratio minima are very close to 1.8, with significant departures from that ratio occurring in summer months. In the case of SM07C2, this ratio can exceed 50 in the summer, dropping back to about 1.8 over the winter. As with any annual signal, however, discerning annual cycles greatly depends upon the number of samples taken

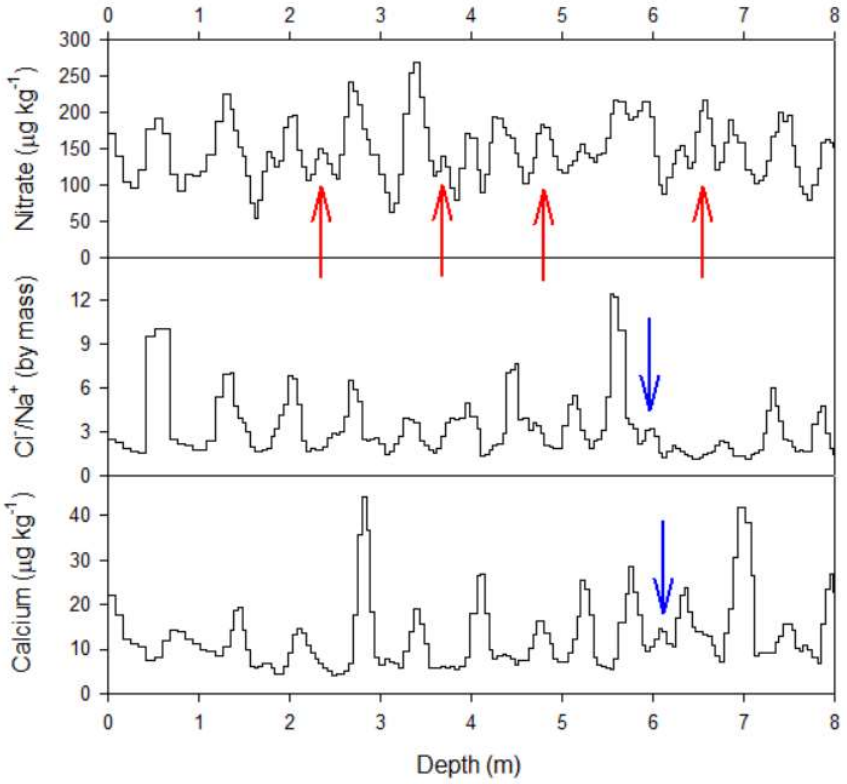

Figure 4. Nitrate concentration, Cl^-/Na^+ mass ratio, and calcium concentration in the top 8 meters of the SM07C2 core. Red arrows indicate years that were counted in the nitrate concentration, but discarded based upon the other two datasets, and blue arrows indicate poorly resolved years that were identified by the strong nitrate peak.

over a one-year thick layer of ice, with some years difficult or impossible to resolve, leading to uncertainty in the age of the ice layers.

The second annual signal evaluated in this work for chronology development in the SM07 core is nitrate, one of the major anions present in snow. In general, nitrate results from the reaction of nitrogen oxides (NO_x) with ozone and hydroxyl radicals. There are many sources of NO_x and its precursors (e.g., NH_3) to the atmosphere, including biomass burning, fossil fuel combustion, emissions from soil and biosphere, and lightning. Owing to the nature of these sources, during pre-industrial periods nitrate exhibits well defined minima in the winter, and maxima in the summer (Legrand and Mayewski, 1997). The winter minima make this a convenient annual signal, since the minima corresponds to the start of a calendar year, as opposed to calcium, discussed below. Nitrate is subject to several post depositional processes in the snowpack, such as photolysis and evaporative loss of HNO_3. However these do not appreciably change the seasonality of the nitrate signal in ice in high accumulation locations (Legrand and Kirchner, 1990; Dibb *et al.*, 2002; Rothlisberger *et al.*, 2002). A complication with nitrate during modern times, however, is the impact of pollution upon nitrate levels. Human emissions in North America after the onset of the industrial revolution constitute a source that can impact the concentrations measured in snow. In Figure 4, nitrate maxima are seen in the winter (red arrows), and if this were the primary ALC proxy, would have been counted as additional years.

Finally, calcium is an effective annual marker, with maxima occurring in the spring (Legrand and Mayewski, 1997). While annual layers are quite well defined (Figure 4), the

spring maxima can be problematic for dating purposes, as the start and end of the year do not align with those of calendar years. If an approximation for the beginning of the calendar year is needed to examine seasonal variation, calcium is not particularly well-suited, requiring a different ALC proxy to be used. However, calcium is invaluable in resolving annual layers when other measurements such as chloride, sodium, and nitrate do not provide clear annual oscillation. In Figure 4, the blue arrows at about 6 meters in depth are an example, where the nitrate signal does not have a well resolved annual peak from the following year, and the peak for the chloride to sodium ratio is quite small. The presence of the calcium peak that occurs just before, however, indicates that the beginning of a year starts at about 5.8 and 6.1 meters, rather than at 5.4 and 6.1 meters, which may have been the case if only the chloride to sodium mass ratio and nitrate were used.

Stratigraphic time markers are used in multiple ways concerning ice core dating. The use of stratigraphic time markers or tie-ins may be used to verify date assignment or used as a dating method by computing average accumulation rate under some circumstances. Certain signals, such as those from very large volcanic eruptions, may appear in multiple ice cores or other environmental archives from distant sampling locations. These events may then be used to assign a specific date to an ice layer through synchronization, providing an estimate of uncertainty at that layer and year, and indicating the needed correction. Stratigraphic time markers may synchronize cores on a continental or hemispheric scale, in the case of high-latitude volcanic eruptions, or in the

case of some large low-latitude eruptions, may be used to synchronize dating schemes between poles.

By combining the three chemical signals discussed above with reference horizons, an annual dating scheme is established with relatively little possibility of missing a year or identifying extra years. Figure 5 depicts a section of ice with all ALC signals used here, and a volcanic eruption as a reference horizon.

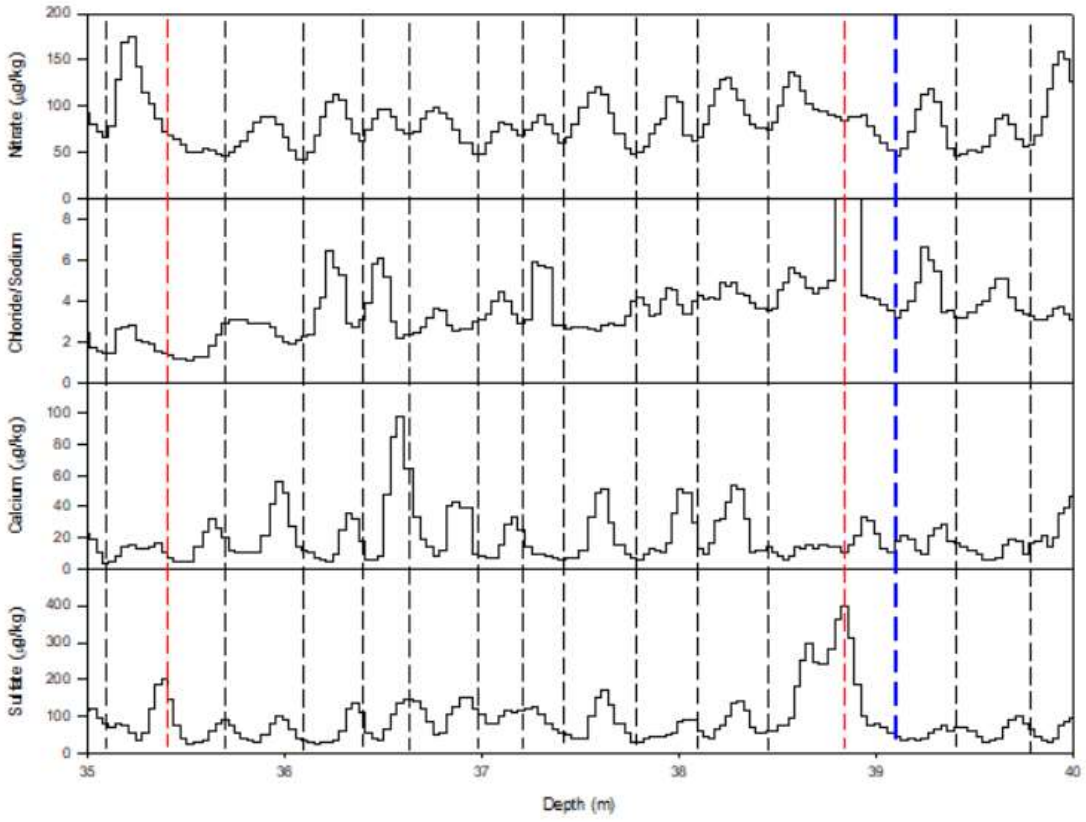

Figure 5. Measurements of nitrate, chloride/sodium ratio, calcium, and sulfate in a 5-meter section of ice from the SM07C2 core. Red lines indicate annual picks with some uncertainty. The blue line indicates the year 1912, which assigned based upon the June 6, 1912 eruption of Novarupta seen in the sulfate signal at about 38.9 meters in depth.

In the SPICE Upstream cores, three reference horizons were used to synchronize to the WAIS Divide 2014 timescale (Sigl *et al.*, 2016). A comparison of continuous ECM measurements was used to identify three eruptions, those of Tambora, the 1809 Event, and a large eruption in 1458, likely that of Kuwae (Global Volcanism Program, accessed April 29, 2020). The Denali Ice Core was dated using ALC, and is described in detail elsewhere (Winski *et al.*, 2017).

2.4.2 Sub Annual Dating

Whereas annual layers present themselves as oscillations in a chemical time series measured in an ice core, no such simple method exists to assign the samples within each year to a specific season, month, or other time interval. Sub annual assignment of dates (or "decimal years") to samples is critical, however, to evaluate a time series in relation to processes that shape the atmosphere and environment throughout the year.

Regardless of how a decimal year is assigned, assumptions on accumulation must be made. While rates of accumulation vary widely on short timescales such as days, weeks, or months, we first assume that accumulation rates are constant throughout the year. This assumption should be evaluated for feasibility though, given the context of varying accumulation. The average accumulation at Summit between 1700 and 2007 is 22.5 cm yr^{-1} water equivalent, and the average number of samples per year is 10.4, thus each sample on average, is about 1.15 months and averages about 2.2 cm water equivalent. The precipitation at Summit Station falls most heavily in the summer than in the winter (Koyama and Stroeve, 2019), constraining the sub annual uncertainty. Assuming that precipitation consistently follows this pattern, even considering actual

monthly variation, the cumulative error introduced by using the constant accumulation assumption for decimal year assignment is small, about 1 month.

To assign the decimal date, first the fraction of annual accumulation, FAA, is assigned for each sample by dividing the sample size (in water) by the total annual layer thickness (also in water). The FAAs of samples since the beginning of the year are then summed to get the cumulative yearly fraction, CYF, for the n^{th} sample of each year, where the first sample of each year is $i = 1$:

$$CYF_n = \sum_{i=1}^{n} FAA_i \quad \text{(E1)}$$

Finally, the CYF is added to the calendar year containing the samples to yield the decimal date (DD) for the bottom depth of each sample. An excerpt of the DD assignment for the major ion time series in the SM07C2 core is shown in Table 1.

Table 1. DD assignment for the year 1996 in the SM07C2 core. This interval comprised 12 samples and covers the depths from 7.124 to 6.514 meters (27.59 cm w.e.).

Sample Size (cm w.e.)	*n*	FAA	CYF	DD
1.98	1	0.07	0.93	1996.93
1.98	2	0.07	0.86	1996.86
1.98	3	0.07	0.78	1996.78
1.99	4	0.07	0.71	1996.71
1.99	5	0.07	0.64	1996.64
2.48	6	0.09	0.55	1996.55
2.00	7	0.07	0.48	1996.48
2.36	8	0.09	0.39	1996.39
2.00	9	0.07	0.32	1996.32
3.86	10	0.14	0.18	1996.18
2.96	11	0.11	0.07	1996.07
2.01	12	0.07	0.00	1996.00

2.6 Data Processing

2.6.1 Flux Calculation and Use

When chemical measurements are made on meltwater from ice core samples, the concentration of the impurity in the meltwater is determined. This concentration, usually in units of mass analyte per mass of the meltwater or ice, as in μg kg^{-1} (parts per billion, ppb), or ng kg^{-1} (parts per trillion, ppt), is then applied to the entire depth interval of the sample. Practically, concentration is a useful measure of analyte content within a matrix. However, when it comes to deposition, what is important in many cases is the flux – amount of mass per unit area for a certain time – rather than concentration. To illustrate the issue with using concentration in lieu of flux, we can consider a situation where the precipitation varies greatly. If a fixed mass of analyte is deposited with a varying amount of precipitation, the concentration varies with precipitation. However, the actual mass of analyte deposited does not change, so if the same mass of analyte is deposited in two locations with differing accumulation, the concentrations would be different. During periods of low accumulation at the same location, the concentration will be high, and during periods of high accumulation, the concentration will be low. Likewise, if there are for example, two identical eruptions from the same volcano occurring at times with different accumulation rates, they may produce different results for concentration, even if the mass (or flux) of analyte deposited, which may be a true measure of the impact of the eruptions, is the same. To quantify deposition, use of flux removes the effect of varied accumulation rates.

Flux, Φ, can be defined as the mass, m, of analyte deposited on a specific area, A, over some amount of time, t, as in E2.

$$\Phi = \frac{m}{A \times t} \quad \text{(E2)}$$

Since the time is governed by the length of time corresponding to the sample, and we are using annual totals, time may be then omitted from E2. To perform the flux calculation, the mass needed to be computed from the measured concentration, which requires that the volume of the ice sample be converted to volume of the meltwater sample, or the water equivalent volume. As snow becomes buried on the ice sheet, it is compacted from soft snow to solid ice. When ice cores are drilled, the volume of the core and a measurement of its mass allows construction of a function that models the density change of the snow due to burial. For flux calculation from units of volume, an analogy is that of measuring rainfall. When rain falls over an area, the true desired measurement is the volume of water, or flux, falling over a specific area in a given amount of time, but rain is measured in units of length, i.e. cm or inches. Since the area of the rain gauge is known, however, the volume may be calculated. With chemicals to be measured in ice cores, the cross sectional area and vertical size of the sample is known. So, by multiplying the sample concentration by its length in water equivalent, the flux for that sample is computed for the time covered by the sample. Then the fluxes over the year are summed for all samples in the year, giving the total mass of analyte deposited over a given unit of area per year. Annual flux is quite convenient and expedient to calculate since relatively

consistent demarcation of annual layers is usually possible and provides a clear and useful metric to gauge the deposition rate of an analyte to the ice sheet.

2.6.2 Time Series Smoothing

Continuous ice core measurements, after creation of the depth-age scale, generate what is known as a time series, which is defined as the magnitude of a signal as a function of time. Generally, the time series generated from measurements of ions contained in ice cores displays noise, as is common with all analytical measurements. In some cases, there arises a need to examine the time series with reduced interference from noise, i.e., to improve the signal-to-noise ratio (S/N), so some technique of smoothing the data may be needed. In general, the easiest method used to increase S/N is a running mean.

The running mean, RM, of the Sample *j* concentration, $\bar{x}_j$, is calculated via a simple algorithm, which may be customized by varying the window size (number of samples in the window), m, around a measurement in the time series, x_j, over the interval, $i = [\frac{1-m}{2}, \frac{m-1}{2}]$ as shown below in (E3):

$$\bar{x}_j = \frac{1}{m}\sum_{i=\frac{1-m}{2}}^{\frac{m-1}{2}} x_{j+i} \qquad \text{(E3)}$$

The RM is simple to calculate, but the bias introduced through assigning equal weight to all measurements becomes more extreme as the window size increases, approaching the arithmetic mean of the dataset. In addition, while a single extreme measurement (large or small) is dealt with well, the occurrence of two extreme signals

may cause unintended biasing of $\bar{x}_j$. In some cases, this may even have the extreme effect of inverting peaks and troughs in the time series. Any use of the RM or adjustment in m must be carefully evaluated for adverse effects on the time series. Obviously, as $m \to \infty$, the time series approaches the arithmetic mean of the entire dataset. The second consideration to make when employing the RM is consistency of x_j over the time domain. Since the total accumulation is proportional to the elapsed time, the measurements should have a consistent depth interval. If the depth interval for x_j is not consistent, then the RM must be weighted for the sample size, derived from the weighted arithmetic mean, as in E4, where w_i is the weight of the i^{th} measurement:

$$\bar{x} = \frac{1}{\sum_{i=1}^{n} w_i} \sum_{i=1}^{n} w_i x_i \tag{E4}$$

The weight in this case is equal to the ratio of the depth interval, z_j, of each measurement divided by the depth interval of the window, z_m. The weighted running mean, WRM, for a set of n observations can be calculated for a window of size m after substituting this ratio for weight, as in (E5):

$$\bar{x}_j = \frac{1}{z_m} \sum_{i=\frac{1-m}{2}}^{\frac{m-1}{2}} z_{j+i} x_{j+i}; \qquad \frac{m-1}{2} \leq j \leq n - \frac{m-1}{2} \tag{E5}$$

Alternatively, the weight may be assigned to preserve the overall shape of the raw signal, in which case the derivation of E4 yields E6, and where α_i is a set of weights for the i^{th} measurement:

$$\bar{x}_j = \frac{1}{\sum \alpha_i} \sum_{i=\frac{1-m}{2}}^{\frac{m-1}{2}} \alpha_i x_{j+i}; \qquad \frac{m-1}{2} \leq j \leq n - \frac{m-1}{2} \tag{E6}$$

Such weighting may be necessary to pick either the exact minima or maxima of an oscillating signal, where the weighted running mean, may shift the minima or maxima by one sample in either direction along the z-axis. If the presence of extreme values is perturbing the time series, some variation of a Savitzky-Golay filter (SGF) may be applied. This method was designed to retain the spectral character (e.g., peak magnitude) of a series of data while removing noise (Savitzky and Golay, 1964; Steinier *et al.*, 1972). In general, the SGF smooths data by convolution, fitting a sub-set of adjacent data points to a polynomial using least-squares analysis. The set of n observations of a dependent variable, y_j, across a window of size m are fit with a set of convolution coefficients, C_i, as in (E7):

$$Y_j = \sum_{i=\frac{1-m}{2}}^{\frac{m-1}{2}} C_i y_{j+i}\,; \qquad \frac{m-1}{2} \leq j \leq n - \frac{m-1}{2} \tag{E7}$$

The convolution coefficients depend on the degree polynomial used for the least-squares analysis may be obtained from a published table (Savitzky and Golay, 1964) or derived, but such derivation is beyond the scope of this work. A macro was developed for Excel to execute this function and is shown in Appendix A for $m = 5, 11, \text{and } 29$. While the SGF excels at retaining the information in the time series while removing noise, it fails when the sample intervals are not similar, and at the ends of the window. This is the same method as locally estimated scatterplot smoothing (LOESS), which was rediscovered and named as such by William Cleveland II in 1979 (Cleveland, 1979), and later refined into the locally weighted scatterplot smoothing (LOWESS) method (Cleveland and Devlin, 1988).

When smoothing is used to present data here, the smoothing method, if any, will be described.

2.6.3 Frequency Domain Time Series Analysis

A useful method for identifying seasonal signals a time series is fast Fourier transform (FFT). Ice core records are collected in the space domain (by depth), then converted to the time domain by assigning a time to each measured signal. Fourier analysis allows conversion of the signal from either space or time domains to the frequency domain. Jean-Baptiste Joseph Fourier recognized that the discrete sinusoids comprising a periodic signal could be separated in the frequency domain (Fourier, 1808; Fourier, 1822). This work provided the foundation for a generalized solution, to quickly perform this task for a wide range of applications (Cooley and Tukey, 1965).

A requirement of these generalized methods, however, is that the series (in time or space) comprise discrete samples of equal weight. Ice core samples do not usually have the same time interval; so, we must first perform some imputation to generate a discrete series. Imputation in general represents some method for assigning a value for a missing data point. In the case of an ice core time series this means that we are solving for a data point that should lie at some discrete time interval, for example each month or each year, when the measured data points are non-discrete. In general, four approaches are used, cold-deck, hot-deck, mean substitution, and regression.

Briefly, cold-deck and hot-deck methods fill the missing point by selecting a donor from another dataset or record, including carrying the last observation forward. Both of

these methods introduce bias to the dataset and are generally not currently used since computing power is no longer a limitation. Mean substitution uses the mean of all observations of the variable as the missing point. While there are some advantages for this method, it cannot be used for a time series where each observation lies in context to neighboring observations. Therefore, the most useful imputation method for ice core time series is regression imputation, where the relationship of neighboring measurements is represented by some function, where any intermediate predicted observation may be interpolated through the regression function.

The simplest and easiest to implement regression imputation is linear imputation, where the domain and range in between two consecutive observations is modeled as a linear function. Here, linear imputation is performed on the SM07C2 dataset to generate a new time series with an interval of exactly one month between data points. Figure 6

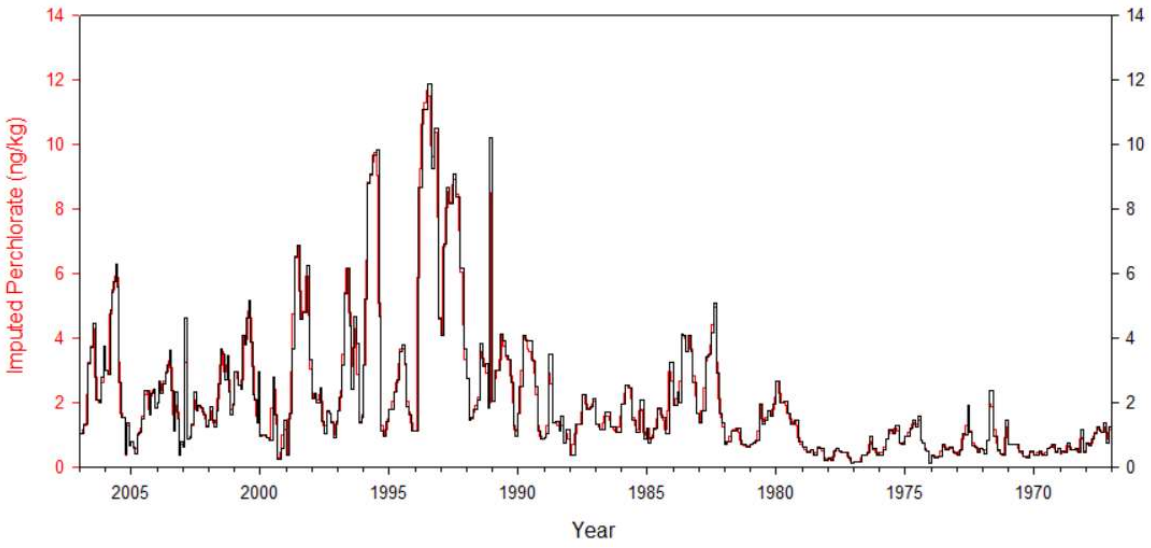

Figure 6. The imputed perchlorate time series (red) is overlaid upon the observed measurements in the time series (black), showing extremely close agreement.

depicts the original perchlorate measurements and imputed concentrations for a section of the SM07C2 perchlorate record from 1967 to 2007. It can be seen that very little bias is introduced, and the now discrete time series closely matches the actual observed time series. Once the discrete time series has been generated, fast Fourier transform was carried out using the periodogram function in the TSA package for R. The scripts written to produce these periodograms are presented in Appendix B.

2.6.4 Time Domain Time Series Decomposition

A time series may be decomposed into three components, the trend, the seasonal or recurring component, and noise using time domain time series decomposition. The trend is how the time series is changing overall, whereas the seasonal component is an oscillating change with some period, be it a day, month, year, etc. The noise is the component of the time series that cannot be explained by the trend or seasonal component. A time series model may be one of two types, additive or multiplicative. In a multiplicative time series, the values of seasonal component and the trend for a data point are multiplied together. The net result is that as a trend increases, the magnitude of the seasonal component of the observed series also increases, and vice versa, because the variation of the seasonal component is *proportional* to the total signal. In an additive time series, the variation of the seasonal signal does not change with respect to the trend, because the seasonal signal is *independent* of the magnitude of the total signal.

In this work, the statistical program R is used to evaluate the SM07C2 monthly perchlorate dataset as an additive time series for the occurrence and magnitude of the perchlorate seasonal signal. The R script for performing this analysis is included in

Appendix C. The additive time series decomposition represents an observed signal as a summation of the noise, seasonal, and trend components. As such, the trend in this case will always be a positive integer. The seasonal and noise components are a positive or negative integer centered on zero that is added to the trend. Summing the noise, seasonal signal, and the trend, then yields the observed measurement for that instance in time. Ideally, the noise should be normally distributed around zero, while there are neither limits to the magnitude of the seasonal component in either the positive or negative direction, nor a need to have a normal distribution around zero.

3.0 Relationship of Perchlorate to Stratospheric Chlorine Chemistry and Ozone

Continuous measurements of perchlorate in ice cores from polar regions allow, for the first time, investigation into chlorine chemistry in the atmosphere through analysis of an environmental archive. The chemistry of halogens in the environment is quite complex, and in the case of chlorine, tied closely with stratospheric ozone. Ozone in the stratosphere is critical for the maintenance of life on Earth, providing an effective shield against the intense ultraviolet radiation that constantly bombards the planet. Indeed, exposure to UV radiation is closely tied to the occurrence of skin cancer in humans. While in recent decades, ozone depletion has been linked to anthropogenic halogen emissions, natural phenomenon such as volcanic eruptions have recently been shown to reduce ozone concentrations in the atmosphere. The effect that volcanic eruptions have had on ozone in the past is largely unknown, as is knowledge of how the ozone layer may have changed over time before anthropogenic emission of CFCs.

In the stratosphere, perchlorate is thought to form from reactions involving chlorine radicals and ozone, and thus may provide a valuable tool for investigation of stratospheric chemistry. While ice cores provide a valuable medium for reconstructing records of atmospheric processes, records which allow investigation of halogen chemistry and ozone do not exist. In this chapter, an overview is provided with respect to general stratospheric chlorine chemistry and proposed perchlorate formation mechanisms; this is followed by a detailed analysis of how ice core perchlorate records are reflective of chemical processes involving chlorine and ozone occurring in a stratosphere unperturbed by volcanic eruptions. Finally, in Chapter 4, the evidence of enhancement of perchlorate

production in the stratosphere by volcanic eruptions is presented, accompanied by an assessment of how perchlorate formation mechanisms are probably affected by volcanic eruptions.

3.1 Overview of Stratospheric Chlorine Chemistry

Chlorine is found in the stratosphere in a variety of chemical forms. The forms include radicals (Cl or ClO, referred to as ClO_x or active chlorine), inorganic compounds (mostly HCl, $ClONO_2$, and HOCl), the diatomic molecule (Cl_2), and organic compounds (CCl_4, CFCs, or referred to as CCl_y). Stratospheric chlorine chemistry can largely be grouped into three categories, gas-phase chemistry, heterogeneous chemistry, and nitrogen coupling. In all three categories, formation of chlorine radicals is directly coupled with ozone chemistry and, therefore can affect the abundance of ozone, and consequently the ozone layer. In contrast to active chlorine species, the chemically inert reservoir species HCl and $ClONO_2$ contain the vast majority of chlorine in the stratosphere. The distribution between these two groups (active and reservoir) is in constant change, with chlorine atoms moving between active moieties and reservoir molecules, largely through interaction with atomic oxygen, molecular oxygen, hydroxyl radicals, methane, various nitrogen species, and ozone. These three categories (chlorine, oxygen, and nitrogen species) interact with each other and respond to various conditions such as the amount of light from the sun and the temperature of the atmospheric regions where reactions are taking place. Each will be briefly discussed, then perchlorate formation mechanisms will be examined in the context of these categories.

Chlorine in the stratosphere exhibits what is known as partitioning, where the distribution of chlorine species varies by altitude and is a critical consideration when investigating stratospheric chemistry. The concentration of chlorine in the stratosphere is quite low, in the range of about 3.7 ppbv (Nassar *et al.*, 2006). Of this amount at high Northern latitudes (60° - 82° N), HCl accounts for about 0.7 ppbv at 15 km altitude, to almost 100% of total chlorine at 55 km. For the same latitudes, the other reservoir species, $ClONO_2$, is largely absent relative to HCl at altitudes above 37 km and accounts for only about 0.2 ppbv at 15 km, with the highest concentration found around 27 km. Active chlorine, as ClO, occurs primarily at altitudes between 30 and 55 km, with the greatest concentration (about 0.8 ppbv) at 40 km. Organic chlorine, which makes up the bulk of chlorine species in the lower stratosphere and troposphere, does not occur in a significant amount above about 30 km, while at 15 km makes up about 60% of all chlorine

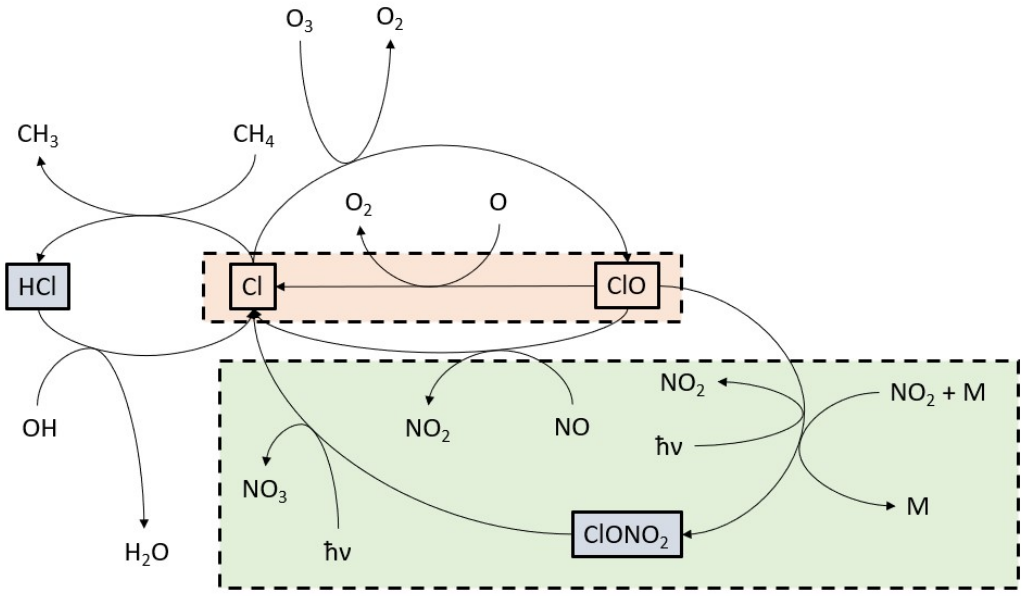

Figure 7. Major gas-phase stratospheric chlorine chemistry. The orange box encompasses ClO_x, and the green box indicates coupling to nitrogen chemistry.

species. These profiles vary seasonally, and with latitude, but the general partitioning behavior remains consistent (Nassar *et al.*, 2006).

Important gas phase chlorine chemistry is shown in Figure 7. In general, HCl is converted to ClO_x through reaction with hydroxyl radicals, and ClO_x can revert back to HCl through reaction with methane. However, methane is also converted to water vapor and CO_2 in the stratosphere through reaction with hydroxyl radicals, competing with both activation of HCl and formation of HCl (Noël *et al.*, 2018). Chlorine is also activated from the $ClONO_2$ reservoir through photolysis. This reaction, however, is strongly seasonal in the polar stratosphere, since models show that, at high solar zenith angles, rates of $ClONO_2$ formation can easily exceed photolysis rates (Solomon *et al.*, 1993). In any case, largely owing to the low concentrations of all gaseous and radical species in the stratosphere, gas phase reactions are quite slow.

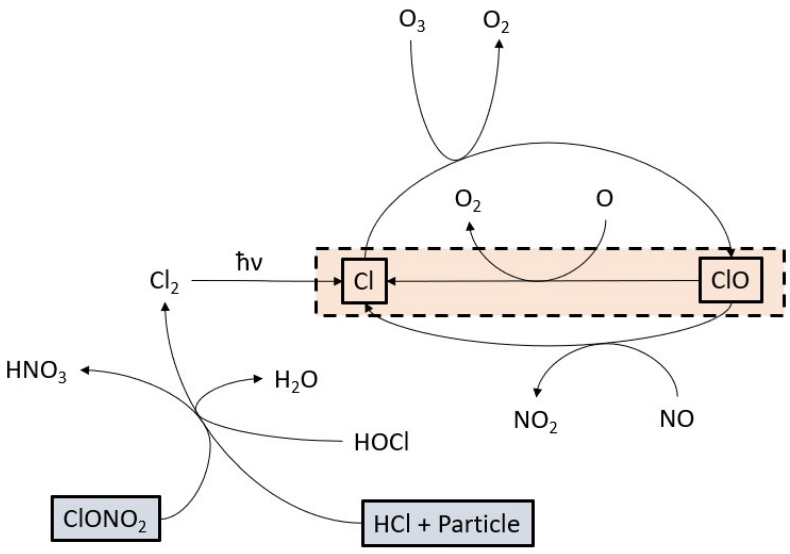

Figure 8. Heterogeneous chlorine chemistry in the stratosphere.

Heterogeneous activation of chlorine (Figure 8), however, can be faster and have a greater impact upon the ozone layer in polar regions, than gas- phase activation:

Step 1a: $HCl + ClONO_2 \rightarrow HNO_3 + Cl_2$

Step1b: $HCl + HOCl \rightarrow H_2O + Cl_2$

Step 2: $Cl_2 + \hbar\nu \rightarrow 2Cl$

In general, reservoir species react on the surface of polar stratospheric clouds (PSCs) or aerosols, forming Cl_2. In the absence of sunlight during polar winter, Cl_2 accumulates. When sunlight reaches the stratosphere in late winter and early spring, Cl_2 is rapidly photolyzed into chlorine radicals, whereupon catalytic destruction of ozone begins. However, in the Arctic, temperatures rarely get cold enough (below 195 K) for PSCs to form, mitigating the ozone loss that may have otherwise occurred. In the

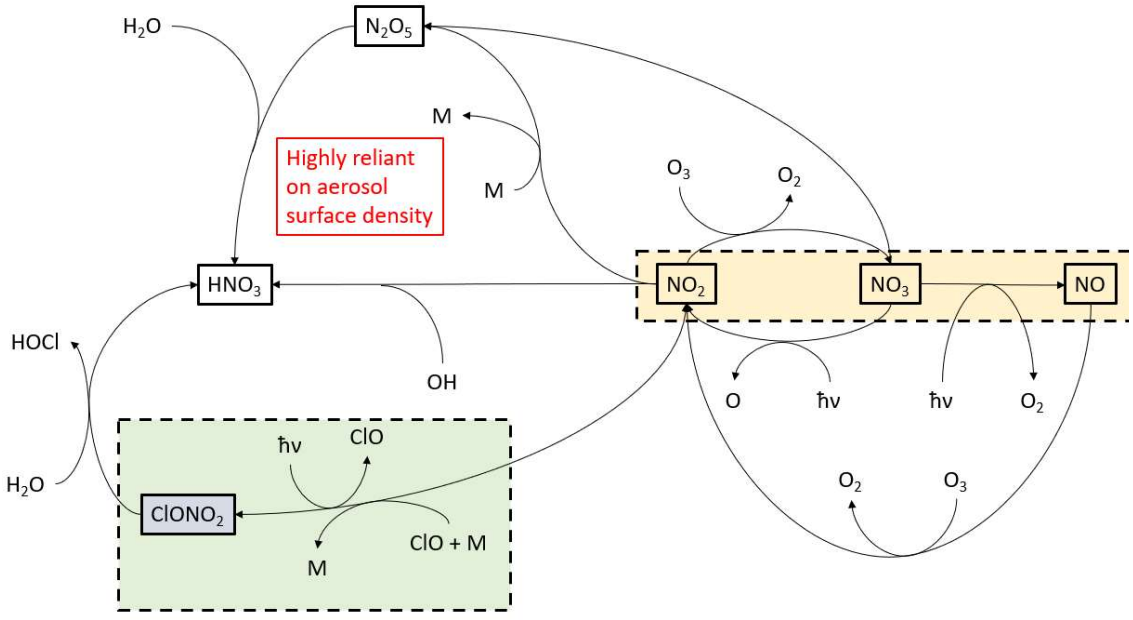

Figure 9. Coupling of the nitrogen cycle to chlorine nitrate in the stratosphere.

Antarctic, temperatures in the stratosphere routinely dip below 185 K, giving rise to more common PSC formation and more extensive chlorine activation, giving rise to catalytic ozone loss, and leading to formation of the springtime Antarctic ozone hole. This process may also occur during periods of high aerosol surface area density, the surface area per volume of aerosol, such as after major volcanic eruptions.

The last major component discussed here is the coupling of the $ClONO_2$ reservoir to the nitrogen cycle in the stratosphere, shown in Figure 9. The coupling of nitrogen and chlorine chemistry is an important part of chemistry in the stratosphere. Chlorine nitrate sequesters about 30% of chlorine in the stratosphere, an important chlorine reservoir, but it is subject to abundance of NO_x, and denitrification of the stratosphere can reduce the abundance of chlorine nitrate through causing denitrification:

$$NO_2 + NO_3 + M \rightarrow N_2O_5$$

$$N_2O_5 + H_2O \rightarrow 2HNO_3$$

Which reduces the NO_2 available to form $ClONO_2$. In particular, during periods of sunlight, when $ClONO_2$ can be photolyzed to ClO, this is especially a consideration for catalytic ozone loss since the formation of chlorine nitrate is hampered during periods of heavy denitrification. Aerosol particle density is a critically important parameter in how quickly N_2O_5 is formed (von Glasow, 2010), as is the abundance of water, which hydrolyzes N_2O_5 into 2 molecules of HNO_3. At sufficiently high aerosol particle densities, the fraction of nitrogen present as HNO_3 can be over 90%, effectively inhibiting the conversion of ClO into chlorine nitrate.

3.2 Mechanisms of Atmospheric Perchlorate Formation

Atmospheric formation of perchlorate is thought to occur in both the troposphere and the stratosphere. Tropospheric processes comprise mainly the direct oxidation of chloride (or HCl) by hydroxyl radicals and ozone, or formation of perchlorate via lightning generated chlorine radicals. Stratospheric processes focus upon the role of chlorine radicals, ozone, and heterogeneous chemistry. In the stratosphere, the abundance and production rate of perchlorate may be crucial to balancing the budget of inorganic chlorine species, chiefly HCl, $ClONO_2$, and chlorine radicals, where a discrepancy has been noted between total observed inorganic chlorine and that which is projected to exist based upon known sources and sinks (Prasad and Lee, 1994; Jaeglé *et al.*, 1996).

Based upon previous work showing that Cl_2O_7 was the final product of chlorine photolysis in the presence of ozone (Byrns and Rollefson, 1934; Cohen and Heicklen, 1972), Simonaitis and Heicklen proposed that perchloric acid is formed in a possible chain terminating step for removal of odd-electron chlorine chemical species in the stratosphere (Simonaitis and Heicklen, 1975):

$$Cl + O_2 + O_3 \rightarrow ClO_3 + O_2$$

$$ClO_3 + OH \rightarrow HClO_4$$

At the time of that work, however, perchlorate had not been measured in the environment, making this a speculative conjecture based upon an estimation of rate coefficients.

Measurements of oxygen isotopes in perchlorate in groundwater and soils showed that at least one oxygen comes from ozone (Bao and Gu, 2004; Jackson *et al.*, 2010), and that photodecomposition of chlorine dioxide is an important intermediate for stratospheric production (Kang *et al.*, 2006; Hatzinger *et al.*, 2017). In addition, if ozone is required, some detectable correlation between ozone and perchlorate may be observed. Some correlations between perchlorate and ozone (Furdui and Tomassini, 2010; Furdui *et al.*, 2017) were found in snow perchlorate concentrations and ozone column measurements from the Arctic, but other work (Cole-Dai *et al.*, 2018) did not arrive at the same conclusions, and it had been previously shown in laboratory experiments that direct oxidation of chloride by ozone produced very little perchlorate (rate of perchlorate production was 2 to 3 orders of magnitude lower than rate of chloride consumption) relative to other formation experiments, and that increasing ozone abundance has diminishing returns on the rate of perchlorate production, suggesting that once a sufficient amount of ozone is present, the addition of excess has little impact on perchlorate production (Rao *et al.*, 2010).

The laboratory experiments conducted by Rao et al. (2010, 2011) provided several other key constraints and findings on perchlorate production. First, it was found that perchlorate production in their experiments was favored at low pH. They concluded that low pH favored the *in-situ* generation of $HClO_2$, leading to a chlorine dioxide radical intermediate. Second, their findings show that production of perchlorate through electrical discharge was favored in conditions of low humidity. Finally, the isotopic

measurements of the perchlorate produced in their laboratory experiments confirm that ozone is a reactant.

Ultimately, perchlorate production mechanisms were summarized, with consideration of all field and laboratory work in a large volume by Hatzinger et al. in 2017. There it was found that perchlorate is produced via a relatively small set of reactions in the atmosphere, the first step of which in all likely cases is formation of either a chlorine radical or gaseous and/or aqueous HOCl from chloride. Pathways with the initial step of forming HOCl:

Step 1a: $O_3 + Cl^-_{(aq)} \rightarrow OCl^-_{(aq)} + O_2$

Step 1b: $O_3 + HCl_{(g)} \rightarrow HOCl_{(g)} + O_2$

Which may form a chlorine radical via:

$$OH + HOCl \rightarrow OCl + H_2O$$

HOCl may also react with HCl to form Cl_2:

$$HCl + HOCl + M \rightarrow H_2O + Cl_2$$

Which undergoes photolytic decay into two chlorine radicals.

The initial steps investigated by Hatzinger et al. considered oxidation of chloride as the first step in the overall mechanism, but it must be clearly understood that in the atmosphere, many other pathways of generating a variety of perchlorate-producing intermediates ($ClONO_2$, ClO_2, Cl, ClO, etc.) exist besides oxidation of chloride, and will be discussed below.

The two chain-terminating steps involve conversion of a chlorine dioxide radical to perchlorate via reactions with ozone and hydroxyl radical:

Chain Termination Step 1: $ClO_2 + O_3 \rightarrow ClO_3 + O_2$

Chain Termination Step 2: $ClO_3 + OH \rightarrow HClO_4$

The most likely pathways involve non-catalytic net destruction of between 2.5 and 4 ozone molecules per molecule of perchlorate formed (Hatzinger *et al.*, 2017), suggesting that ozone is an important precursor and directly linked to perchlorate abundance. These pathways are shown in Figure 10, as part of the stratospheric chlorine chemistry introduced above. For clarity, formation of ClO from HOCl will not be shown on diagrams (other than Figure 35, when discussed later in context of volcanic eruptions) but is considered when discussing chlorine activation. On this and similar diagrams, species

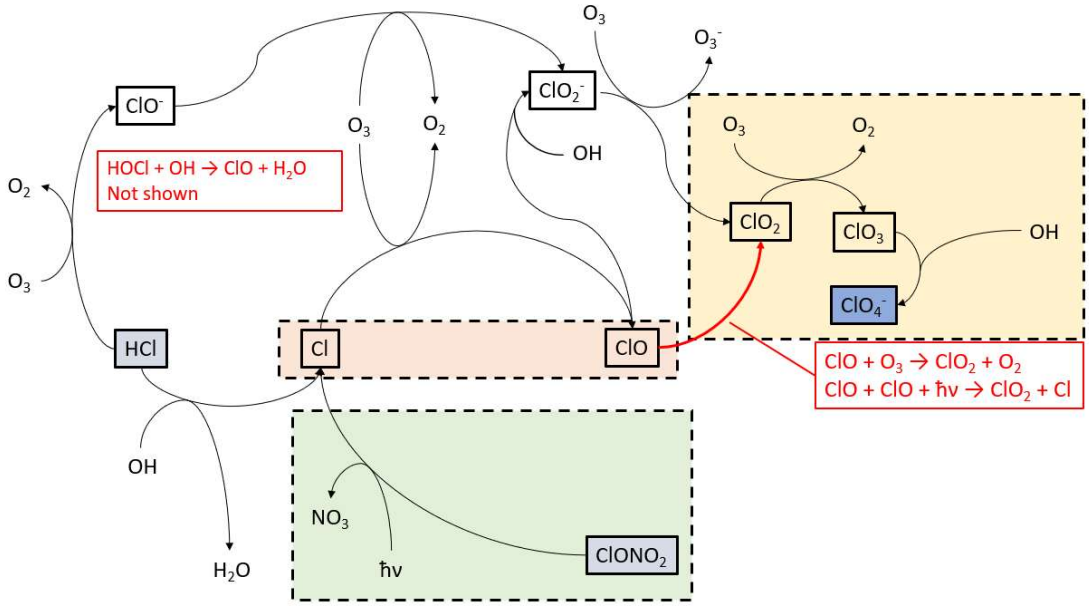

Figure 10. Perchlorate production pathways integrated into stratospheric chlorine chemistry.

with an acidic hydrogen may be shown either protonated or not, since the exact form of these species may vary and is not precisely known at any given time; rather, the particular species thought to be involved in a given step is shown. Heterogeneous chlorine chemistry is not shown here but is shown later in Figure 33.

An important note must also be made here concerning the formation of chlorine dioxide. This molecule occurs in two isomers, OClO, and ClOO, and here a distinction is not made between the two since both can form ClO_3. In the figures presented here, the reaction

$$BrO + ClO + \hbar\nu \rightarrow ClO_2 + Br$$

is not shown, though it is thought to be the primary pathway to generating chlorine nitrate in the stratosphere (Cicerone, 1981; Solomon *et al.*, 1993). Experiments have, however, shown that the self-reaction (ClO + ClO) to produce OClO does indeed occur, and may be significant (Birk *et al.*, 1989). Regardless, the reaction pathways discussed here are those deemed pertinent by Hatzinger et al. (2017). Under typical conditions, namely before significant anthropogenic input or injection of volcanic HBr, the abundance of bromine in the stratosphere is quite limited. For this reason, formation pathway involving bromine for chlorine activation will be discussed later, in the context of enhanced perchlorate production during a volcanic eruption.

Upon inspection of proposed perchlorate formation mechanisms in the context of stratospheric chlorine chemistry, several features become apparent. First, ozone is required in all pathways, as mentioned above. The number of ozone molecules varies by

specific path but is required even in the pathway not proceeding through chlorine radicals. Second, all pathways have the same chain terminating steps (shown above), the addition of an oxygen atom from ozone, and addition of a hydroxyl radical. Third, while sunlight is not required in all pathways (except in the generation of NO_x and ozone), it is required for pathways beginning with chlorine nitrate, and for one pathway to generate chlorine dioxide from a ClO radical, indicating that perchlorate production may be enhanced in periods of sunlight if the rate limiting step involves photolysis. These three characteristics have significant ramifications for interpreting perchlorate records in ice cores and will be discussed further in Chapter 4.

3.3 Seasonality of Perchlorate

Early measurements of perchlorate in precipitation during recent decades indicated that the rate of deposition appears to vary according to a seasonal cycle (Rajagopalan *et al.*, 2009; Furdui and Tomassini, 2010) in some North American locations. Recent work on Antarctic perchlorate also identified that the concentration of perchlorate in snow appears to vary seasonally (Jiang *et al.*, 2016; Crawford *et al.*, 2017). In addition, a seasonal oscillation in perchlorate appears present in the SM07C2 record, shown in Figure 11. As seen in the figure, annual oscillations are easily identified in the calcium and nitrate concentrations, while comparison of perchlorate and sulfate signals reveals that the perchlorate concentration in snow appears to reach a maximum in the fall.

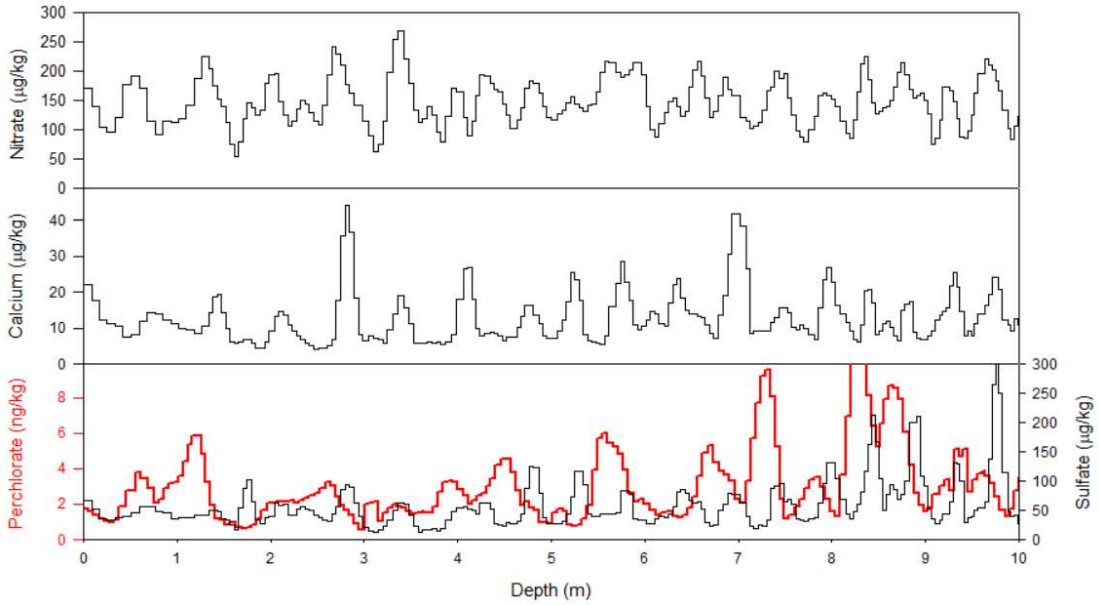

Figure 11. Nitrate, calcium, sulfate (black), and perchlorate (red) concentrations from the top 10 meters of the SM07C2 core. Data has been smoothed with a weighted 3 sample running mean.

Here, the seasonality of perchlorate is quantitatively evaluated through spectral and time-series analysis. This evaluation includes an examination of the periodicity of the perchlorate signal, the relative timing of the perchlorate maxima and minima, and a search for changes in seasonality over time.

3.3.1 Spectral Analysis of the Summit Perchlorate Record

The perchlorate concentration data was converted to the time domain using procedures described in methods. A time period with high levels of atmospheric organic chlorine, from 1980 to 2007, is analyzed. This period overlaps with those in previous studies where seasonality was observed (Rajagopalan *et al.*, 2009; Furdui and Tomassini, 2010). The periodogram (depicting spectral density) generated using the program R is

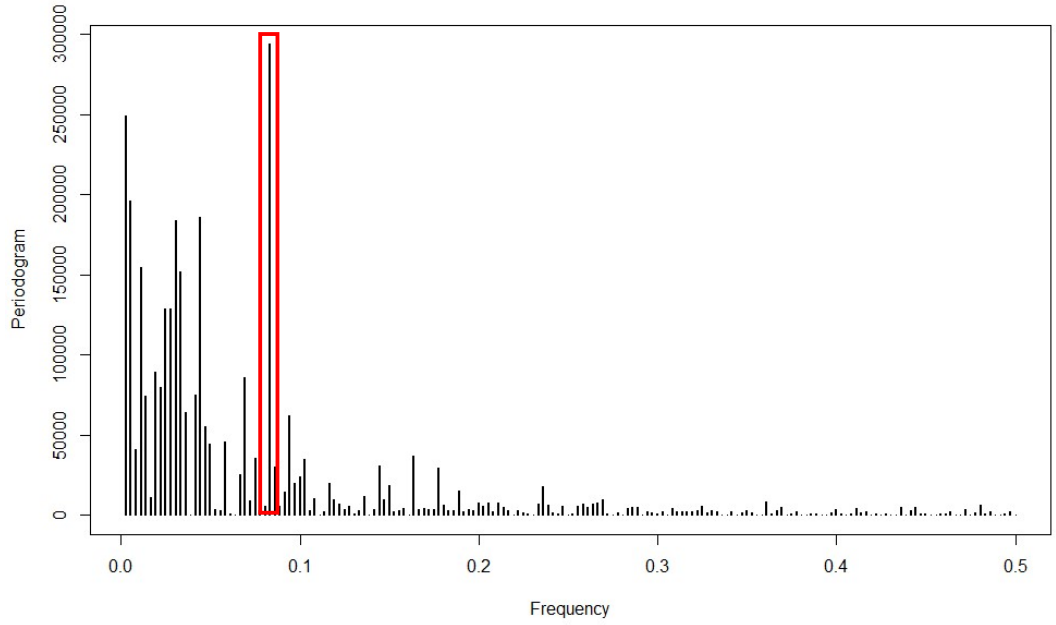

Figure 12. The FFT of the perchlorate SM07C2 time series from 1980 to 2007. Units on the Periodogram axis are $[(\mu g\ kg^{-1})^2]/f$, and units of frequency are in cycles per month. The signal with a 12-month period is highlighted in red.

depicted in Figure 12 (see Appendix for code). It appears that the highest spectral density occurs at the f = 0.083, which corresponds to a period of exactly 12 months (t = 1/f). The second and third strongest frequency correspond to a period of 3 years and 1.5 years, but these are likely artifacts from the trend of data over this 27 year length of time, discussed later.

To evaluate the impact of anthropogenic organic chlorine emission on perchlorate seasonality, a period of time (1967 to 1980) with low levels of organic chlorine in the environment is investigated, and the results are shown in Figure 13.

In Figure 13, it can be seen that no significant signal at f = 0.083 is present, indicating that during periods of low perchlorate levels, there is no perchlorate

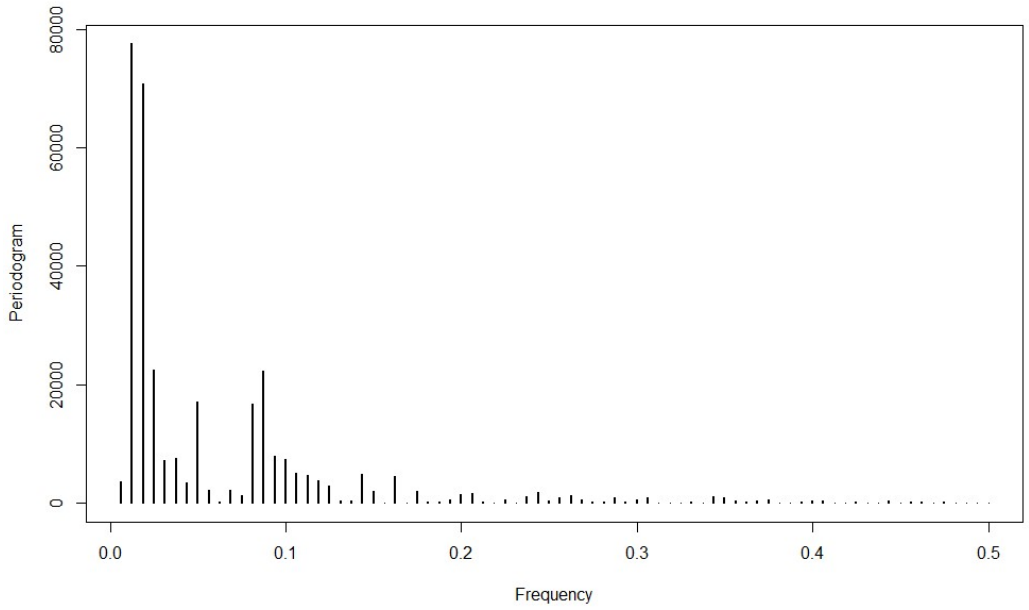

Figure 13. The FFT for the perchlorate time series from the year 1967 to 1980. Units on the Periodogram axis are $[(\mu g\ kg^{-1})^2]/f$, and units of frequency are in cycles per month.

seasonality at Summit. Given evidence of the relationship between perchlorate and organic chlorine in the stratosphere (Cole-Dai *et al.*, 2018), this suggests that seasonality and high levels of stratospheric organic chlorine are related.

The bipolar nature of perchlorate seasonality is confirmed by performing FFT on the perchlorate signal from a WAIS Divide snow pit, shown in Figure 14. Here, the maximum frequency corresponds to a period of 12.8 months. Given the short length of time for this record, this appears to be broadly consistent with an approximately 1 year period.

The FFT is not sensitive to the absolute magnitude of the measurement, but rather the relative magnitude of variation of the component sinusoids. These findings suggest

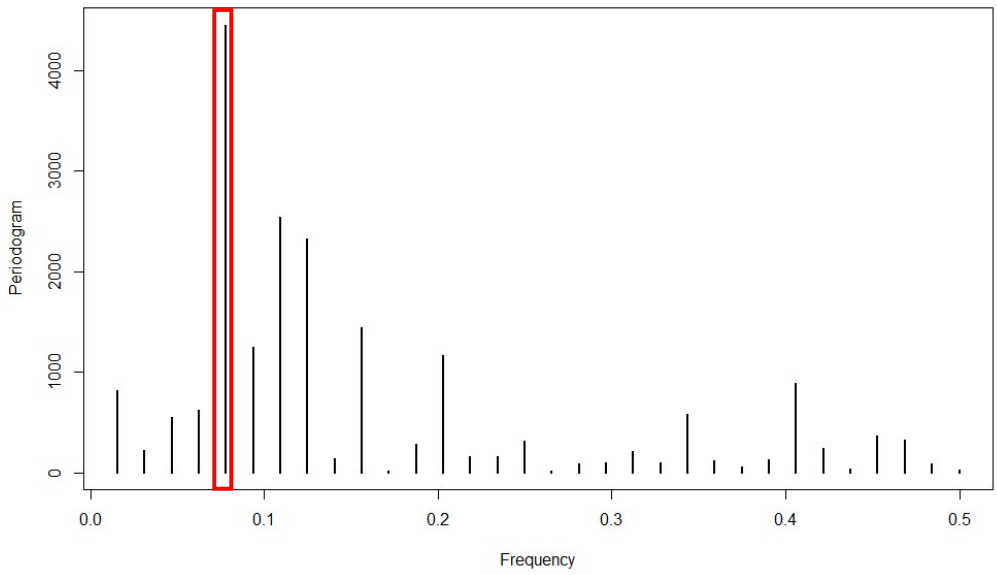

Figure 14. The FFT for the WAIS Divide snow pit samples covering the years 2008 to 2013. Units on the Periodogram axis are $[(\mu g\ kg^{-1})^2]/f$, and units of frequency are in cycles per month. The red box indicates a signal with a period of 12.8 months.

that at very low perchlorate concentrations, either measurement noise is occluding the seasonal signal due to small magnitude of the seasonal signal, or indeed the seasonal component is nonexistent. To the effect of signal magnitude on whether seasonality is detectable, and to evaluate the seasonal variation of the perchlorate concentration of the time series in detail, time-domain time series decomposition is used.

3.3.2 Time Series Decomposition of the Summit Perchlorate Record

Three time periods were selected for this analysis: 1980 to 2007, 1967 to 1979, and 1916 to 1925. The first two intervals were selected based upon analysis of the spectral power density from each period, representing two periods with vastly different spectral power in the 0.083 cycles/month band. The interval from 1916 to 1925 was selected because it was not influenced by volcanic activity or any other large

perturbations, and it represented a time long before atmospheric chlorine concentrations were influenced by anthropogenic chlorine emission.

In Figure 15, a prominent annual signal is seen, which is superimposed upon a relatively stable level of background noise, and on a trend clearly showing the effect of the 1991 eruption of Mt. Pinatubo. Also reflected in the trend is the effect of the rise and decline of anthropogenic chlorine emission (Cole-Dai *et al.*, 2018) in this time period. The decomposed seasonal signal for perchlorate is from -1.12 ppt from the trend in January, to +0.96 ppt in August. This equates to inducing a change from the trend of 2.08 ppt peak to peak, a quite strong variation. For this time period, the mean concentration in August is about 3.2 ppt, while in January through March is consistently about 1.8 ppt (Figure 15). However, the absolute lowest measurements are made in January, and while the mean concentration in July and August is similar, concentrations in August can regularly exceed any observed in July. The average perchlorate concentration for these years is 2.76 ppt, so the relative magnitude of variance in the seasonal signal is -40.6% to +34.8% of the mean for this period.

When considering the seasonality of perchlorate during this time period, it is important to consider the effect of chlorofluorocarbon (CFC) emission. When CFCs reach the stratosphere, they are destroyed via photolysis and ultimately release a chlorine radical. Thus, since perchlorate levels in snow at Summit have been shown to have increased with total chlorine in the atmosphere, the seasonal component must be evaluated against a period of time before increased atmospheric chlorine to determine if CFC emission amplifies the seasonal signal.

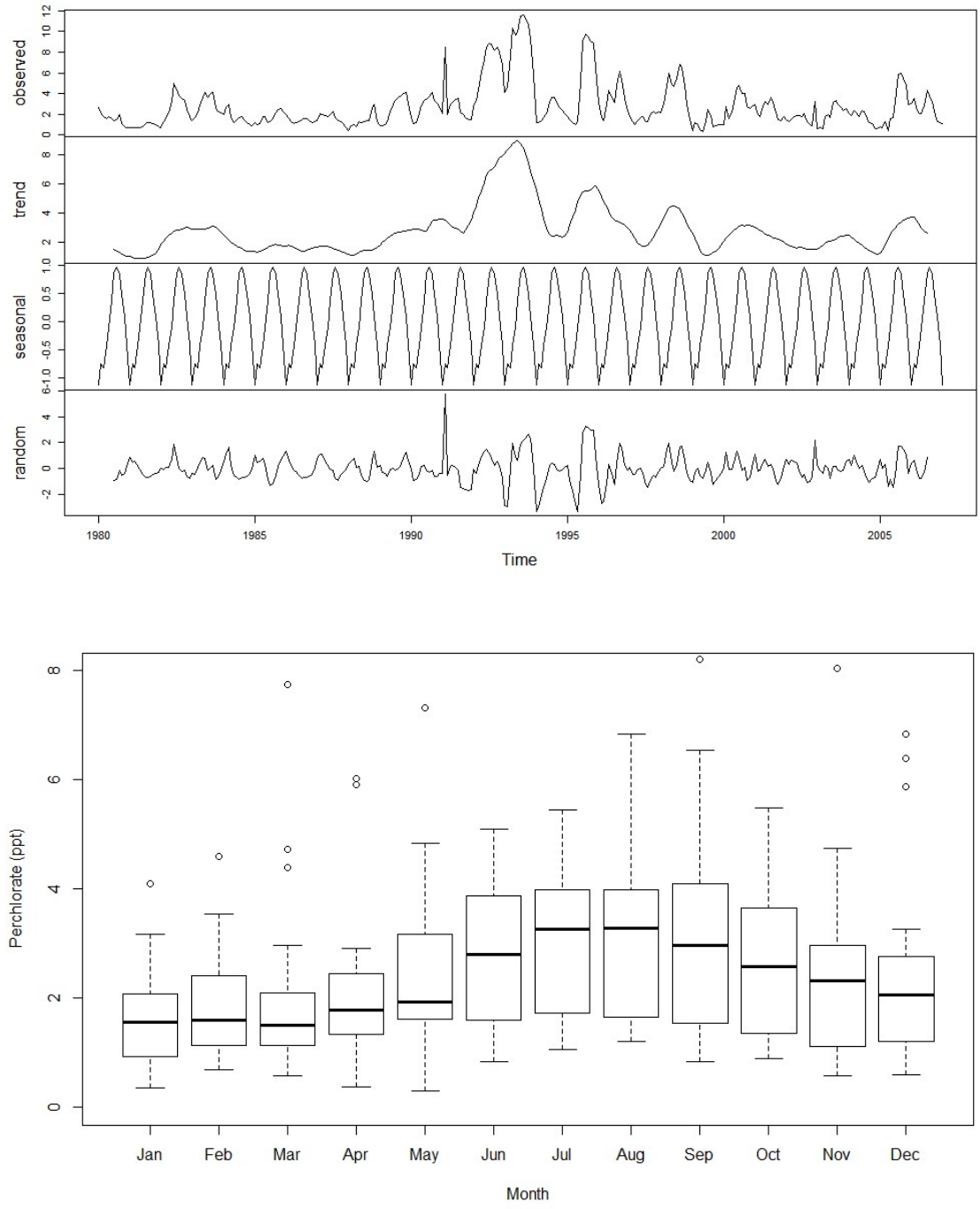

Figure 15. Time series decomposition (top), and plot of monthly concentrations (bottom) for the period 1980 to 2007 in the SM07C2 core. The decomposition depicts the observed signal, trend, seasonal component, and noise.

The years 1967-1979 displayed a very weak seasonal signal, depicted in Figure 16, a period when CFC use first became widespread. It is immediately seen that the magnitude of the seasonal signal is much lower, only -0.15 ppt in January, with a high of +0.20 ppt in September, or 0.35 ppt peak to peak, than the seasonality observed in the period from 1980 to 2007. In addition, the monthly mean concentrations are much more consistent and very close to the average perchlorate concentration for these years of 0.76 ppt. This yields a relative magnitude for the seasonal variance from the mean of between -19.7% and 26.3%, about half that observed from 1980 to 2007.

Finally, the period, 1916 through 1925, that was not impacted by either volcanic eruptions or organic chlorine emission was selected for time series analysis. The time series decomposition is shown in Figure 17. Clearly, no seasonal signal is present, even though the average concentration of perchlorate is not significantly different from that in the period 1967-1979 (p-value = 0.9268). Accordingly, in the boxplot for this period, no large variation between the monthly means is seen, indicating that in this period perchlorate production was not constrained by a mechanism reliant upon photolysis

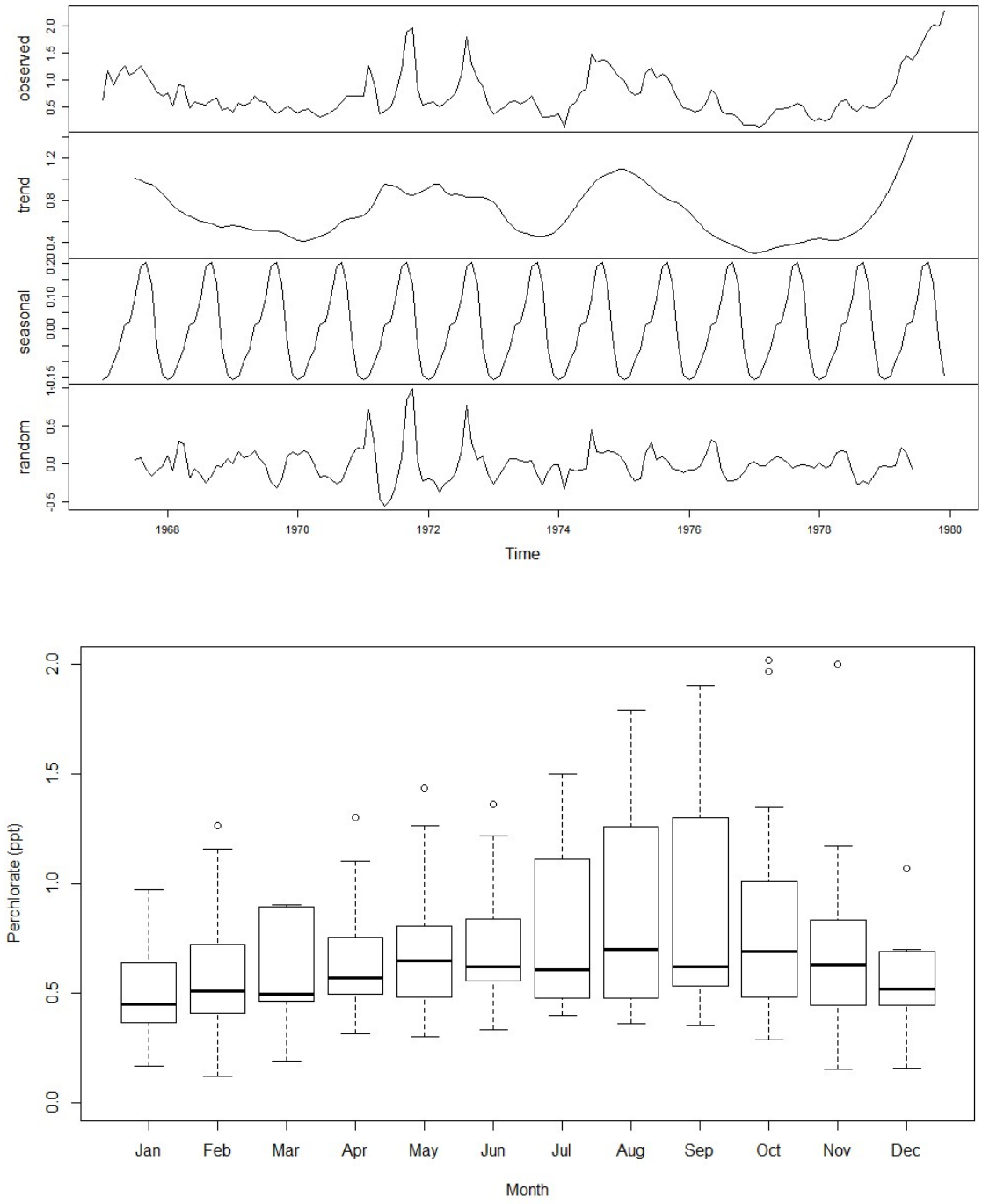

Figure 16. Time series decomposition (top), and plot of monthly concentrations (bottom) for the period 1967 to 1979 in the SM07C2 core.

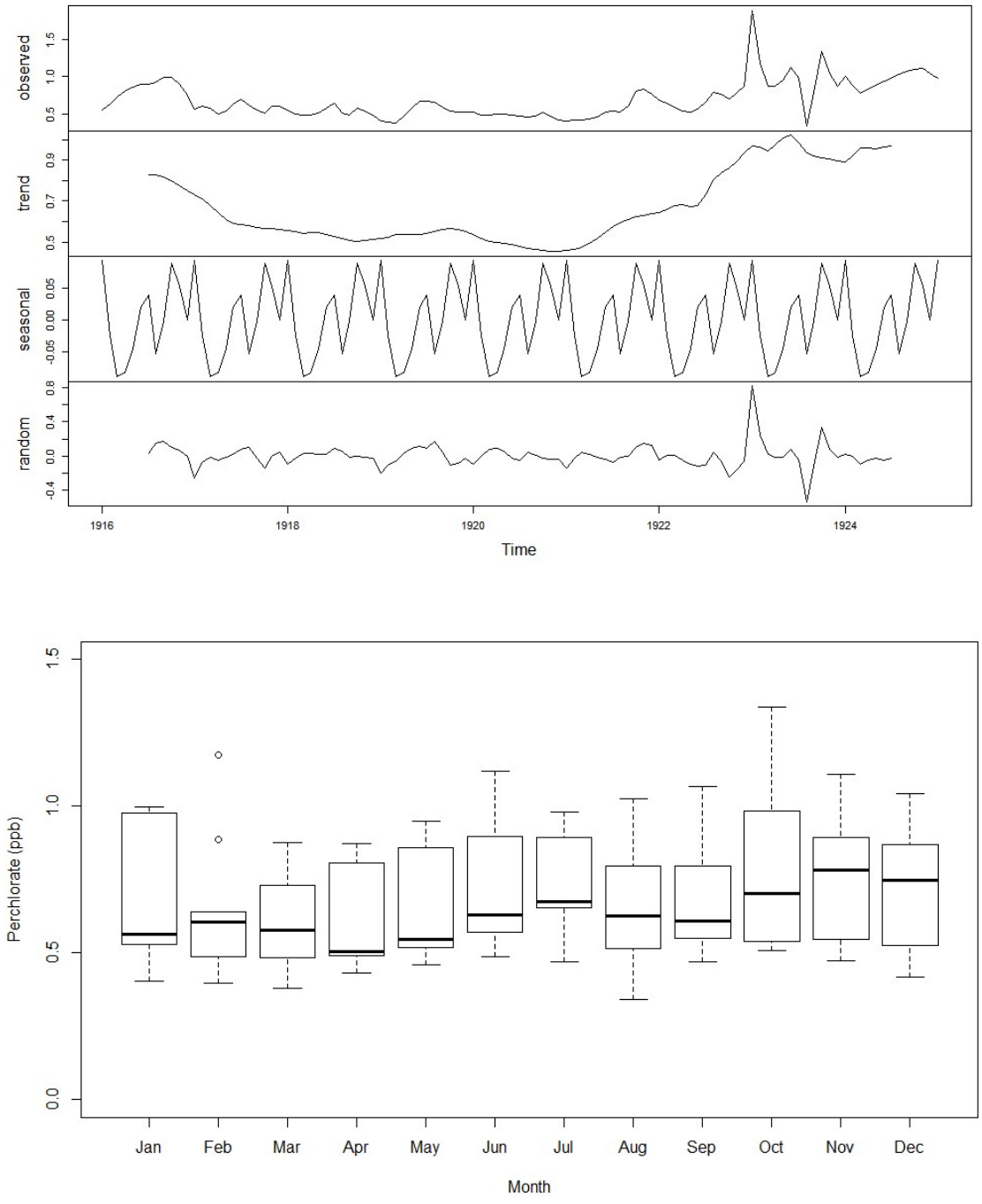

Figure 17. Time series decomposition (top), and plot of monthly concentrations (bottom) for the period 1916 to 1925 in the SM07C2 core.

After imputation and time series decomposition, the *sarima* function in R, which generates an autoregressive integrated moving average (ARIMA model) allows forecasting. The R script for forecasting as used here is shown in Appendix D. Taking the period from 1980 to 2007, the forecast perchlorate signal in snow for Summit, Greenland is displayed in Figure 18. While samples could now be collected to cover this period, the model predicts that seasonality will continue to be a dominant factor in perchlorate deposition in snow deposited after 2007, when the core was collected.

The time series analyses for these three time periods support the conclusion (Cole-Dai *et al.*, 2018) that the emission of CFCs has played a role in atmospheric perchlorate production in recent decades. The increase in seasonal signal magnitude in

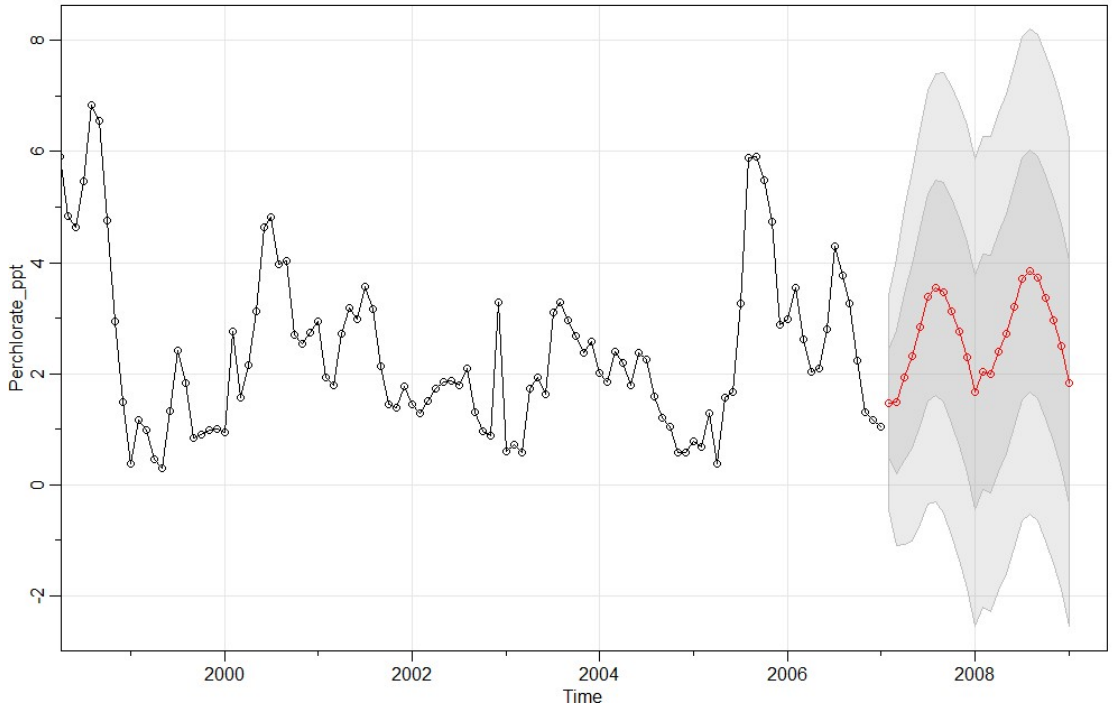

Figure 18. Forecasting prediction for perchlorate at Summit for the years 2008 and 2009, with +/- 1σ and 2σ prediction bands in dark and light gray, respectively.

polar regions in 1980 is indicative of a relative increase in photolytic production. However, a critical piece of the CFC/ozone relationship must be resolved, since perchlorate in snow appears to be at its maximum in the late summer, when it has been repeatedly observed that ozone destruction rates peak in the early spring. This is addressed in the following section.

3.4 Relationship to Ozone

Stratospheric chlorine is directly linked to ozone and can affect its abundance. Mario Molina, Sherwood Roland, and Paul Crutzen demonstrated the impact that the oxidizing power of ozone and the reactive potential of chlorine radicals can have upon chemical processes in the stratosphere. As shown in the sections and figures above, both ozone and chlorine radicals are an integral part of stratospheric perchlorate formation, so here the link is investigated in detail.

3.4.1 Sub Annual Relationship

If indeed ozone and active chlorine are critical to perchlorate formation, a predictable seasonal change should exist based upon current understanding of the seasonality of ozone abundance and chlorine activation. The seasonality of perchlorate has been mentioned in recent work (Furdui and Tomassini, 2010; Jiang *et al.*, 2016; Crawford *et al.*, 2017), and some early attempts at interpreting the seasonality with respect to ozone have been made (Peterson, 2016). However, conflicting conclusions have been reached, where the work of Furdui and Tomassini contrasted with other research in terms of seasonal variation of perchlorate. While they observed seasonal

variation in the Arctic, measurements of perchlorate at several North American sites found no such annual variation (Rao *et al.*, 2012).

In the work of Furdui and Tomassini (2010), a relatively strong correlation (R^2 = 0.6153) between total column ozone and levels of perchlorate in snow was found; however, at WAIS Divide in Antarctica, perchlorate appeared to reach its maximum concentration in the autumn, when ozone levels were still low and recovering from large losses during the spring (Jiang *et al.*, 2016; Peterson, 2016; Crawford *et al.*, 2017). It should be noted, that only in the case of the work of Furdui and Tomassini was a correlation analysis conducted. All of these analyses though, treat the perchlorate concentration in snow as contemporaneous with real-time ozone measurements.

The transfer of a chemical from the stratosphere to the surface through scavenging or sedimentation does not occur instantly, and to perform a correlation analysis with such an assumption is quite problematic. Through comparison of optical aerosol measurements and sulfate analysis of well dated ice samples, it was shown that the sulfate formed after volcanic eruptions of Mt. Pinatubo and Cerro Hudson may have taken several months to reach the surface from the stratosphere (Cole-Dai *et al.*, 1997). In addition, ^{10}Be measurements in a more recent work revealed that stratospheric aerosol has a residence time of between 103 and 205 days, or between about 3 and 7 months before descending to the troposphere (Długosz-Lisiecka and Bem, 2012). While many variables can affect the movement of particles from the stratosphere to the troposphere, it is clear that the assumption that perchlorate measurements at the surface are contemporaneous with ozone measurements should not be considered valid.

However, this type of correlation does serve as an initial starting point for evaluating the relationship between perchlorate and ozone. A program of weekly monitoring of ozone was started in 2005 at Summit Station in Greenland (NOAA; Frith *et al.*, 2012). The measurements of total column ozone taken there are shown along with perchlorate concentrations in the well-dated SM07C2 core in Figure 19. Though only 2 years of the ice core overlaps with the ozone measurements, some useful conclusions can be made regarding timing.

By far, most ozone resides in the lower stratosphere. In the year 2005, ozone reaches its maximum concentration of about 400 DU in spring, April-May, whereas the maxima in the perchlorate concentration (≈ 6 ppt) occurs in the autumn, in about September, which is consistent with the analysis of seasonality conducted above. In 2006, the ozone maxima (≈ 450 DU) occurs in March, and the Perchlorate maxima (≈ 4 ppt) that year occurs in summer, around July or August. In each case, there is about 5-6 months in

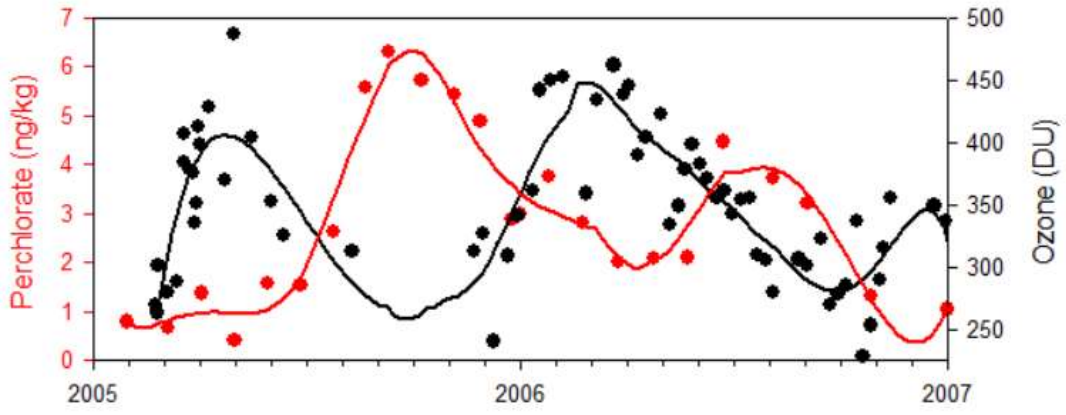

Figure 19. Ozone sonde measurements (black circles) made at Summit Station and ice-core perchlorate concentrations (red circles). Data treated with LOESS smoothing (red and black lines).

between the relative maxima of ozone and perchlorate, within the window for stratospheric aerosol residence times discussed above. Second, and more importantly, the wintertime ozone levels coming out of 2005 appear generally lower than those in the winter of 2005-6. The perchlorate levels are higher in 2005 and 2006, suggesting that there may be an underlying common link, though the assumption that perchlorate concentration and ozone abundance are directly related in terms of cause and effect must not be made. The air-snow transfer of perchlorate is not well understood, though, making a sub annual analysis difficult. Examination of annual data gives a way to expand this analysis without the confounding effect of air to snow transfer. Since annual totals and averages are used, an extrapolation made possible so long as the transfer of perchlorate to snow is less than a year.

3.4.2 Annual Relationship

To evaluate the relationship between perchlorate and ozone on an annual timescale, the annual perchlorate deposition flux was calculated; and annual zonal mean total ozone (ZMO) abundance from 35-65° N wad calculated from the NASA Solar Backscatter Ultraviolet (SBUV) Merged Ozone Dataset (McPeters *et al.*, 2013) for the years 1980 to 2007. The plots are shown in Figure 20 as a function of time. It should be noted that the ozone scale is inverted to better investigate the correlation. A scatterplot of ZMO vs perchlorate flux for the same period is shown in Figure 21.

The slight lack of fit in 1982 (Figure 20) is the result of high ZMO abundance, and very high perchlorate flux for that year. It is plausible that this is the result of unusual perturbation by the eruption of either Mt. St. Helens in 1980 or El Chichon in 1982, or

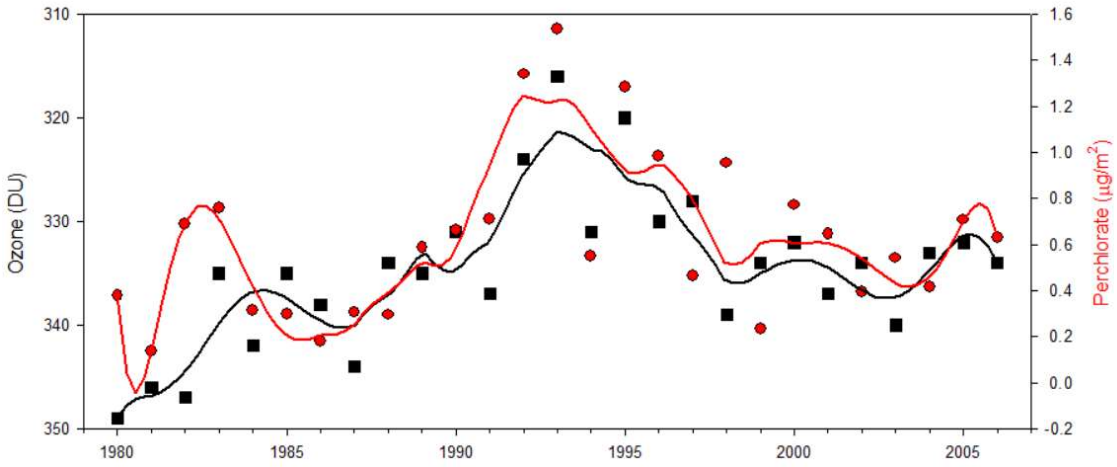

Figure 20. Zonal mean total ozone from 35-65°N (black squares), and perchlorate flux (red circles) from the SM07C2 ice core. Data are fitted (solid curves) with a LOESS algorithm.

both. Such a scenario could possibly be expected of a large release of chlorine to the upper troposphere, where interaction with ozone was limited, but long-range dispersion may still be possible. At this time, however, that line of reasoning is only speculation.

Regardless, the negative correlation between ZMO and perchlorate flux over the 27-year period is quite good (R^2 = 0.4785). This is in direct contrast to the findings by Furdui and Tomassini (2010), where a positive correlation was found between ozone and perchlorate. First, the question must be asked if a positive or negative correlation may be expected. As shown earlier, the link between ozone and perchlorate in the stratosphere is through chlorine radicals. As the abundance of chlorine radicals increases and begin to catalytically destroy ozone, ozone abundance decreases, and given the excess of ozone relative to chlorine an increase in perchlorate is expected. With the ozone concentration in the stratosphere being vastly greater than the abundance of chlorine, much less chlorine radicals, ozone abundance is likely not a limiting reagent in

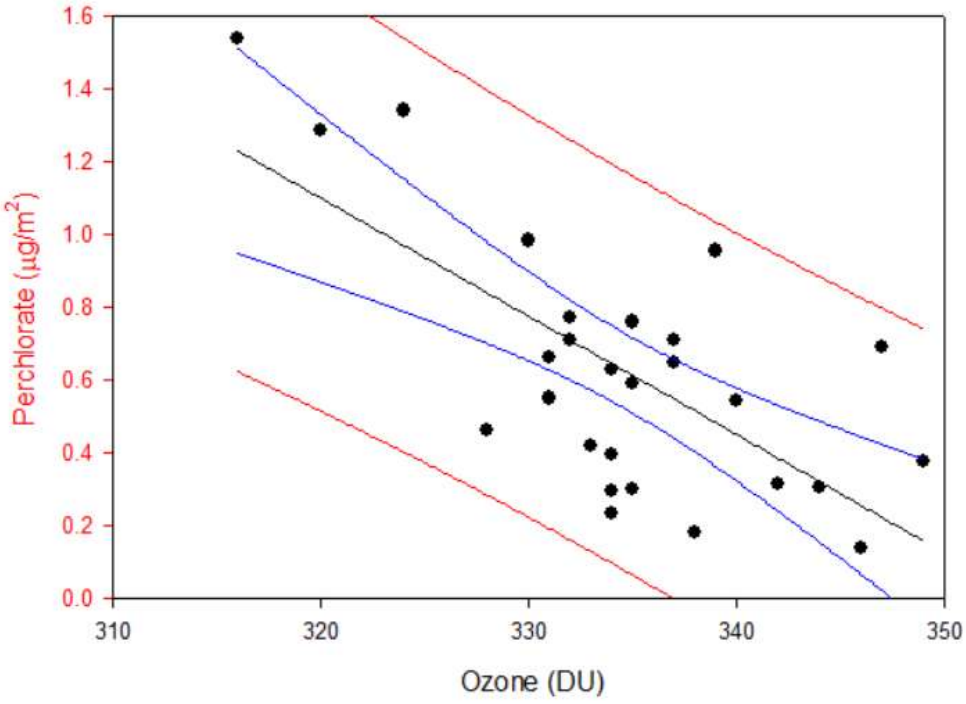

Figure 21. Annual zonal mean total ozone from 35-65°N and annual perchlorate flux from the SM07C2 ice core. The regression (black line), prediction interval (blue line), and 95% confidence interval (red line) are shown.

the formation of perchlorate. One explanation put forth by Furdui and Tomassini for the positive correlation observed in their work may be that an important source of perchlorate is in the troposphere. The coastal location of their study sites may subject those locations to a larger contribution of chloride from sea salt aerosol relative to central Greenland, leading to increased tropospheric production from a chloride precursor.

As mentioned earlier, it has been noted that chloride may be oxidized into perchlorate without transitioning through a chlorine or chlorine monoxide radical. In addition, the background level of perchlorate observed by Furdui and Tomassini is much higher ($\bar{x}_{perch\ .} = 5.5 \pm 3.9$ ppt) than that at Summit ($\bar{x}_{perc\ \ .} = 1.2 \pm 1.2$ ppt),

indicating that there is a difference in the magnitude or number of sources. The latitudes of the Furdui and Tomassini study sites are not significantly different than the latitude of Summit Station, and the initial assumption made here is that the stratospheric deposition of perchlorate should be consistent zonally across the Arctic.

A plausible hypothesis could be formed here where ozone is a limiting reactant in perchlorate production in the troposphere at those locations, whereas the location of Summit, far from the coast, is isolated from a sea-salt chloride perchlorate source (i.e., a tropospheric source) , thus sea salt chloride is the limiting reagent for tropospheric production. While the authors agree that a positive correlation between ozone and perchlorate can only be possible if ozone is a limiting reagent, they state that this must happen at stratospheric altitudes. However, the abundance of ozone in the stratosphere, even during the lowest periods is still several orders of magnitude greater than the abundance of chloride or chlorine radicals, whereas in the upper troposphere, the abundance of organic chlorine and chloride far exceeds that of ozone. The hypothesis seeking to explain the positive correlation between perchlorate and ozone in their works neglects to address those relative abundances and the rather strong seasonal variation in ozone at altitudes between 5 and 10 km, which decreased by about 80% at 10 km in their dataset during the year 2004. At these extremely low ozone levels, it is conceivable that ozone may be a limiting factor in perchlorate production via oxidation of chloride in a region with high levels of sea-salt aerosol.

Furdui and Tomassini state that there is a small amount of perchlorate that is not produced from chloride, but rather must stem from a chlorine radical precursor. In that

work, it was determined that if the perchlorate generated from a chloride precursor is excluded, there should be about 1.0 ppt in snow remaining that is generated via a chlorine radical precursor, extremely close to that observed during nonvolcanic periods prior to the 1970s at Summit. These factors support several conclusions: that the bulk of perchlorate deposited at Summit is stratospheric in nature, and that the negative correlation of perchlorate with ozone observed at Summit on an annual scale and the positive correlation observed in the Furdui and Tomassini work on a sub annual scale are not mutually exclusive. The implications are that the correlation of ozone and perchlorate conveys a great deal of information regarding formation pathway and layer of the atmosphere where the bulk of the generation is occurring.

4.0 Response of Perchlorate to Volcanic Eruptions

Increased perchlorate levels in 1996 were noted in an ice core collected from Devon Ice Cap in Canada by Furdui and Tomassini (2010). The researchers suspected that volcanic eruptions such as the 1991 eruption of Pinatubo would enhance perchlorate production based upon speculation by others (Jaeglé *et al.*, 1996), but no conclusive evidence could be found since that ice core only dated as far back as 1996. Later, a link between volcanic eruptions are perchlorate formation was again proposed (Rao *et al.*, 2012) in an analysis of perchlorate in wet deposition from sites across North America, but conclusive evidence was still not found.

Another investigation into volcanic perchlorate was published by Furdui et al. (2017). Here, the relationships between perchlorate, chloride, and sulfate were investigated to determine the contribution of volcanic activity to perchlorate production relative to nonvolcanic periods. However, no conclusions were reached from their chemical analysis on how or to what extent volcanic activity perturbs perchlorate production. In that work, aerosol depth was also investigated because it is a direct response to volcanic emission, but it was concluded that stratospheric volcanic aerosol had little effect on perchlorate levels observed at Agassiz Ice Cap (80°30’N, 075°00’W).

Other recent work, however, has found clear evidence of a perchlorate response to some large eruptions (Peterson, 2016; Cole-Dai *et al.*, 2018). Peterson only identified a few eruptions, with no particularly large perchlorate response. Several volcanic eruptions were identified by Cole-Dai et al. (2018) through an increase in volcanic sulfate

where the snow also had an increased concentration of perchlorate. Cole-Dai et al. (2018) examined more eruptions, found perchlorate response to several eruptions, and identified a very large volcanic perchlorate signal. It was also found in the 300-year perchlorate record that only large eruptions with stratospheric impact have a perchlorate response.

However, the only perchlorate response to volcanic eruptions at this time has only observed at Summit; so, whether this phenomenon could be found at other sampling locations, including the Southern Hemisphere, remained unclear. In addition, detailed features of the perchlorate response, which may preserve some aspects of the atmospheric chemistry of perchlorate formation, has never been conducted.

4.1 Observation of Volcanic Perchlorate Signals

The phenomenon of a perchlorate response to some large volcanic eruptions could not be readily extended globally, or considered a general response to eruptions, based upon the sparse suite of measurements made on the Summit, Greenland ice cores. Additional analyses were needed to confirm that volcanic impact on perchlorate production is a large-scale (hemispheric and/or global) atmospheric phenomenon. To verify that the perchlorate response to some eruptions was not confined locally to Greenland, a section of core from Denali, Alaska dated to around the 1912 eruption of Katmai (details about and discussion on Katmai are presented later in this work) was analyzed. This section of ice indeed contained high concentrations of perchlorate co-deposited with the volcanic sulfate from that eruption (discussed later in more detail,

Figure 32), consistent with those observed at Summit. Indeed, the magnitude of the perchlorate signal was even larger than the response seen at Summit, but the background levels of perchlorate were also higher than at Summit, similar to the background levels observed at other sites near the coast and at other North American sites (Rajagopalan *et al.*, 2009; Furdui and Tomassini, 2010; Rao *et al.*, 2012; Furdui *et al.*, 2017). This finding confirms that this phenomenon is probably across the Northern Hemisphere, not restricted to Greenland.

Evidence that the perchlorate response could be observed in the Southern Hemisphere was needed to confirm that perchlorate would respond to an eruption globally. Two short sections from the Antarctic SPC14 core were dated by synchronizing continuous ECM measurements to the WAIS Divide ECM record (Winski *et al.*, 2019). The sulfate deposition of three large eruptions (Tambora, a widely-known but unattributed event in the early 19th century, and the suspected eruption of Kuwae in the 15th century)

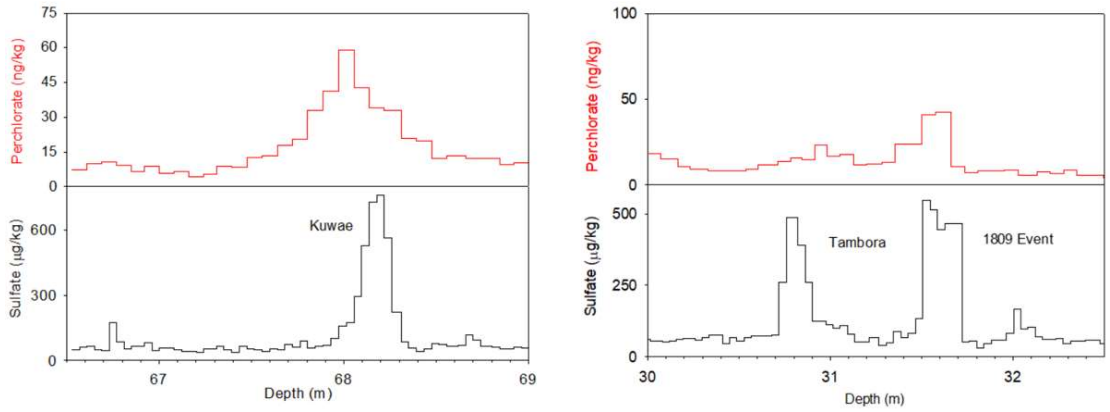

Figure 22. Volcanic sulfate signals (black, bottom), and perchlorate responses (red, top) of the suspected eruption of Kuwae (left), and of Tambora and the 1809 Unidentified Event (right) in the SPICE Core.

was identified in the two sections, and perchlorate measurements were made for the same samples.

Strong perchlorate responses were observed in concert with the sulfate response for all three of these eruptions (Figure 22), indeed verifying that the perchlorate response could be extended to the Southern Hemisphere. The list of eruptions analyzed for this study producing a perchlorate response are shown in Table 2.

Table 2. Table of volcanic eruptions where a clear perchlorate response was identified.

Ice Core	Sample Location	Year	Volcano
SM07	Summit, Greenland	1991	Pinatubo[1]
SM07	Summit, Greenland	1982	El Chichon[1]
SM07	Summit, Greenland	1912	Katmai[1]
SM07	Summit, Greenland	1883	Krakatoa[1]
SM07	Summit, Greenland	1835	Cosigüina[1]
SM07	Summit, Greenland	1831	Babuyan Claro[1]
SM07	Summit, Greenland	1815	Tambora[1]
SM07	Summit, Greenland	1601	Huaynaputina[2]
DIC	Denali, AK, USA	1912	Katmai[2]
SPC14	South Pole, Antarctica	1815	Tambora[2]
SPC14	South Pole, Antarctica	1809	Unknown[2]
SPC14	South Pole, Antarctica	1453	Kuwae[2]

[1]Cole-Dai, et al., 2018
[2]This work

The fact that the perchlorate response to volcanic eruptions has been found in ice cores from both the Arctic and Antarctica demonstrates that volcanic impact on perchlorate production is global. The volcanic eruptions in Table 2 are large enough to inject material into the stratosphere. In the SM07 core, two known Icelandic eruptions were investigated that showed a well-defined sulfate signal, those of the 1728 CE

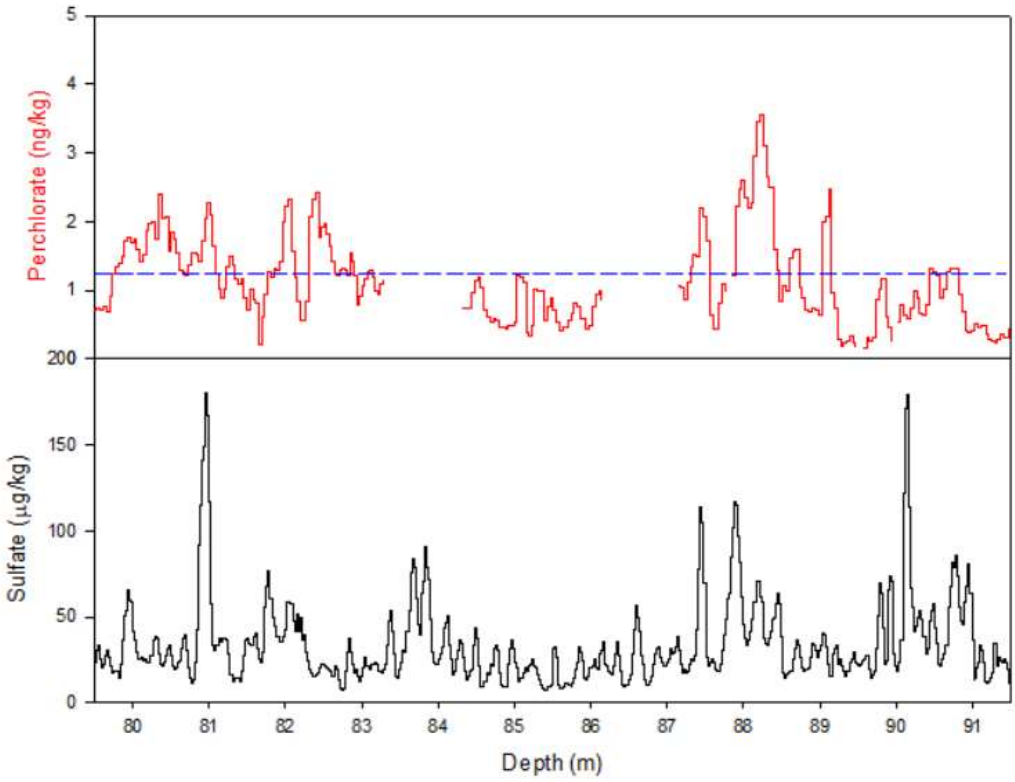

Figure 23. The sulfate (bottom, black), and perchlorate (top, red) concentrations measured in SM07 for Öraefajökull (1728 CE, 90.2 meters), and Hekla (1768 CE, 80.9 meters). The mean perchlorate concentration is shown as a horizontal blue line.

eruption of Öraefajökull, and the 1768 CE eruption of Hekla (Global Volcanism Program, Smithsonian Institution).

While both very large (VEI 4), these eruptions were not thought to have injected material into the stratosphere (Global Volcanism Program, Smithsonian Institution). The sulfate and perchlorate concentrations for these eruptions are shown in Figure 23. In Figure 23, the blue line indicates the mean perchlorate concentration, and it is seen that at no point does the perchlorate concentration exceed even one standard deviation in perchlorate concentration (± 1.2 ppt) for this period, indicating that neither of these

eruptions produced a detectable perchlorate response. This suggests that large eruptions without stratospheric injection do not elicit a perchlorate response.

4.2 Magnitude of Perchlorate Response to Katmai and Huaynaputina

Here, the perchlorate responses in the SM07C4 core to the June 6, 1912 eruption of Novarupta (Katmai) and a second eruption of similar magnitude, the 1600 eruption of Huaynaputina, are examined in detail. Though Novarupta is the geological name of the volcano, due to its proximity and formation of a caldera on neighboring Mt. Katmai the volcano is colloquially referred to as Katmai and will be referred to as such in this work. Both of these massive eruptions are from stratovolcanoes located in continental volcanic arcs, where an oceanic plate is being subducted by continental crust and were of similar explosive magnitude in the Volcanic Explosivity Index (VEI), VEI 6. Katmai lies at the base of the Alaskan Peninsula, about 300 miles southwest of Anchorage, AK (Figure 24). The eruption occurred about 10.5 km from the summit of Mt. Katmai, where the magma chamber was actually located. During the eruption, emptying of the Katmai magma chamber through a series of interconnected sills and vents caused the summit of Katmai to collapse, leaving a 600 m deep, 12 km^2 caldera (Brantley, 1996). The eruption of Katmai emitted an estimated rhyolitic/dacitic magma volume of 13 km^3 over three eruptive phases in a span of only 60 hours, and produced a plume reaching a modeled altitude of up to 26 km, well above the tropopause (Fierstein and Hildreth, 1992; Hildreth *et al.*, 2003).

Huaynaputina is located in the Central Volcanic Zone of the Andes in southern Peru (Figure 24), one of three igneous provinces in South America arising from subduction of the Nazca Plate. The eruption took place in three phases between February 19 and March 6, 1600 and is the largest historic eruption known in South America (Global Volcanism Program, Smithsonian Institution). It contributed to the coldest Northern

Figure 24. Map of the Western Hemisphere depicting the relative locations of Katmai, Denali, Huaynaputina, and Summit, Greenland.

Hemisphere summers in 600 years, comparable to the climate impact of the 1815 eruption of Tambora. Tambora, in what is now Indonesia, was the largest volcanic eruption in recorded history (Adams *et al.*, 2001). Models of the climate impact indicate that the eruption altered the Atlantic meridional overturning current, increased Arctic sea ice extent for several years, and strengthened Little Ice Age climate conditions (Slawinska and Robock, 2018). Unlike Katmai, severe human impacts followed the eruption, including disease, widespread famine, flooding, and the complete burial of several villages by ash (Adams *et al.*, 2001; Finizola *et al.*, 2017). It erupted an estimated volume of 11 km^3 chiefly dacitic magma, with an estimated 85% ejected during the 20-hour long first phase (Adams *et al.*, 2001). The plume height during the Plinian phase of the Huaynaputina eruption reached an estimated altitude of 27-35 km (Thouret *et al.*, 2002), deep into the stratosphere, similar to Katmai.

To evaluate the magnitude of a chemical signal in ice cores, an appropriate background must be established. The background represents the concentration measured in snow, or the flux of a species being deposited, that is the result of processes unrelated to that which causes an unusual signal response. In the case of sulfate, the marine emissions of sulfur-containing products which are oxidized to sulfuric acid comprise the source of sulfate in polar snow and ice during non-volcanic time periods. This amount varies throughout the year, with the largest concentration occurring during times of high marine productivity, in the late spring and summer. For perchlorate, the background is usually very low, and for most of the record shows no seasonal change. The response or signal associated with an event such as a volcanic eruption is then

superimposed upon this background; thus, to evaluate the magnitude of the chemical signal for a volcanic event, an appropriate threshold above which the chemical concentration or deposition is no longer attributable to the background, must be calculated or estimated. Background levels of both sulfate and perchlorate will be discussed in the appropriate sections below, in the context of the signals for the investigated volcanic eruptions.

Typical nonvolcanic sulfate concentrations for the early 20th century lie in the range of 50 to 75 µg kg^{-1}, whereas the peak sulfate concentration for the eruption of Katmai reaches 440.6 µg kg^{-1} around October of 1912 (Figure 25). A second sulfate peak of 343.9 µg kg^{-1} appears about June 1913. At around these depths, we detected a very large perchlorate signal in the ice core. Background levels of perchlorate at Summit, Greenland have been shown to be about 1.2 ng kg^{-1} before the late 20th Century, and

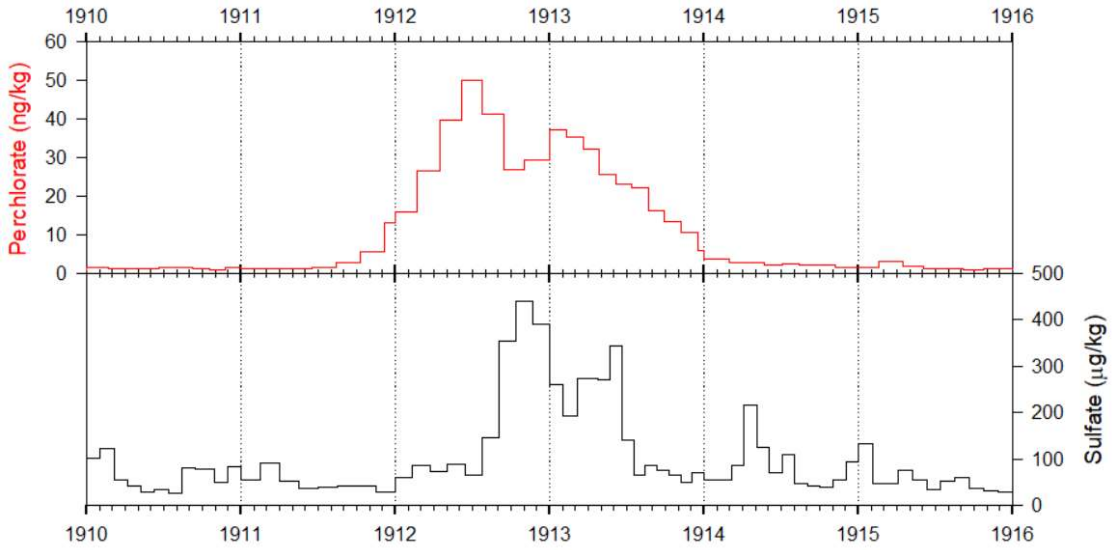

Figure 25. Perchlorate response (top, red) and volcanic sulfate (bottom, black) deposition recorded at Summit, Greenland to the eruption of Katmai in 1912.

stable throughout several hundred years (Cole-Dai *et al.*, 2018). For the eruption of Katmai, perchlorate levels reach a maximum of 50.0 ng kg^{-1} in late June 1912, with a second peak (37.1 ng kg^{-1}) in about January of 1913. The period of elevated perchlorate for this eruption is about 2 years in length. Without anthropogenic influence, or that of volcanic eruptions, the distribution of the perchlorate background flux is not quite lognormal, so here the flux attributed to volcanic eruptions is calculated by summing that portion of perchlorate flux during the event above the mean plus two standard deviations for 1916-1930, a period with an unperturbed background. For Katmai, the perchlorate flux deposited at Summit and attributed to influence from the eruption is 12.9 g km^{-2}, or about 7.2 g km^{-2} yr^{-1} for the duration of the signal.

The peak sulfate concentration for the Huaynaputina eruption is 367.5 µg kg^{-1} in about January of 1602, and a second smaller peak (304.4 µg kg^{-1}) appears earlier, in March

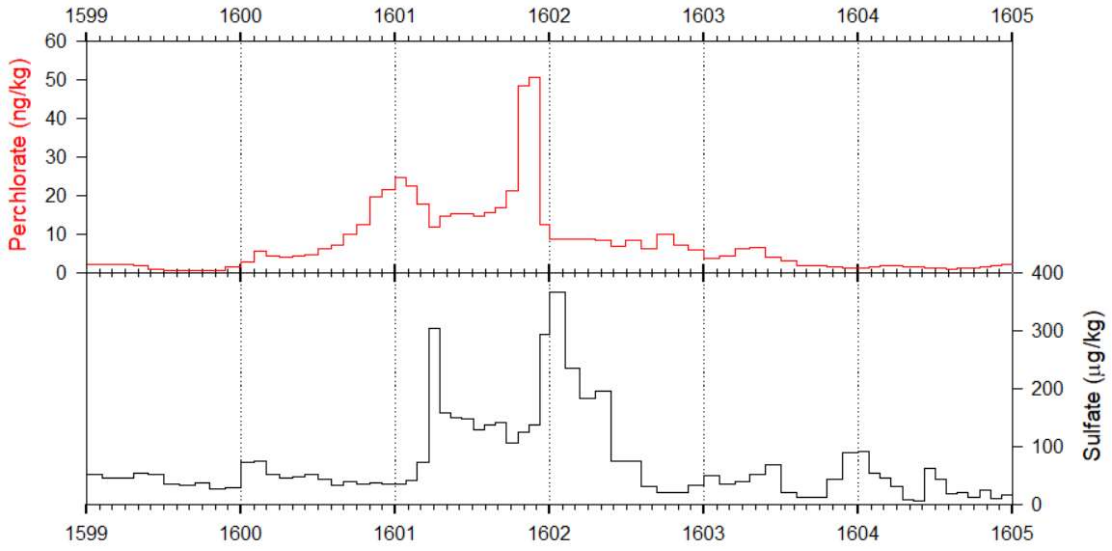

Figure 26. Perchlorate response (top, red) and volcanic sulfate (bottom, black) deposition recorded at Summit, Greenland to the eruption of Huaynaputina in 1600.

1601 (Figure 26). As with Katmai, typical background sulfate concentrations comprise a range of about 50 to 75 μg kg^{-1}. A period of high of perchlorate concentration was also encountered around this volcanic signal and there are two perchlorate maxima. The first maximum occurs in January 1601 and reaches a concentration of 24.7 ng kg^{-1}, and the second occurs in November 1601, reaching 50.6 ng kg^{-1}. Here, the period of perchlorate deposition higher than the background level is almost 4 years. Flux for Huaynaputina is calculated in the same manner as for Katmai using the years 1604-1607 as a background. For this eruption, the total perchlorate flux attributed to the eruption is about 8.1 g km^{-2} for the duration of the signal or about 2.3 g km^{-2} yr^{-1}.

The perchlorate flux from these two eruptions is extremely large compared to both that of the typical background levels. For instance, the flux of perchlorate from 1980 to 2007 is 16.8 g km^{-2}, and averages about 0.6 g km^{-2} yr^{-1} from all sources (Cole-Dai *et al.*, 2018). From 1916 to 1980, the perchlorate flux is much lower, 10.9 g km^{-2}, or <0.2 g km^{-2} yr^{-1}. The chlorine atom in perchlorate may be contributed either from a chlorine species present in the stratosphere prior to the eruption or emitted from the eruption. In either case, however, perchlorate deposited after these two eruptions may represent a large sink for chlorine in the Arctic atmosphere during volcanic eruptions, supporting earlier hypotheses (Simonaitis and Heicklen, 1975; Jaeglé *et al.*, 1996).

If significant HCl is injected into the stratosphere, it may be that the large increase in the supply of chlorine-containing source material is helping drive production of perchlorate. Whether the chlorine in perchlorate is injected to the atmosphere from the eruption or removed from existing chlorine reservoirs without additional chlorine

injection is unclear. This amount of perchlorate removed from the stratosphere following a volcanic eruption appears to be inconsistent with historically low pre-anthropogenic stratospheric chlorine levels. The discrepancy suggests that at least some of the chlorine in perchlorate is injected directly from the eruption (Dasgupta *et al.*, 2005).

The quantitative relationship between perchlorate flux and sulfate flux was examined to characterize the relationship between perchlorate production and volcanic aerosol. Since the stratospheric HCl injection from volcanic eruptions can vary easily from almost none to over 10% of gaseous emissions (Cadle, 1975; Textor *et al.*, 2003; Kutterolf *et al.*, 2015), how the perchlorate response is related to the sulfate produced from the eruption may indicate the degree to which perchlorate production is related to stratospheric aerosol versus chlorine emission. The total perchlorate flux was calculated for each of the volcanic events in Table 2, and is shown in Table 3, and the sulfate flux for the same depth interval was also calculated. These results are shown in Figure 27.

Table 3. Volcanic sulfate signals and perchlorate responses for identified eruptions, with total sulfate and perchlorate fluxes for that section of ice.

Ice Core	SO_4^{2-} (kg km^{-2})	ClO_4^- (g km^{-2})	Eruption Year	Volcano
SM07	102.1	6.4	1991	Pinatubo
SM07	252.2	2.1	1982	El Chichon
SM07	101.2	13.9	1912	Katmai
SM07	60.3	3.9	1883	Krakatoa
SM07	45.1	1.6	1835	Cosigüina
SM07	58.0	2.9	1831	Babuyan Claro
SM07	79.5	9.7	1601	Huaynaputina
DIC	178.2	27.2	1912	Katmai
SPC14	60.6	5.3	1815	Tambora
SPC14	71.5	7.3	1809	Unknown
SPC14	137.5	21.6	1458/9	Kuwae

The 1982 eruption of El Chichon in Southern Mexico proved to be a peculiar case and was omitted from the regression (triangle in Figure 27). First, the perchlorate response was not very pronounced. Second, this eruption occurred during a period where the sulfate background was unusually high and variable, at the peak of sulfur dioxide emission to the environment. The fluctuating background can lead to under- or overestimation of both perchlorate and sulfate background levels, resulting in large errors in volcanic flux calculation. With these considerations, the signal of El Chichon is not included in this examination.

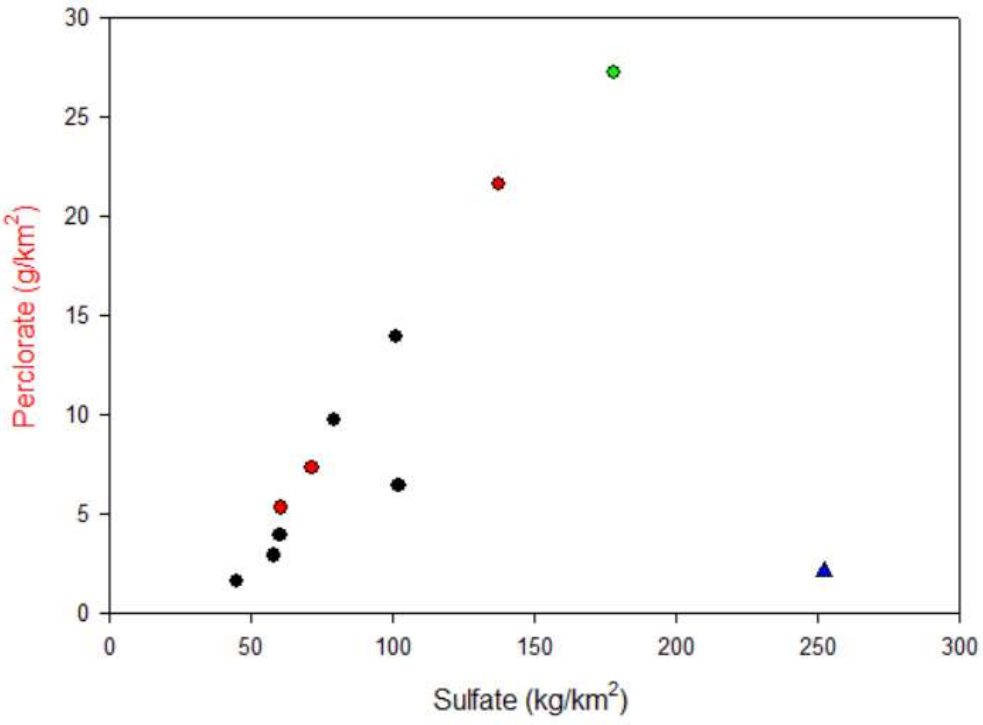

Figure 27. Perchlorate flux plot as a function of sulfate flux for eruptions recorded at Summit, Greenland (black), the South Pole (red), and at Denali, Alaska (green). The 1982 eruption of El Chichon (blue triangle), is not included in the regression.

The correlation between sulfate and perchlorate deposition fluxes is extremely high (R^2 = 0.9231), suggesting that perchlorate formation is strongly related to the presence of sulfuric acid aerosol in the stratosphere. Observations of volcanic gas composition have shown that the relative abundances of HCl and SO_2 vary considerably (Textor *et al.*, 2003; Kutterolf *et al.*, 2015; Carn *et al.*, 2017), and it is assumed that this behavior extends to this suite of eruptions when no direct gas measurements were possible. The correlation between perchlorate and sulfate fluxes exists across volcanoes producing plumes with widely varying chemical composition and in samples collected from wide-ranging locations. This indicates both that the volcanic production of perchlorate is largely independent of volcanic HCl injection into the stratosphere, rather that the dominant formation pathway following these large eruptions is dependent upon increased aerosol abundance.

To compare volcanic correlation to nonvolcanic periods, the annual sulfate and perchlorate fluxes for two periods of nonvolcanic years (1870 to 1840, and 1775 to 1725 CE) were examined for correlation (Figure 28). As seen here, the correlation is low (R^2 = 0.1719) during periods with no volcanic sulfate signals. During nonvolcanic periods, the variance in the perchlorate concentration is high relative to the mean of the signal (1.2 ± 1.2 ng kg^{-1}). The poor correlation during these periods suggest that during periods with low levels of stratospheric aerosol, perchlorate formation in both the troposphere and stratosphere gives rise to the background abundance. Because sulfate during nonvolcanic periods originates from marine emissions of organic sulfur, the non-correlation suggests

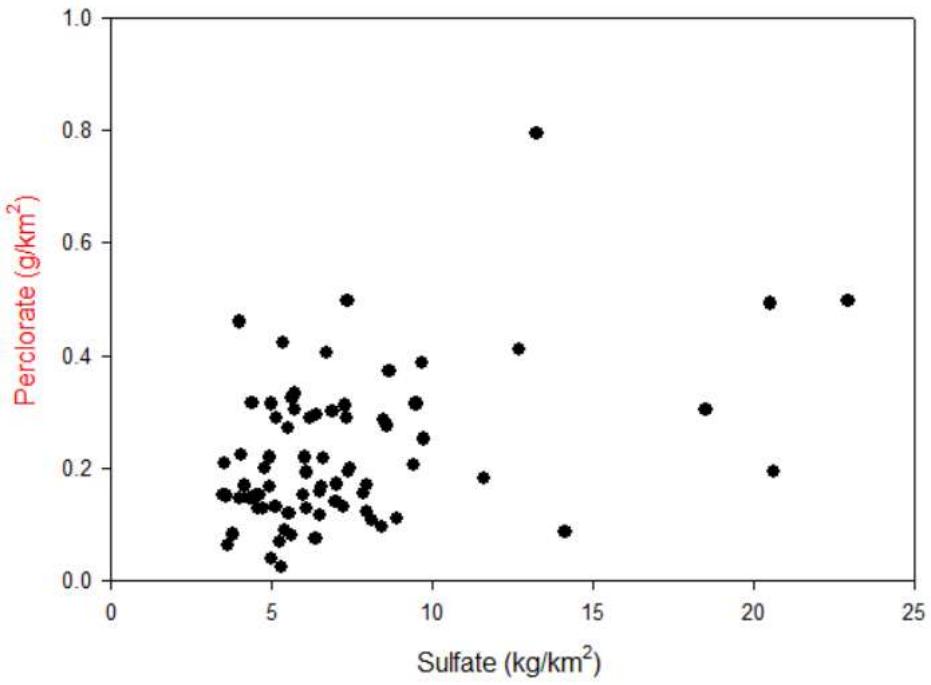

Figure 28. Annual total perchlorate flux plot as a function of annual total sulfate flux for the years 1870-1840 and 1775-1725.

that perchlorate formation is largely independent of variation in marine sulfate input to the atmosphere.

4.3 Perchlorate Response Signal Characteristics

There are two primary differences between the volcanic sulfate and perchlorate signals. First, their timing appears to be slightly different in terms of when the peaks begin to appear in the ice core, and when maxima and minima are reached. Second, the shape of the leading and trailing edges of the perchlorate signals differs significantly from those of the sulfate signal. Since the volcanic sulfate and the ice core perchlorate response are from the same volcanic event, the differences in shape and timing between the two ice core signals are likely due to differences in (1) atmospheric chemistry

(formation from precursors), (2) deposition (removal from atmosphere), and/or (3) signal preservation in snow.

4.3.1 Timing of Perchlorate and Sulfate Concentration Peaks

The sulfate signal from the eruption of Katmai is found in the depth interval of from 38.90 to 38.58 meters in SM07C2, corresponding approximately to the time period of August 1912 to August 1913 (Figure 24). The depth interval of elevated perchlorate concentration is from 39.26 to 37.93 meters, from about October 1911 to May 1915, about 3.5 years. For Huaynaputina, the sulfate signal appears between 122.48 to 122.18 meters in SM07C4, of from about March 1601 to July 1602 (Figure 25). The perchlorate signal associated with this eruption spans from 121.92 to 122.78 meters in depth, or from about February 1600 to August 1603.

If chlorine activation occurs solely from heterogeneous activation of HCl or $ClONO_2$ on sulfuric acid aerosol, perchlorate and sulfate should be co-deposited. The early appearance of the perchlorate peaks, relative to the sulfate peaks, may indicate that perchlorate deposition began earlier than sulfate, suggesting that alternative pathway(s) to chlorine activation and perchlorate production exist. In addition, this difference in peak deposition timing may be due to how efficiently and by what mechanism these species are scavenged from the stratosphere.

One possibility is extremely rapid chlorine activation, immediately after or concurrent with the eruption and independent of sulfate aerosol, which takes some time to form (Cole‐Dai *et al.*, 1997). Uptake of chlorine in sulfuric acid aerosol is favored at

low temperatures and dilute concentrations (Hanson and Ravishankara, 1993; Hanson and Ravishankara, 1994), and it is also possible that the young aerosol is neither cold nor dilute enough to promote extremely rapid chlorine activation. Alternatively, rapid chlorine activation may occur from HCl adsorbed on volcanic ash. The uptake and activation of HCl on the surface of ash has been experimentally shown to favor low temperatures and certain chemical compositions of ash, but can also occur in higher-temperature plume conditions (Zelenski and Taran, 2012; Ayris *et al.*, 2014; Gutiérrez *et al.*, 2016). However, the positive correlation between sulfate and perchlorate deposition fluxes supports that chlorine activation is strongly dependent on the abundance of sulfate aerosol, which suggests that this timing difference must be due to scavenging efficiency and mechanism.

Finally, another possibility for the difference in signal onset timing may be that the transport of impurities was somehow stratified in the atmosphere after the eruption, leading to an offset in timing between the perchlorate and sulfate peaks. The eruption of Katmai consisted of multiple phases; the eruption plume of the initial phase reached as high as 30 km, whereas the later plume height reached only 15-20 km (Palais and Sigurdsson, 1989). This is an important consideration for interpretation of volcanic evidence in ice cores if rapid transport from the eruption location to the sampling site in the upper troposphere occurred, followed by deposition of impurities from the stratosphere some months later. Rapid ash transport near the tropopause coupled with high HCl adsorption may have led to rapid chlorine activation and subsequent perchlorate deposition months before deposition of sulfate from the stratosphere occurred.

While identifications of ash and tephra from specific eruptions are both limited in number, and pose significant uncertainties with regard to the physical processes that led to ash deposition at the sample location (from eruption plume, or remobilization from areas remote from the sample site), ash readily scavenges HF from the atmosphere and leads to a high fluoride to sulfate deposition flux ratio (Óskarsson, 1980). The ash from Katmai was observed over Europe within two weeks of the eruption (Volz, 1975). Indeed, in a core collected from Summit, Greenland, an increase in fluoride was observed to occur shortly before the sulfate signal for Katmai (De Angelis and Legrand, 1994), and it was concluded that the signal characteristics reflected both rapid transport in the upper troposphere, and slower stratospheric transport. Further, this hypothesis is supported by H_2O_2 measurements made at summit, that show rapid transport of SO_2 to Greenland just weeks after the eruption (Laj *et al.*, 1990).

4.3.2 Diffusion of Perchlorate in Ice Cores

In Figures 25 and 26, it can be seen that perchlorate concentration begins to increase from its background before sulfate, and it continues to be elevated after sulfate concentration has returned to baseline levels. In addition, the rates of concentration reduction from the last maxima to baseline levels are not the same for perchlorate and sulfate. This suggests differences in their deposition mechanisms and removal rates from the stratosphere, or diffusion in snow.

While some portion of the elevated perchlorate may begin being deposited before sulfate due to different deposition mechanisms, deposition cannot explain the early onset of elevated perchlorate as observed in SM07C2, or the seemingly long duration of

elevated perchlorate concentration in the eruption records of both Katmai and Huaynaputina. A possible explanation for the shape and broadening of the perchlorate peak may, however, be that diffusion of perchlorate, following deposition, occurs in snow or ice.

Fick's First Law governs diffusion rates, and relates diffusion flux, J, to the diffusion coefficient (or diffusivity), D, concentration (φ) gradient:

$$J = -D\frac{d\varphi}{dx} \tag{E8}$$

Diffusivity then, in terms of unit area per unit time, is the rate at which the concentration gradient changes. In an ice sheet, each layer of snow can be modeled as an infinitely thin plane with a uniform concentration of impurity, where the z-axis is the depth of the layer of snow below the surface. As the layer of snow becomes buried, the concentration of impurities slowly begins to diffuse in a Gaussian manner from layers of high concentration to adjacent layers in the depth direction. In this diffusion model to account for the perchlorate peak shape, the layer of high concentration begins as an infinitely thin center of molecules; over time, diffusion results in a Gaussian peak and the standard deviation increases with time at a rate determined by the diffusivity. Fick's Second Law then relates diffusivity to the relative changes of concentration gradient as a function of distance and time:

$$\frac{\partial\varphi}{\partial t} = D\frac{\partial^2\varphi}{\partial x^2} \tag{E9}$$

Which has the general solution:

$$\varphi(x,t) = \frac{1}{\sqrt{4\pi Dt}} e^{\left(-\frac{x^2}{4Dt}\right)} \quad \text{(E10)}$$

Comparison with the Gaussian distribution,

$$f(x) = \frac{1}{\sigma\sqrt{2\pi}} e^{-\frac{1}{2}\left(\frac{x}{\sigma}\right)^2}$$

yields the substitution:

$$\sigma = \sqrt{2Dt}$$

This provides a method for estimating the effective diffusivity, D_{eff}, from the standard deviation of the Gaussian peak and when the amount of time for diffusion is known (E11), where l is the diffusion length, i.e., standard deviation of the Gaussian curve, and t is the elapsed time (Johnsen, 1977):

$$D_{eff} = \frac{l^2}{2t} \quad \text{(E11)}$$

In an ice core, the diffusion rate or diffusivity is not constant as snow is compacted into ice. Thus, for ice cores, we can assign the square of the overall diffusion length, l, as that part of the signal standard deviation due to effective diffusion.

The observed signal shape of an impurity in ice cores may be caused by other processes than diffusion, such as transport and gradual deposition, as discussed above. To determine the diffusion length, the perchlorate signal must be compared to a reference with known diffusion characteristics. In the case of volcanic signals, sulfate is a convenient reference, since perchlorate and sulfate are generally deposited at the same time (from the same precipitating event, assuming the same transport and deposition

processes for sulfate and perchlorate. The diffusion of sulfate in ice cores has been studied, and is well characterized (Barnes *et al.*, 2003). The proposed diffusion mechanism for sulfate yields little diffusion over the span of one or a few hundred years. Sulfate is non-volatile, undergoes negligible diffusion in the gas phase, and in ice has effective diffusion coefficients (D_{eff}) in the range of between 2.4 x 10^{-8} and 4.7 x 10^{-8} m^2 yr^{-1} (Barnes *et al.*, 2003). For $t = 95$ years (for Katmai) and $D = 4.7 \times 10^{-8}$ m^2 yr^{-1}, the diffusion length of sulfate is only about 3 mm (l^2 = 8.9 x 10^{-6} m^2), if we take the upper limit of the effective diffusion coefficient for sulfate. Since this is a negligible contribution to the overall variance of the sulfate signal, we can assume the peak shape of sulfate in the case of Katmai is entirely due to non-diffusive processes. The sulfate signal is then taken as an undiffused initial condition to evaluate perchlorate diffusion rate and estimate the diffusion coefficient.

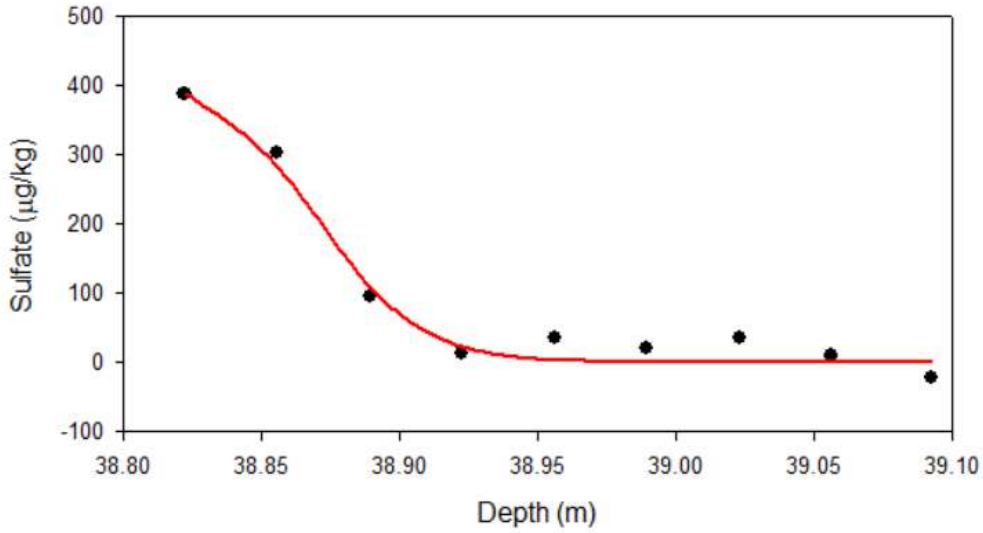

Figure 29. Sulfate measurements (solid black circles) and fitted Gaussian curve (red line) for the eruption of Katmai.

To estimate the diffusive length of perchlorate, the variance of the leading edges of the recorded sulfate and perchlorate signals are compared. A gaussian model is used to construct a shape to fit the data of the leading edge of the peak by minimizing sums of squares. The variance of the sulfate model (i.e., the variance due to non-diffusive processes) may then be subtracted from the variance of the fit to the perchlorate peak to yield that portion of the perchlorate signal due to diffusion. The sulfate signal and fit are shown in Figure 29. For the perchlorate signal, the interval from 38.879 to 39.381 meters was selected for evaluation and is shown in Figure 30 with a gaussian curve fitted.

The variance of the sulfate fit was 1.764 x 10^{-3} m^2 (Figure 29), and that of the perchlorate fit (Figure 30) is 6 x 10^{-3} m^2. Taking the square root of the difference in variances yields a diffusion length of about 6.5 cm (≈ 3.6 months, based upon decimal

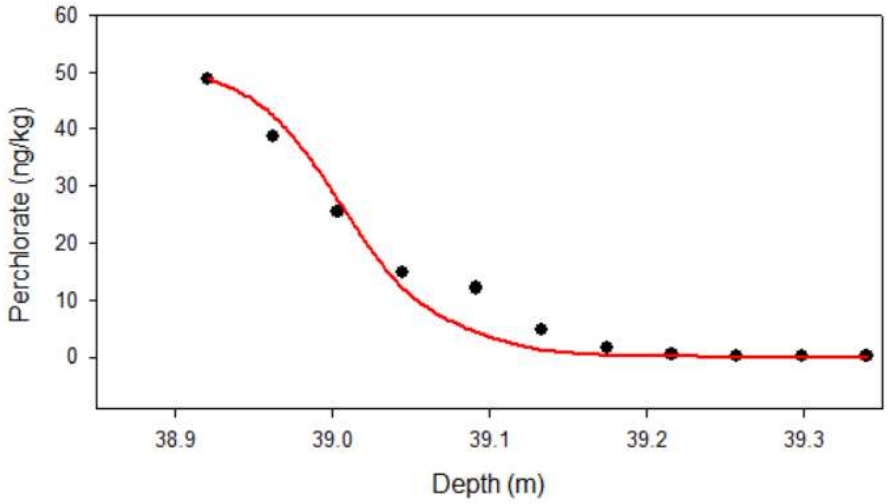

Figure 30. Perchlorate measurements (solid black circles) and fitted Gaussian curve (red line) for the eruption of Katmai.

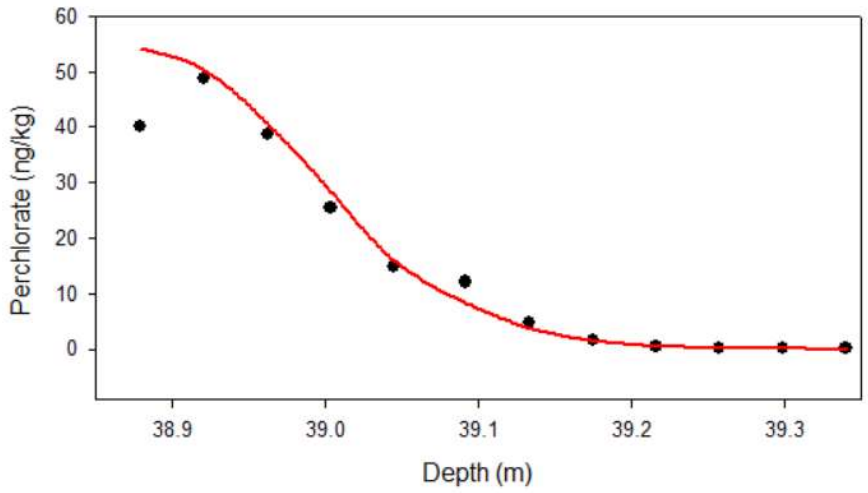

Figure 31. Alternate selection of perchlorate measurements (solid black circles) and fitted Gaussian curve (red line) for the eruption of Katmai.

year calculation as explained in Chapter 2) and an estimated effective diffusion coefficient of 2.2 x 10^{-5} m^2 yr^{-1}. This diffusion length, however, appears too short, so an evaluation of leading edge selection is warranted. Location of the top of the Gaussian function is of critical importance for this method. If the first slight dip of the perchlorate signal is considered to be a low reading due to measurement uncertainty and the peak of the perchlorate signal is selected slightly later, as in Figure 31, the estimated effective diffusivity is 5.4 x 10^{-5} m^2 yr^{-1}, with a diffusion length of 10.1 cm (≈ 5.5 months), a better fit with the observed data for Katmai.

To test the validity of the estimated diffusion coefficient, it is applied to the signal of Huaynaputina, though the low quality symmetry of the peak shape makes any quantitative estimation from it difficult. For Huaynaputina t = 407 years, yielding a perchlorate diffusion length of between 13.4 and 21.0 cm (≈ 7.3 – 11.5 months), generally consistent with the observed breadth of the signal (diffusion length decreases in

proportion to the square root of time). Also, like Katmai, an effective diffusivity towards the high end of the estimate range appears to give the best fit with observations.

If diffusion is only occurring in the firn layer, i.e., no significant diffusion in solid ice or below the pore close-off depth, sampling sites subject to high accumulation rates and higher strain rates experience less diffusion than other locations due to rapid densification (Morris and Wingham, 2014). The signal for the 1910 Katmai eruption in an ice core (Figure 32) collected from Denali, Alaska, was analyzed for major soluble ions including sulfate, and for perchlorate. The signal for the Katmai eruption occurs much deeper in the DIC1 core; about 122 meters in depth, compared to about 39 meters at Summit. In the DIC1 core, no diffusion is seen at the onset of the perchlorate signal.

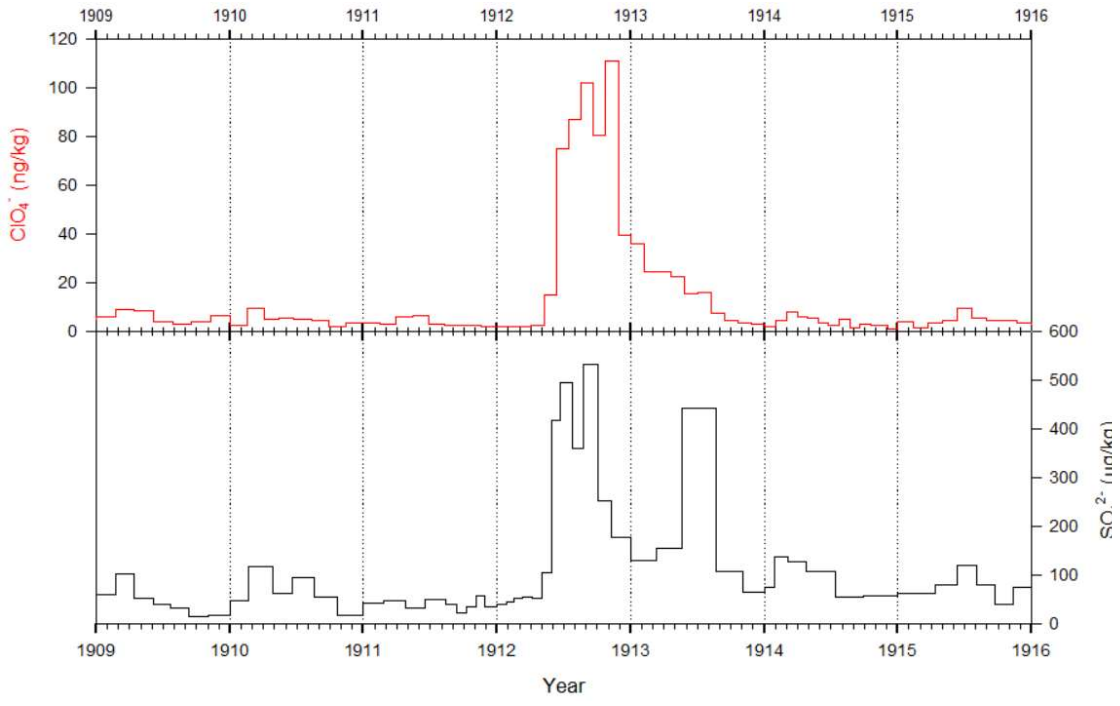

Figure 32. Perchlorate response (top, red) and volcanic sulfate (bottom, black) deposition recorded at Denali, Alaska to the eruption of Katmai in 1912.

Densification of snow into ice creates very different environments for diffusion to take place, from rapid gas phase diffusion in the upper unconsolidated snow, to very slow diffusion in solid ice. The depth at which air bubbles are closed off during densification is the pore close-off depth. Below this depth, gas phase diffusion can no longer occur, as the air bubbles are now closed off from each other.

The signal for Katmai in the SM07 core is still far from pore close-off depth; at 39 meters in depth, the density is still only about 0.69 g cm^{-3} (unpublished data). In DIC1, the density of solid ice (≈ 0.91 g cm^{-3}) is reached at about 75 meters in depth (corresponding to about 38 years of accumulation), whereas at Summit, this depth is at about 120 meters (about 370 years of accumulation). If we apply an effective diffusion constant of 2.2 x 10^{-5} m^2 yr^{-1} to about 38 years of diffusion in the firn at Denali, a diffusion length of only 3.9 cm is expected; this indicates that no diffusion could be observed, since the sample resolution of perchlorate analysis was approximately 4.2 cm per sample. If the effective diffusion coefficient 2.2 x 10^{-5} m^2 yr^{-1} is applied to the DIC1 data for t = 104 (from 2016 to 1912 CE), the diffusion length becomes 6.8 cm. This equates to 1.9 months on the time domain and would indicate that there should only be a 1- or 2-sample lead of increasing perchlorate concentration vs. increasing sulfate concentration.

Similarly, using the upper estimate for perchlorate diffusivity and a 35-year time, the diffusion length would be 6.1 cm. This suggests that the diffusive process slows down with more rapid densification, and that diffusion is occurring predominantly in the firn layer of the ice column. A complicating factor, however, could be the proximity of the DIC1 sampling site with respect to Katmai, which lies only a few hundred kilometers away.

The cause of the large sulfate signal towards the middle of 1913 in the DIC1 core is unexplained and is coincident with a large spike in dust content and nitrate (Osterberg, 2017, personal communication). Interestingly, the profile of perchlorate appears to match closely with that of sulfate in the years following the eruption.

Finally, a major cause for variation in diffusivity is the dependence of D_{eff} upon densification characteristics of the sample site. The effective diffusivity, if taken as an overall metric from the snow surface to the signal depth, comprises a wide range of effects resulting from variations, as the peak depth increases, in vertical strain, density, and temperature, all of which have an effect upon diffusion rate. Applying diffusivity for sulfate derived from a sample site in Antarctica to a site in Greenland carries some uncertainty as to suitability a static initial condition to estimate diffusivity of perchlorate, although this is largely mitigated by the extremely slow diffusion of sulfate in snow. However, in the case of perchlorate, the application of the D_{eff} derived at Summit to other sites must be taken with caution in light of the difference in densification rates between those sites. Nevertheless, these estimates show that the effective diffusivity for perchlorate in snow is on the order of 10^{-5} m^2 yr^{-1}, or 10^{-9} cm^2 s^{-1}, somewhere in the range of diffusivity of liquid to that of solid (Haynes, 2015).

4.4 Perchlorate Formation after Major Volcanic Eruptions

Here, perchlorate formation in the atmosphere perturbed by large and explosive eruptions is explored in the context of stratospheric chlorine chemistry outlined above. The strong correlation between volcanic sulfate and volcanic perchlorate flux indicates

that primary perchlorate formation pathways likely perturbed during these large eruptions involve heterogeneous chlorine activation and possibly reaction of chlorine and bromine radicals. Other pathways experiencing perturbation when volcanic aerosol is present in the stratosphere are gas phase formation from hydrogen chloride with or without a chlorine radical intermediate and gas phase formation from chlorine nitrate. The hypothesis under investigation here is that perchlorate responds so heavily to volcanic eruptions as a result of extremely rapid and widespread chlorine activation. The following sections discuss how volcanic eruptions perturb these pathways, leading to chlorine activation, and to increases in important immediate perchlorate precursors such as chlorine nitrate.

4.4.1 Primary Volcanically Perturbed Pathways

4.4.1.1 Heterogeneous Chlorine Activation

As depicted above, the correlation between perchlorate flux and volcanic sulfate flux indicates a clear connection between perchlorate production rates and sulfate aerosol abundance. This connection indicates that the significant perturbation to primary perchlorate production pathways during a stratospheric volcanic eruption likely arises from heterogeneous chlorine activation, shown in Figure 33, rather than from injection of volcanic HCl. Activation of chlorine on sulfuric acid aerosol is similar to activation in PSCs, where the heterogeneous reaction between HCl and $ClONO_2$ or HOCl on aerosol results in the formation and release of Cl_2 gas. This Cl_2 gas can subsequently be photolyzed to generate chlorine radicals:

Step 1a: $HCl + ClONO_2 \rightarrow HNO_3 + Cl_2$

Step1b: $HCl + HOCl \rightarrow H_2O + Cl_2$

Step 2: $Cl_2 + \hbar\nu \rightarrow 2Cl$

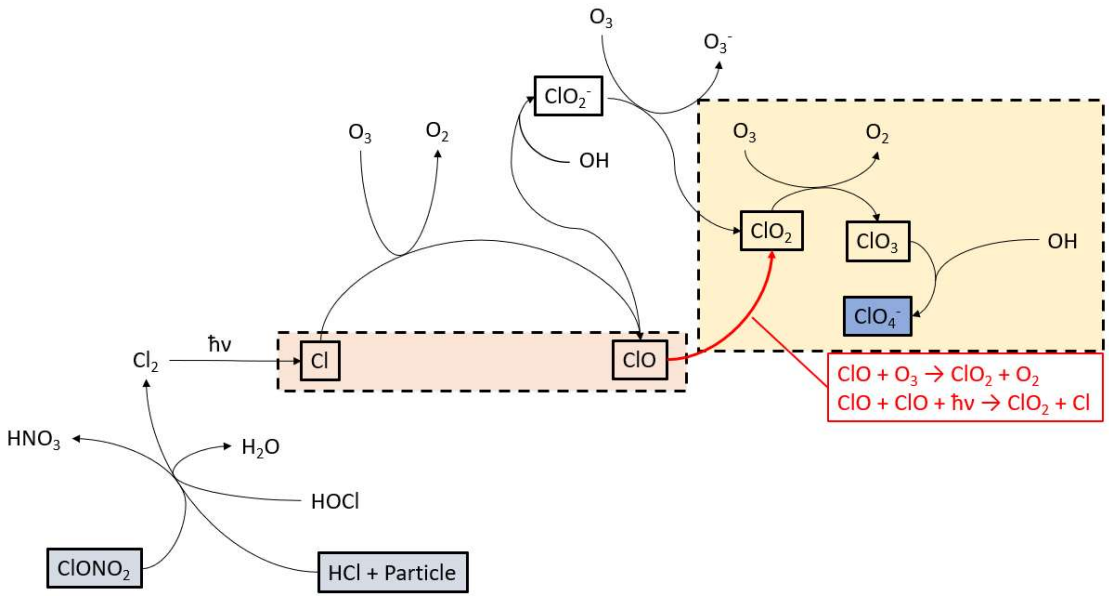

Figure 33. Formation of perchlorate from heterogeneous chlorine activation.

In fact, the heterogeneous chlorine activation on sulfuric acid aerosol surface has been shown to be a significant source of ozone depletion in the few years immediately following eruptions with plumes reaching the stratosphere (Solomon *et al.*, 1993).

The photolytic decomposition of chlorine gas in this formation pathway suggests that seasonality in the perchlorate signal should be observed in samples collected from polar regions. In the case of Katmai, the second perchlorate peak occurs in the boreal winter, as do both peaks for the Huaynaputina volcanic perchlorate response. Time series analysis indicates, however, that peak perchlorate concentrations are typically reached in

the autumn. During non-volcanic years, aerosol abundance is low, and in the Arctic PSCs rarely form, thus chlorine activation occurs slowly. In polar regions, Cl_2 builds up over the winter and is then photolyzed rapidly as soon as the atmosphere is exposed to sunlight again. However, in the spring, PSCs no longer form and the photolytic decay rate of Cl_2 greatly exceeds its formation rate, rapidly and completely depleting the temporary Cl_2 reservoir, explaining the timing of the ozone hole in a non-volcanically perturbed stratosphere.

In the case of a volcanic eruption injecting sulfur to the stratosphere, a different picture emerges. In this case, aerosol density in the stratosphere can be several orders of magnitude above the background level, along with injection of water and ash. Under these conditions, particle surface area is abundant, facilitating widespread chlorine activation which can lead to unusual and unseasonal active chlorine abundances, such as those observed in the Antarctic stratosphere after the eruption of Mt. Pinatubo (Solomon *et al.*, 1993).

4.4.1.2 Bromine Coupled Chlorine Activation

In all of the mechanisms discussed in this work, chlorine dioxide, a key perchlorate precursor, is depicted as a product of the ClO + ClO reaction, or oxidation of ClO by ozone:

$$ClO + ClO + \hbar\nu \rightarrow ClO_2 + Cl$$

$$ClO + O_3 \rightarrow ClO_2 + O_2$$

However, the reaction of BrO with ClO is also thought to be a source of ClO_2 in the stratosphere, and becomes important during large volcanic eruptions, which can emit significant quantities of HBr (von Glasow, 2010):

$$ClO + BrO + \hbar\nu \rightarrow ClO_2 + Br$$

The bromine radical is then rapidly converted to BrO through reaction with ozone. Unlike chlorine, there is no reservoir for bromine in the stratosphere, resulting in higher ozone-destroying efficiency by bromine than chlorine. Important bromine-chlorine coupling reactions are shown in Figure 34. It should be noted, however, that bromine does not activate chlorine, and therefore some other mechanism of chlorine activation must precede ClO_2 formation via BrO.

In the volcanic plume, bromine has only been measured as HBr and as BrO, which is thought to account for the majority of ozone destruction in the plume immediately

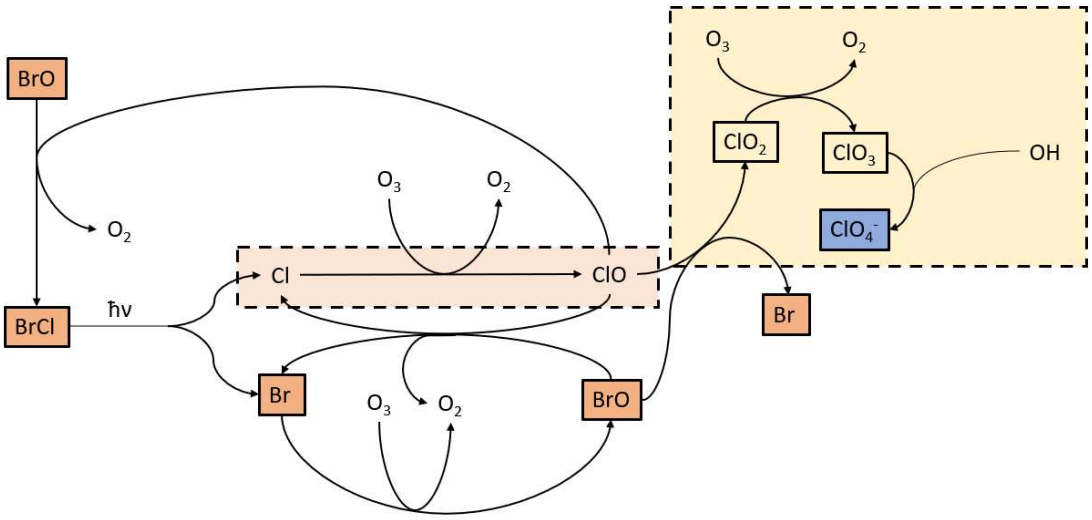

Figure 34. Stratospheric bromine chemistry shown coupled to chlorine activation.

after eruption from the vent and in the following few hours (von Glasow, 2010). Bromine as HBr appears to become rapidly converted to BrO in volcanic plumes, driving chlorine dioxide concentrations to high levels. This mechanism is thought to have been responsible for the high chlorine dioxide levels observed after the eruption of Pinatubo (Solomon *et al.*, 1993). Since high levels of bromine enhance abundance of chlorine dioxide, this leads to speculation that volcanic eruptions featuring large bromine emission may enhance perchlorate production through more extensive and rapid chlorine dioxide formation, but this will not be investigated here.

4.4.2 Other Volcanically Perturbed Pathways

4.4.2.1 Gas Phase Oxidation of HCl

If eruptions emit significant amounts of HCl to the atmosphere, it can be oxidized to perchlorate via the pathways shown in Figure 35. The relative significance of these pathways as contributors to perchlorate after large explosive eruptions is undetermined, however. While volcanic eruptions do emit significant quantities of HCl, little reaches the

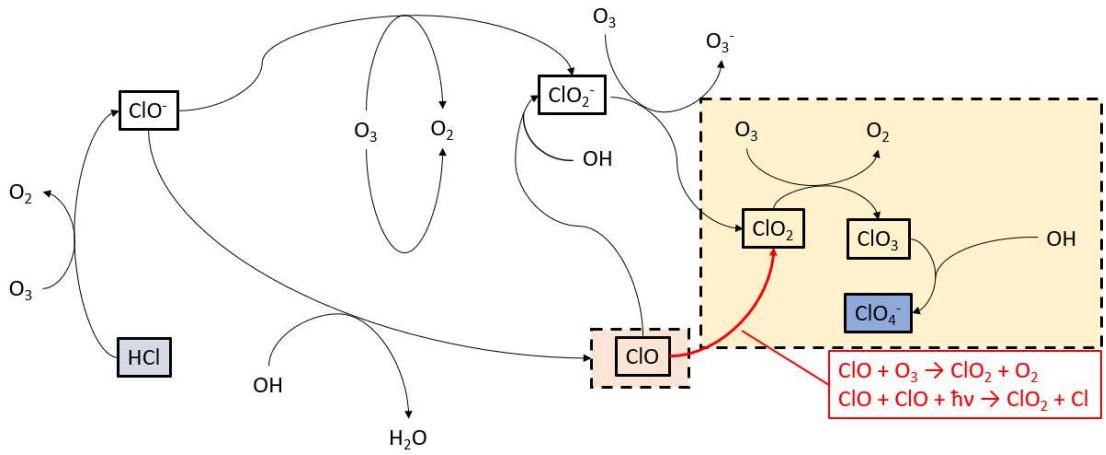

Figure 35. Gas phase formation of perchlorate without a Cl or ClO intermediate.

stratosphere due to washout by condensing water vapor in the rapidly cooling plume during the eruption. While the plume in certain eruptions where reaches stratospheric altitudes, estimates of the amount of HCl that is not washed out and enters the stratosphere vary widely, from almost none to about 10%. In addition, formation via ClO_2^- requires the formation of a rather unusual ozonide (O_3^-) molecule through oxidation by ozone, which to this authors knowledge, has not been measured in the environment:

$$ClO^- + O_3 \rightarrow ClO_2^- + O_2$$

$$ClO_2^- + O_3 \rightarrow ClO_2 + O_3^-$$

However, it should be noted that this pathway does not require aerosol or sunlight (except for indirectly for ozone formation), so may, if valid, proceed both during polar night and in a non-volcanic atmosphere. Such conditions may help explain the discrepancy between this work and Furdui and Tomassini (2010) with respect to ozone/perchlorate correlation. In the troposphere, and particularly locations where chloride concentrations are high and ozone concentrations are low, a positive correlation between ozone and perchlorate and ozone may be expected with pathways such as this. Extensive formation of the perchlorate observed after volcanic eruptions in polar ice via this mechanism, then, would be restricted to cases in which a massive injection of HCl to the stratosphere occurs.

Due to the pronounced seasonality observed at Summit, and the lack of reliance of this mechanism upon a seasonal component such as sunlight, this pathway likely has a relatively small contribution to perchlorate production in the stratosphere. In addition,

the strong negative correlation between ZMO and annual flux (discussed in Chapter 3) of perchlorate indicates strong coupling between ozone and perchlorate, and in this pathway, there is no catalytic ozone loss occurring. Due to the rather large discrepancy between ozone concentration and chlorine concentration, even though 4 molecules of ozone are involved for each molecule of chlorine in this pathway, the ozone loss is negligible, even if 100% of HCl was converted to perchlorate.

Gas-phase mechanisms of chloride oxidation may also involve formation of a Cl radical from HCl as an initial step, as in Figure 36:

$$HCl + OH \rightarrow Cl + H_2O$$

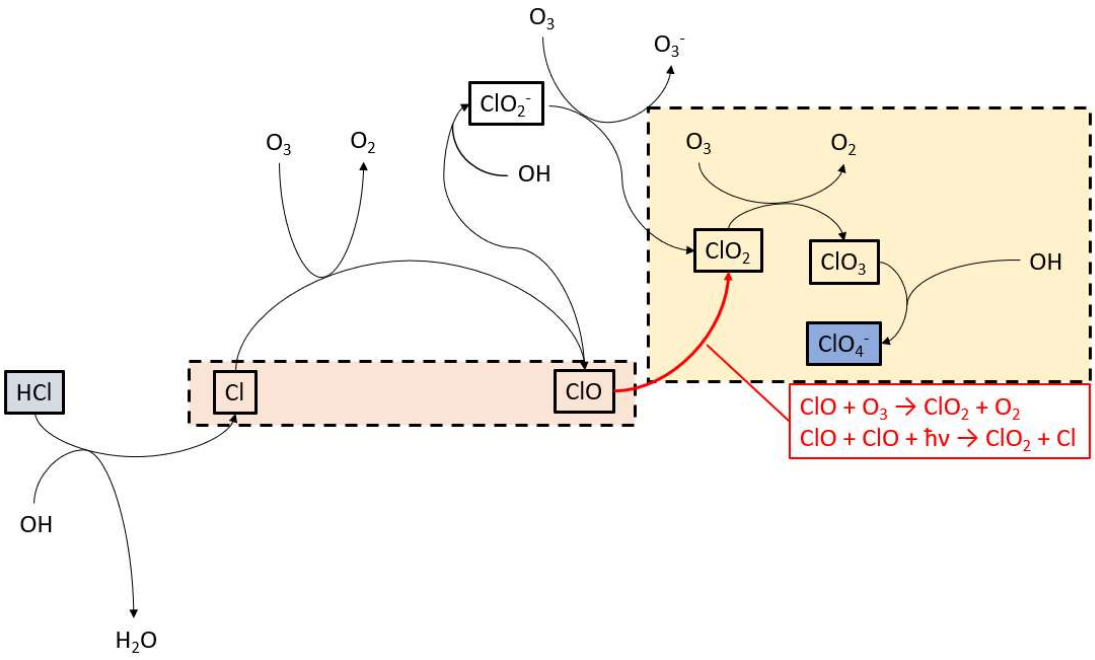

Figure 36. Gas phase formation of perchlorate from oxidation of HCl with Cl or ClO intermediate.

Here, the initial step is attack of HCl by a hydroxyl radical, which generates a chlorine radical that can participate in catalytic ozone destruction. Also, an important factor with this mechanism is that there is a photolytic component, and a non-photolytic component; the conversion of Cl to ClO does not require sunlight, and ClO can proceed to ClO_2^- through reaction with a hydroxyl radical (Hatzinger *et al.*, 2017):

$$ClO + OH \rightarrow ClO_2^- + H^+$$

Typically, the ratio of Cl to OH in the stratosphere is about 10 (Li *et al.*, 2018), with values of about 10^5 molecules cm^{-3} for OH, and 10^4 molecules cm^{-3} for Cl. For comparison, not only are OH concentrations in the troposphere on average an order of magnitude greater than those in the stratosphere, but also display a large variation due to variations in relative strengths of tropospheric sources and sinks (Lelieveld *et al.*, 2016). In volcanic plumes however, OH is thought by some to be rapidly consumed during the conversion of SO_2 to H_2SO_4 and little would be available for formation of Cl (Pinto *et al.*, 1989; von Glasow *et al.*, 2009; von Glasow, 2010), and thought by others to be generated in some conditions (Gerlach, 2004). That OH concentrations are not enhanced, and indeed most likely depleted in the volcanically perturbed atmosphere indicates that activation of HCl to Cl radicals is likely not a significant initial step responsible for perchlorate generation, nor the intermediate reaction of ClO with OH.

However, measurements of OH after the eruptions of Eyjafjallajökull (1728 CE) and Hekla (1768 CE) support that excess OH was not generated (Millard *et al.*, 2006; Rose *et al.*, 2006), but the concentrations of Cl radicals increased; in the case of Eyjafjallajökull,

the tropospheric OH/Cl ratio was about 37 (rather than >100 under quiescent conditions), indicating significant chlorine activation in the plume itself. Such a case opens the door for significant generation of perchlorate by direct generation of Cl or ClO inside the plume, both in the troposphere and the stratosphere, in conjunction with catalytic ozone loss. Also, this pathway may proceed in polar day and night since there is both a photolytic and a non-photolytic pathway between ClO and ClO_2.

4.4.2.2 Chlorine Activation from $ClONO_2$

One pathway to generation of chlorine radicals is the photolysis of chlorine nitrate, shown in Figure 37:

$$ClONO_2 + \hbar\nu \rightarrow ClO + NO_2$$

$$ClONO_2 + \hbar\nu \rightarrow Cl + NO_3$$

and indirectly via Cl_2 in the heterogeneous reaction sequence:

$$\text{Step 1:} \quad ClONO_2 + HCl + M \rightarrow Cl_2 + HNO_3$$

$$\text{Step 2:} \quad Cl_2 + \hbar\nu \rightarrow 2Cl$$

Finally, the following aqueous phase reaction takes place in sulfuric acid aerosol:

$$ClONO_2 + H_2O \rightarrow HOCl + HNO_3$$

where the HOCl is photolyzed to ClO as discussed in Chapter 3.

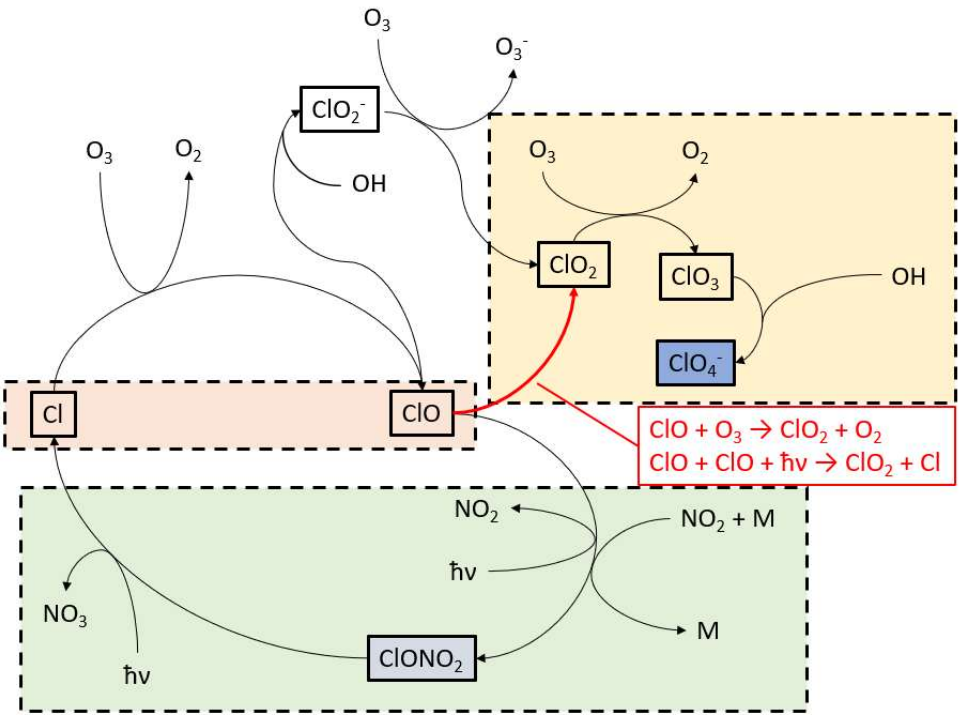

Figure 37. Gas-phase formation of perchlorate from the chlorine nitrate reservoir.

The radical-forming reaction ensembles above exist in a delicate balance with the gas-phase reaction that generates chlorine nitrate and consumes a chlorine radical (deactivation):

$$ClO + NO_2 + M \rightarrow ClONO_2$$

The steady state abundance of chlorine nitrate, then, is a function of the abundance of sunlight, which is required for all radical generating reactions involving chlorine nitrate, and the abundance of NO_2. In conditions of adequate sunlight, the rate of photolysis of chlorine nitrate can exceed the formation rate from NO_2, whereas in conditions of little sunlight, i.e., polar winter, $ClONO_2$ can accumulate, especially in conditions where there are no particles to support heterogeneous reaction with HCl.

In the volcanically perturbed stratosphere, however, all of the pathways involving chlorine nitrate are highly perturbed. In sulfuric acid aerosol, the reaction:

$$N_2O_5 + H_2O + M \rightarrow 2HNO_3$$

proceeds rapidly, due to the large dependence of this reaction to aerosol surface density, inducing denitrification of the stratosphere (Hanson *et al.*, 1994; Borrmann *et al.*, 1997; von Glasow *et al.*, 2009). This in turn limits the NO_2 available for formation of $ClONO_2$. Without sufficient NO_x for chlorine nitrate formation, an important mechanism for removal of ClO from the stratosphere becomes very slow. Following the eruption of Mt. Pinatubo, where very high aerosol surface density was present in the Antarctic stratosphere, very high levels of chlorine dioxide, a critical perchlorate precursor, were observed due to the impact of volcanic aerosol upon chlorine nitrate chemistry (Solomon *et al.*, 1993). Also, of importance is that this mechanism can provide significant chlorine activation at temperatures far too warm (≈ 215K) for the formation of PSCs to form when heterogeneous activation occurs rapidly.

5.0 Conclusions and Future Work

5.1 Conclusions

Ice cores from Greenland, Antarctica, and Alaska were analyzed to investigate the effect of volcanic eruptions on the level of perchlorate in polar snow, the chemistry of perchlorate formation during nonvolcanic periods, and the impact on perchlorate formation chemistry by volcanic eruptions. A perchlorate response was found in both the Arctic and the Antarctic, and in a coastal Alpine glacier in North America. This response was observed in those eruptions occurring both before and during high levels of anthropogenic chlorine in the stratosphere.

Only very large eruptions were found to increase perchlorate deposition, but it was unknown whether additional HCl was injected into the stratosphere after the eruption. It is important to note that for this study, perchlorate response is found for every stratospheric volcanic eruption identified by a sulfate signal. The largest volcanic perchlorate deposition flux (12.9 g km^{-2}) is measured following the eruption of Katmai in 1912.

Careful analysis of the ice core perchlorate data and atmospheric ozone levels lead to a picture where perchlorate formation is driven by chlorine activation. Perchlorate deposition at Summit, Greenland shows significant seasonality, implying at least one major photochemical pathway is present. This seasonality has been enhanced over the last few decades, probably by the increased organic chlorine in the environment. The correlation of mean ozone levels to perchlorate flux on an annual time scale indicates that

both are related to stratospheric chlorine activation, and that the lag of 4-5 months between perchlorate deposition and ozone column concentration at Summit is due to perchlorate transport from the stratosphere to the snow surface. This implies that perchlorate production in the volcanically quiescent stratosphere peaks in the polar spring, likely from photolysis of Cl_2 and/or $ClONO_2$. Some characteristics of the volcanic perchlorate response may be related to seasonal activation patterns, such as timing of peak perchlorate deposition.

During volcanic eruptions emitting large quantities of SO_2 to the stratosphere, a high correlation is seen between perchlorate and sulfate fluxes. This high correlation indicates that sulfate aerosol is the driving factor in perchlorate formation during volcanic eruptions and that perchlorate formation arises from enhanced heterogeneous chlorine activation when the stratosphere is perturbed by high aerosol abundance.

The diffusion of perchlorate in snow was investigated in the perchlorate and sulfate signals of one eruption at two sampling locations of different accumulation rates, and of two eruptions separated by time from the same sampling location. It is found that perchlorate diffusion occurs at an effective rate (diffusion coefficient) of 10^{-5} m^2 yr^{-1}. Diffusion of perchlorate, which happens about 10^3 times faster than sulfate, is still relatively slow compared to diffusion of in aqueous solution and appears to happen in the firn column before densification turns firn into ice.

5.2 Future Work

When perchlorate formation begins is important to understanding the characteristics of the signal in ice cores. If perchlorate formation critically depends upon chlorine activation, then any activation mechanism other than heterogeneous activation (i.e., on sulfate aerosols) should result in enhanced production. Since chlorine activation is known to occur immediately at the vent, and continuously as the plume evolves, perchlorate may begin to be deposited before sulfate (formed gradually), and some evidence suggests that formation of perchlorate in the upper troposphere may be important. Therefore, perchlorate measurement *in situ* in eruption plumes would demonstrate whether heterogenous activation is a dominant pathway. However, logistics of deploying and designing suitable analytical equipment and predicting the location where the equipment must be deployed make this a daunting proposition.

Likewise, measurement of perchlorate in the stratosphere will help determine the lag time between peak perchlorate concentration and the annual ozone minimum. The characterization of air-snow transfer is critical to understanding the timing of perchlorate deposition signal, and how perchlorate is scavenged from the atmosphere. Variations of sulfate and perchlorate concentrations in snow reveal differences in how these two chemicals are removed from the atmosphere; however, without a better understanding of perchlorate air-snow transfer, a comparison of their physical deposition cannot be made.

Post-depositional change of perchlorate concentrations in snow and ice should be investigated further. The diffusion modeling presented here was based upon an analysis of limited data from a small number of samples, as these ice cores were not analyzed to investigate diffusion. Two experiments should be conducted as expansion of those performed here. First, to fully evaluate perchlorate diffusion, a high-resolution measurement of perchlorate and sulfate concentrations in the same samples are needed for the same event in multiple ice core locations. The extremely small sample volumes for the DIC1 core permitted only coarse resolution, and no repeat analyses. Second, more high-quality data need to be obtained on signals in a single core. While the signals for Katmai and Huaynaputina are unusual in their magnitude, that they are observed in a 300-year period indicates that such signals are not exceedingly rare. However, only the signal of Katmai has sufficiently well-preserved features to allow a study of diffusion. Other eruptions with large perchlorate responses should be identified for diffusion examination.

As suggested by Jaegle et al. (1996), the incorporation of perchlorate into stratospheric chlorine chemistry models would serve to satisfy several objectives. First, the propensity and extent to which perchlorate acts as a sink for stratospheric chlorine can be better evaluated. It is unknown how and to what extent the addition of volcanic HCl to the stratosphere affects perchlorate formation, but modelling can help answer if increased perchlorate requires an additional source of chlorine atoms to the stratosphere. In turn, better understanding the role of volcanic HCl can help constrain overall perchlorate formation rates. Also, modelling will help in understanding the

mechanism(s) by which perchlorate is scavenged from the stratosphere, possibly helping to explain some of the differences between features of the sulfate and volcanic perchlorate response.

Appendix A, Visual Basic LOESS Smoothing Macro for Excel

The following VBA code programs an Excel macro that allows selection of 5, 11, and 29 sample window sizes. The code may be altered to any window size of an odd integer by substituting appropriate coefficients.

```
      Sub SG_five()
          '5 Point Savitzky-Golay Smoothing Filter
          'Multiple InputBoxes are used so the macro is self-contained.
          'Note that this is a fixed output calculation and does not
update if input data is changed.
          On Error GoTo NotValidInput
          Dim i As Integer       'counter
          Dim Lrow As Integer    'low cell of data column
          Dim Urow As Integer    'high cell of data column
          Dim Ic As Integer      'column NUMBER for input data
          Dim Cnum As Integer    'column NUMBER for output
          Ic = InputBox("Enter column NUMBER of input data (A=1, B=2
etc.)")
          Lrow = InputBox("Enter row number of first data cell.")
          Urow = InputBox("Enter row number of last data cell.")
          Cnum = InputBox("Enter column NUMBER for output (A=1, B=2
etc.).")
          '5 point S-G coefficients are -3, 12, 17, 12, -3 and the divisor
is 35
          For i = (Lrow + 2) To (Urow - 2)
               Cells(i, Cnum).Value = (-3 * Cells(i - 2, Ic).Value + 12
* Cells(i - 1, Ic).Value _
                                      + 17 * Cells(i, Ic).Value + 12 *
Cells(i + 1, Ic).Value - 3 * Cells(i + 2, Ic).Value) / 35
          Next i
          Exit Sub
      NotValidInput:
          MsgBox ("Non valid entry- terminating.")

      End Sub

      Sub SG_eleven()
          '11 Point Savitzky-Golay Smoothing Filter
          'Multiple InputBoxes are used so the macro is self-contained.
          'Note that this is a fixed output calculation and does not
update if input data is changed.
          On Error GoTo NotValidInput
          Dim i As Integer       'counter
          Dim Lrow As Integer    'lower cell of data column
          Dim Urow As Integer    'uppper cell of data column
          Dim Ic As Integer      'column NUMBER for input data
          Dim Cnum As Integer    'column number for output
          Ic = InputBox("Enter column NUMBER of input data (A=1, B=2
etc.)")
          Lrow = InputBox("Enter row number of first data cell.")
          Urow = InputBox("Enter row number of last data cell.")
```

```
          Cnum = InputBox("Enter column NUMBER for output (A=1, B=2
etc.).")
          For i = (Lrow + 5) To (Urow - 5)
               Cells(i, Cnum).Value = (-36 * Cells(i - 5, Ic).Value + 9
* Cells(i - 4, Ic).Value + 44 * Cells(i - 3, Ic).Value + 69 * Cells(i -
2, Ic).Value _
                                       + 84 * Cells(i - 1, Ic).Value + 89
* Cells(i, Ic).Value + 84 * Cells(i + 1, Ic).Value + 69 * Cells(i + 2,
Ic).Value _
                                        + 44 * Cells(i + 3, Ic).Value + 9
* Cells(i + 4, Ic).Value - 36 * Cells(i + 5, Ic).Value) / 429
          Next i
          Exit Sub
      NotValidInput:
          MsgBox ("Non valid entry- terminating.")

      End Sub

      Sub SG_twentynine()
          '29 Point Savitzky-Golay Smoothing Filter
          'Multiple InputBoxes are used so the macro is self-contained.
          'Note that this is a fixed output calculation and does not
update if input data is changed.
          On Error GoTo NotValidInput
          Dim i As Integer       'counter
          Dim Lrow As Integer    'lower cell of data column
          Dim Urow As Integer    'uppper cell of data column
          Dim Ic As Integer      'column NUMBER for input data
          Dim Cnum As Integer    'column NUMBER for output data
          Ic = InputBox("Enter column NUMBER of input data (A=1, B=2
etc.)")
          Lrow = InputBox("Enter row number of first data cell.")
          Urow = InputBox("Enter row number of last data cell.")
          Cnum = InputBox("Enter column NUMBER for output data (A=1, B=2
etc.)")
          For i = (Lrow + 14) To (Urow - 14)
               Cells(i, Cnum).Value = (-351 * Cells(i - 14, Ic).Value -
216 * Cells(i - 13, Ic).Value + -91 * Cells(i - 12, Ic).Value _
                                        + 24 * Cells(i - 11, Ic).Value +
129 * Cells(i - 10, Ic).Value + 224 * Cells(i - 9, Ic).Value _
                                       + 309 * Cells(i - 8, Ic).Value +
384 * Cells(i - 7, Ic).Value + 449 * Cells(i - 6, Ic).Value _
                                       + 504 * Cells(i - 5, Ic).Value +
549 * Cells(i - 4, Ic).Value + 584 * Cells(i - 3, Ic).Value _
                                       + 609 * Cells(i - 2, Ic).Value +
624 * Cells(i - 1, Ic).Value + 629 * Cells(i, Ic).Value _
                                       + 624 * Cells(i + 1, Ic).Value +
609 * Cells(i + 2, Ic).Value + 584 * Cells(i + 3, Ic).Value _
                                       + 549 * Cells(i + 4, Ic).Value +
504 * Cells(i + 5, Ic).Value + 449 * Cells(i + 6, Ic).Value _
                                       + 384 * Cells(i + 7, Ic).Value +
309 * Cells(i + 8, Ic).Value + 224 * Cells(i + 9, Ic).Value _
                                       + 129 * Cells(i + 10, Ic).Value +
24 * Cells(i + 11, Ic).Value - 91 * Cells(i + 12, Ic).Value _
                                       - 216 * Cells(i + 13, Ic).Value -
351 * Cells(i + 14, Ic).Value) / 8091
          Next i
          Exit Sub
      NotValidInput:
          MsgBox ("Non valid entry- terminating.")

      End Sub
```

Appendix B, Fast Fourier Transform Script for R

```
# load file path and file
setwd("file path")
my.data <- read.table(file="file_name.csv",sep=",")

library(TSA)
p = periodogram(my.data)
title(main = "periodogram title")
dd = data.frame(freq=p$freq, spec=p$spec)
order = dd[order(-dd$spec),]
top2 = head(order, 2)

# display the 2 highest "power" frequencies
top2

# convert frequency to time periods
time = 1/top2$f
time
```

Appendix C, Time Series Analysis Script for R

```
      # load file path and file
      setwd("file path")
      data<-
read.table(file="file_name.csv",sep=",",row.names=1,header=TRUE)
      data
      my.ts <- ts(data = data, start = 1916, frequency = 12)
      is.ts(my.ts)
      class(my.ts)
      start(my.ts)
      end(my.ts)
      summary(my.ts)
      frequency(my.ts)
      plot(my.ts)
      cycle(my.ts)
      aggregate(my.ts)
      aggregate(my.ts, FUN = mean)
      plot(aggregate(my.ts))
      boxplot(my.ts~cycle(my.ts),
              names=c("Jan",
"Feb","Mar","Apr","May","Jun","Jul","Aug","Sep","Oct","Nov","Dec"),
              xlab = "Month", ylab = "Perchlorate (ppt)", ylim =
c(0,1.5))
      decompose(my.ts)
      plot(decompose(my.ts))
```

Appendix D, Forecasting Script for R

```
      # must be performed after construction of an R time series
      # Will perform autocorrelation analysis, quantiles analysis,
      # and provide useful data such as monthly means

      library(astsa)

      diff12=diff(my.ts, lag = 12)
      plot(diff12)
      acf2(diff12)
      diff1and12 = diff(diff12, lag = 1)
      acf2(diff1and12)
      acf2(my.ts, max.lag = 48)
      sarima(diff1and12, 1,0,0,0,1,1,12)
      sarima(diff12, 1,0,0,0,1,1,12)
      sarima(my.ts, 1,0,0,0,1,1,12)
      sarima(my.ts, 12,0,0,0,1,1,12)
      sarima.for(my.ts, 24, 1,0,0,0,1,1,12)
      themodel = arima(my.ts, order = c(1,0,0), seasonal = list(order =
c(0,1,1), period = 12))
      themodel
      predict(themodel, n.ahead=24)
      tsm = matrix(my.ts, ncol=12,byrow=TRUE)
      col.means=apply(tsm,2,mean)
      plot(col.means,type="b",   main="Monthly   Means",   xlab="Month",
ylab="Mean")
```

References

Adams, N. K., S. L. de Silva, S. Self, G. Salas, S. Schubring, J. L. Permenter and K. Arbesman (2001). The physical volcanology of the 1600 eruption of Huaynaputina, southern Peru. *Bull. Volcanol.* **62**(8): 493-518.

Ayris, P. M. and P. Delmelle (2012). The immediate environmental effects of tephra emission. *Bull. Volcanol.* **74**(9): 1905-1936.

Ayris, P. M., P. Delmelle, C. Cimarelli, E. C. Maters, Y. J. Suzuki and D. B. Dingwell (2014). HCl uptake by volcanic ash in the high temperature eruption plume: mechanistic insights. *Geochem. Cosmochim. Acta* **144**: 188-201.

Bao, H. and B. Gu (2004). Natural perchlorate has a unique oxygen isotope signature. *Environ. Sci. Technol.* **38**(19): 5073-5077.

Barnes, P., E. Wolff, H. Mader, R. Udisti, E. Castellano and R. Röthlisberger (2003). Evolution of chemical peak shapes in the Dome C, Antarctica, ice core. *J. Geophys. Res.* **108**(D3).

Birk, M., R. R. Friedl, E. A. Cohen, H. M. Pickett and S. P. Sander (1989). The rotational spectrum and structure of chlorine peroxide. *J. Chem. Phys.* **91**(11): 6588-6597.

Blanchard, D. C. and A. H. Woodcock (1980). The production, concentration, and vertical distribution of the sea‐salt aerosol. *Ann. N. Y. Acad. Sci.* **338**(1): 330-347.

Borrmann, S., S. Solomon, J. E. Dye, D. Baumgardner, K. K. Kelly and K. R. Chan (1997). Heterogeneous reactions on stratospheric background aerosols, volcanic sulfuric acid droplets, and type I polar stratospheric clouds: Effects of temperature fluctuations and differences in particle phase. *J. Geophys. Res.* **102**(D3): 3639-3648.

Brantley, S. R. (1996). *Volcanoes of the United States*.

Brown, G. M. and B. Gu (2006). The chemistry of perchlorate in the environment. *Perchlorate*: 17-47.

Buat-Menard, P., J. Morelli and R. Chesselet (1974). Water-soluble elements in atmospheric particulate matter over tropical and equatorial Atlantic. *J. Rech. Atmos.* **8**(3): 661-673.

Byrns, A. C. and G. K. Rollefson (1934). The formation of chlorine heptoxide on illumination of mixtures of chlorine and ozone. *J. Am. Chem. Soc.* **56**(5): 1250-1251.

Cadle, R. D. (1975). Volcanic emissions of halides and sulfur compounds to the troposphere and stratosphere. *J. Geophys. Res.* **80**(12): 1650-1652.

Carn, S., V. Fioletov, C. McLinden, C. Li and N. Krotkov (2017). A decade of global volcanic SO2 emissions measured from space. *Sci. Rep.* **7**.

Catling, D. C., M. W. Claire, K. J. Zahnle, R. C. Quinn, B. C. Clark, M. H. Hecht and S. Kounaves (2010). Atmospheric origins of perchlorate on Mars and in the Atacama. *J. Geophys. Res.* **115**(E00E11): 1-15.

Cicerone, R. J. (1981). *Halogens in the atmosphere*.

Cleveland, W. S. (1979). Robust locally weighted regression and smoothing scatterplots. *J. Am. Stat. Assoc.* **74**(368): 829-836.

Cleveland, W. S. and S. J. Devlin (1988). Locally weighted regression: an approach to regression analysis by local fitting. *J. Am. Stat. Assoc.* **83**(403): 596-610.

Cohen, N. and J. Heicklen (1972). Comprehensive Chemical Kinetics, Elsevier. **8**.

Cole-Dai, J. (2010). Volcanoes and climate. *Wiley Interdiscip. Rev.: Clim. Change* **1**(6): 824-839.

Cole-Dai, J., K. M. Peterson, J. A. Kennedy, T. S. Cox and D. G. Ferris (2018). Evidence of Influence of Human Activities and Volcanic Eruptions on Environmental Perchlorate from a 300-Year Greenland Ice Core Record. *Environ. Sci. Technol.*

Cole‐Dai, J., E. Mosley‐Thompson and L. G. Thompson (1997). Quantifying the Pinatubo volcanic signal in south polar snow. *Geophys. Res. Lett.* **24**(21): 2679-2682.

Cooley, J. W. and J. W. Tukey (1965). An algorithm for the machine calculation of complex Fourier series. *Math. Comput.* **19**(90): 297-301.

Crawford, T. Z., A. D. Kub, K. M. Peterson, T. S. Cox and J. Cole-Dai (2017). Reduced perchlorate in West Antarctica snow during stratospheric ozone hole. *Antarct. Sci.* **29**(3): 292-296.

Dansgaard, W. (1964). Stable isotopes in precipitation. *Tellus* **16**(4): 436-468.

Dasgupta, P. K., J. V. Dyke, A. B. Kirk and W. A. Jackson (2006). Perchlorate in the United States. Analysis of relative source contributions to the food chain. *Environ. Sci. Technol.* **40**(21): 6608-6614.

Dasgupta, P. K., P. K. Martinelango, W. A. Jackson, T. A. Anderson, K. Tian, R. W. Tock and S. Rajagopalan (2005). The origin of naturally occurring perchlorate: the role of atmospheric processes. *Environ. Sci. Technol.* **39**(6): 1569-1575.

De Angelis, M. and M. Legrand (1994). Origins and variations of fluoride in Greenland precipitation. *J. Geophys. Res.* **99**(D1): 1157-1172.

Delmas, R., M. Briat and M. Legrand (1982). Chemistry of south polar snow. *J. Geophys. Res.* **87**(C6): 4314-4318.

Dibb, J. E., M. Arsenault, M. C. Peterson and R. E. Honrath (2002). Fast nitrogen oxide photochemistry in Summit, Greenland snow. *Atmos. Environ.* **36**(15-16): 2501-2511.

Długosz-Lisiecka, M. and H. Bem (2012). Determination of the mean aerosol residence times in the atmosphere and additional 210 Po input on the base of simultaneous determination of 7 Be, 22 Na, 210 Pb, 210 Bi and 210 Po in urban air. *J. Radioanal. Nucl. Chem.* **293**(1): 135-140.

Duce, R. A. (1969). On the source of gaseous chlorine in the marine atmosphere. *J. Geophys. Res.* **74**(18): 4597-4599.

Duce, R. A., J. W. Winchester and T. W. Van Nahl (1965). Iodine, bromine, and chlorine in the Hawaiian marine atmosphere. *J. Geophys. Res.* **70**(8): 1775-1799.

Ferris, D. G., J. Cole‐Dai, A. R. Reyes and D. M. Budner (2011). South Pole ice core record of explosive volcanic eruptions in the first and second millennia AD and evidence of a large eruption in the tropics around 535 AD. *J. Geophys. Res.* **116**(D17308): 1-11.

Fierstein, J. and W. Hildreth (1992). The plinian eruptions of 1912 at Novarupta, Katmai national park, Alaska. *Bull. Volcanol.* **54**(8): 646-684.

Finizola, A., L. Macedo, R. Antoine, J.-C. Thouret, E. Delcher, C. Bacri, C. Fauchard, R. Gusset, S. Japura and I. Lazarte (2017). Physical impacts of the CE 1600 Huaynaputina eruption on the local habitat: Geophysical insights. International Congress on Climate Change and its Impacts, 1, Huaraz-Ancash, PE, 29 nov.-1 dic., 2017,-Abstracts Volume., Sociedad Geológica del Perú-SGP.

Fourier, J. (1808). Mémoire sur la Propagation de la Chaleur dans les Corps Solides (Extrait). *Nouveau Bulletin des Sciences, par la Société Philomathique de Paris* **1**: 112-116.

Fourier, J. B. J. (1822). *Théorie analytique de la chaleur*, F. Didot.

Frith, S., R. McPeters, N. Kramarova, P. K. Bhartia, G. Labow, R. S. Stolarski, S. Taylor, B. Fisher and M. DeLand (2012). A 40-year Record of Profile Ozone from the SBUV (/2) Instrument Series. Guadrennial Ozone Symposium.

Furdui, V. I. and F. Tomassini (2010). Trends and Sources of Perchlorate in Arctic Snow. *Environ. Sci. Technol.* **44**(2): 588-592.

Furdui, V. I., J. Zheng and A. Furdui (2017). Anthropogenic Perchlorate Increases since 1980 in the Canadian High Arctic. *Environ. Sci. Technol.* **52**(3): 972-981.

Gerlach, T. M. (2004). Volcanic sources of tropospheric ozone‐depleting trace gases. *Geochem. Geophys.* **5**(9): 1-16.

Gow, A. J. (1965). On the accumulation and seasonal stratification of snow at the South Pole. *J. Glaciol.* **5**(40): 467-477.

Gu, B. and J. D. Coates (2006). *Perchlorate: Environmental Occurrence, Interactions and Treatment*. New York, Springer Science & Business Media.

Gutiérrez, X., F. Schiavi and H. Keppler (2016). The adsorption of HCl on volcanic ash. *Earth Planet. Sci. Lett.* **438**: 66-74.

Hanson, D. and A. Ravishankara (1993). Uptake of hydrochloric acid and hypochlorous acid onto sulfuric acid: solubilities, diffusivities, and reaction. *J. Phys. Chem.* **97**(47): 12309-12319.

Hanson, D. R. and A. Ravishankara (1994). Reactive uptake of ClONO2 onto sulfuric acid due to reaction with HCl and H2O. *J. Phys. Chem.* **98**(22): 5728-5735.

Hanson, D. R., A. R. Ravishankara and S. Solomon (1994). Heterogeneous reactions in sulfuric acid aerosols: A framework for model calculations. *J. Geophys. Res.* **99**(D2): 3615-3629.

Hatzinger, P. B., G. Harvey, W. A. Jackson, J. K. Böhlke, N. C. Sturchio, B. Gu, D. Grantz, K. Burkey and M. McGrath (2017). Identification and Characterization of Natural Sources of Perchlorate, CB and I Federal Services, LLC. Lawrenceville United States.

Haynes, W. H. (2015). CRC Handbook of chemistry and physics-A ready reference book of chemical and physical data. 96. Auflage, CRC Press/Taylor & Francis Group, Boca Raton (Florida).

Hildreth, W., M. A. Lanphere and J. Fierstein (2003). Geochronology and eruptive history of the Katmai volcanic cluster, Alaska Peninsula. *Earth Planet. Sci. Lett.* **214**(1): 93-114.

Hitchcock, D. R., L. L. Spiller and W. E. Wilson (1980). Sulfuric acid aerosols and HCl release in coastal atmospheres: evidence of rapid formation of sulfuric acid particulates. *Atmos. Environ.* **14**(2): 165-182.

Jackson, W. A., J. K. Böhlke, B. Gu, P. B. Hatzinger and N. C. Sturchio (2010). Isotopic composition and origin of indigenous natural perchlorate and co-occurring nitrate in the southwestern United States. *Environ. Sci. Technol.* **44**(13): 4869-4876.

Jaeglé, L., Y. L. Yung, G. C. Toon, B. Sen and J. F. Blavier (1996). Balloon observations of organic and inorganic chlorine in the stratosphere: The role of HClO4 production on sulfate aerosols. *Geophys. Res. Lett.* **23**(14): 1749-1752.

Jiang, S., J. Cole-Dai, Y. Li, D. G. Ferris, H. Ma, C. An, G. Shi and B. Sun (2012). A detailed 2840 year record of explosive volcanism in a shallow ice core from Dome A, East Antarctica. *J. Glaciol.* **58**(207): 65-75.

Jiang, S., T. S. Cox, J. Cole‐Dai, K. M. Peterson and G. Shi (2016). Trends of perchlorate in Antarctic snow: Implications for atmospheric production and preservation in snow. *Geophys. Res. Lett.* **43**(18): 9913-9919.

Johnsen, S. J. (1977). Stable isotope homogenization of polar firn and ice. *Isotopes and Impurities in Snow and Ice* **118**: 210-219.

Kang, N., T. A. Anderson and W. A. Jackson (2006). Photochemical formation of perchlorate from aqueous oxychlorine anions. *Anal. Chim. Acta* **567**(1): 48-56.

Kirk, A. B. (2006). Environmental perchlorate: why it matters. *Anal. Chim. Acta* **567**(1): 4-12.

Kirk, A. B., P. K. Martinelango, K. Tian, A. Dutta, E. E. Smith and P. Dasgupta (2005). Perchlorate and iodide in dairy and breast milk. *Environ. Sci. Technol.* **39**(7): 2011-2017.

Knight, B., B. Shields, E. Pearce, L. Braverman, X. He, R. Sturley and B. Vaidya (2017). Perchlorate exposure affects thyroid function in third trimester pregnant women from South-West England. Endocrine Abstracts.

Kounaves, S. P., S. T. Stroble, R. M. Anderson, Q. Moore, D. C. Catling, S. Douglas, C. P. McKay, D. W. Ming, P. H. Smith and L. K. Tamppari (2010). Discovery of natural perchlorate in the Antarctic Dry Valleys and its global implications. *Environ. Sci. Technol.* **44**(7): 2360-2364.

Koyama, T. and J. Stroeve (2019). Greenland monthly precipitation analysis from the Arctic System Reanalysis (ASR): 2000–2012. *Polar Sci.* **19**: 1-12.

Kritz, M. A. and J. Rancher (1980). Circulation of Na, Cl, and Br in the tropical marine atmosphere. *J. Geophys. Res.* **85**(C3): 1633-1639.

Kumarathilaka, P., C. Oze, S. P. Indraratne and M. Vithanage (2016). Perchlorate as an emerging contaminant in soil, water and food. *Chemosphere* **150**: 667-677.

Kutterolf, S., T. H. Hansteen, A. Freundt, H. Wehrmann, K. Appel, K. Krüger and W. Perez (2015). Bromine and chlorine emissions from Plinian eruptions along the Central American Volcanic Arc: From source to atmosphere. *Earth Planet. Sci. Lett.* **429**: 234-246.

Laj, P., S. M. Drummey, M. J. Spencer, J. M. Palais and H. Sigurdsson (1990). Depletion of H2O2 in a Greenland ice core: Implications for oxidation of volcanic SO2. *Nature* **346**(6279): 45-48.

Lawrence, J. E., S. H. Lamm, S. Pino, K. Richman and L. E. Braverman (2000). The effect of short-term low-dose perchlorate on various aspects of thyroid function. *Thyroid* **10**(8): 659-663.

Legrand, M. and R. J. Delmas (1985). Spatial and temporal variations of snow chemistry in Terre Adelie (East Antarctica). *Ann. Glaciol.* **7**: 20-25.

Legrand, M. and P. Mayewski (1997). Glaciochemistry of polar ice cores: a review. *Rev. Geophys.* **35**(3): 219-243.

Legrand, M. R. and R. J. Delmas (1984). The ionic balance of Antarctic snow: a 10-year detailed record. *Journal of Atmospheric Environment* **18**(9): 1867-1874.

Legrand, M. R. and R. J. Delmas (1988). Formation of HCl in the Antarctic atmosphere. *J. Geophys. Res.* **93**(D6): 7153-7168.

Legrand, M. R. and S. Kirchner (1990). Origins and variations of nitrate in south polar precipitation. *J. Geophys. Res.* **95**(D4): 3493-3507.

Lelieveld, J., S. Gromov, A. Pozzer and D. Taraborrelli (2016). Global tropospheric hydroxyl distribution, budget and reactivity. *Atmos. Chem. Phys.* **16**(19): 12477-12493.

Li, M., E. Karu, C. Brenninkmeijer, H. Fischer, J. Lelieveld and J. Williams (2018). Tropospheric OH and stratospheric OH and Cl concentrations determined from CH 4, CH 3 Cl, and SF 6 measurements. *npj Clim. Atmos. Sci.* **1**(1): 1-7.

Lybrand, R. A., G. Michalski, R. C. Graham and D. R. Parker (2013). The geochemical associations of nitrate and naturally formed perchlorate in the Mojave Desert, California, USA. *Geochem. Cosmochim. Acta* **104**: 136-147.

Martens, C. S., J. J. Wesolowski, R. C. Harriss and R. Kaifer (1973). Chlorine loss from Puerto Rican and San Francisco Bay area marine aerosols. *J. Geophys. Res.* **78**(36): 8778-8792.

McPeters, R. D., P. K. Bhartia, D. Haffner, G. J. Labow and L. Flynn (2013). The version 8.6 SBUV ozone data record: An overview. *J. Geophys. Res.* **118**(14): 8032-8039.

Millard, G. A., T. A. Mather, D. M. Pyle, W. I. Rose and B. Thornton (2006). Halogen emissions from a small volcanic eruption: Modeling the peak concentrations, dispersion, and volcanically induced ozone loss in the stratosphere. *Geophys. Res. Lett.* **33**(L19815): 1-6.

Morris, E. and D. Wingham (2014). Densification of polar snow: Measurements, modeling, and implications for altimetry. *J. Geophys. Res.* **119**(2): 349-365.

Motzer, W. E. (2001). Perchlorate: problems, detection, and solutions. *Environ. Forensics* **2**(4): 301-311.

Mulvaney, R., G. F. J. Coulson and H. F. J. Corr (1993). The fractionation of sea salt and acids during transport across an Antarctic ice shelf. *Tellus B* **45**(2): 179-187.

Nassar, R., P. F. Bernath, C. D. Boone, C. Clerbaux, P.-F. Coheur, G. Dufour, L. Froidevaux, E. Mahieu, J. C. McConnell and S. D. McLeod (2006). A global inventory of stratospheric chlorine in 2004. *J. Geophys. Res.* **111**(D22312): 1-13.

NOAA. ESRL/GMD Ozonesondes. Retrieved November 19, 2019, from https://www.esrl.noaa.gov/gmd/ozwv/ozsondes/sum.html.

Noël, S., K. Weigel, K. Bramstedt, A. Rozanov, M. Weber, H. Bovensmann and J. P. Burrows (2018). Water vapour and methane coupling in the stratosphere observed using SCIAMACHY solar occultation measurements. *Atmos. Chem. Phys.* **18**(7): 4463-4476.

Óskarsson, N. (1980). The interaction between volcanic gases and tephra: fluorine adhering to tephra of the 1970 Hekla eruption. *J. Volcanol. Geotherm. Res.* **8**(2-4): 251-266.

Palais, J. M. and H. Sigurdsson (1989). Petrologic Evidence of Volatile Emissions from Major Historic and Pre‐Historic Volcanic Eruptions. *Understanding Climate Change* **52**: 31-53.

Peterson, K. (2016). PERCHLORATE VARIATIONS OVER 300 YEARS: INFLUENCE OF HUMAN ACTIVITIES, VOLCANIC ERUPTIONS, AND BOLIDE EVENTS.

Peterson, K., J. Cole-Dai, D. Brandis, T. Cox and S. Splett (2015a). Rapid measurement of perchlorate in polar ice cores down to sub-ng L^{-1} levels without pre-concentration. *Anal. Bioanal. Chem.* **407**(26): 7965-7972.

Peterson, K., J. Cole-Dai, D. Brandis and E. Manandhar (2015b). Assessment of anthropogenic contribution to perchlorate in the environment using an ice core record. *Emerging Micro-Pollutants in the Environment: Occurrence, Fate, and Distribution*, ACS Publications**:** 175-185.

Pinto, J. P., R. P. Turco and O. B. Toon (1989). Self‐limiting physical and chemical effects in volcanic eruption clouds. *J. Geophys. Res.* **94**(D8): 11165-11174.

Plummer, L. N., J. K. Böhlke and M. W. Doughten (2006). Perchlorate in Pleistocene and Holocene groundwater in north-central New Mexico. *Environ. Sci. Technol.* **40**(6): 1757-1763.

Prasad, S. S. and T. J. Lee (1994). Atmospheric chemistry of the reaction ClO + O2 ↔ ClO· + O2: where it stands, what needs to be done, and why? *J. Geophys. Res.* **99**(D4): 8225-8230.

Rajagopalan, S., T. Anderson, S. Cox, G. Harvey, Q. Cheng and W. A. Jackson (2009). Perchlorate in Wet Deposition Across North America. *Environ. Sci. Technol.* **43**(3): 616-622.

Rajagopalan, S., T. A. Anderson, L. Fahlquist, K. A. Rainwater, M. Ridley and W. A. Jackson (2006). Widespread presence of naturally occurring perchlorate in high plains of Texas and New Mexico. *Environ. Sci. Technol.* **40**(10): 3156-3162.

Rao, B., T. A. Anderson, G. J. Orris, K. A. Rainwater, S. Rajagopalan, R. M. Sandvig, B. R. Scanlon, D. A. Stonestrom, M. A. Walvoord and W. A. Jackson (2007). Widespread natural perchlorate in unsaturated zones of the southwest United States. *Environ. Sci. Technol.* **41**(13): 4522-4528.

Rao, B., T. A. Anderson, A. Redder and W. A. Jackson (2010). Perchlorate formation by ozone oxidation of aqueous chlorine/oxy-chlorine species: Role of Cl_xO_y radicals. *Environ. Sci. Technol.* **44**(8): 2961-2967.

Rao, B. A., C. P. Wake, T. Anderson and W. A. Jackson (2012). Perchlorate depositional history as recorded in North American ice cores from the Eclipse Icefield, Canada, and the Upper Fremont Glacier, USA. *Water Air Soil Pollut.* **223**(1): 181-188.

Rose, W. I., G. A. Millard, T. A. Mather, D. E. Hunton, B. Anderson, C. Oppenheimer, B. F. Thornton, T. M. Gerlach, A. A. Viggiano and Y. Kondo (2006). Atmospheric chemistry of a 33–34 hour old volcanic cloud from Hekla Volcano (Iceland): Insights from direct sampling and the application of chemical box modeling. *J. Geophys. Res.* **111**(D20).

Rothlisberger, R., M. A. Hutterli, E. W. Wolff, R. Mulvaney, H. Fischer, M. Bigler, K. Goto-Azuma, M. E. Hansson, U. Ruth and M.-L. Siggaard-Andersen (2002). Nitrate in Greenland and Antarctic ice cores: a detailed description of post-depositional processes. *Ann. Glaciol.* **35**(1): 209-216.

Rubin, R., M. Pearl, M. Kharrazi, B. C. Blount, M. D. Miller, E. N. Pearce, L. Valentin-Blasini, G. DeLorenze, J. Liaw and A. N. Hoofnagle (2017). Maternal perchlorate exposure in pregnancy and altered birth outcomes. *Environ. Res.* **158**: 72-81.

Savitzky, A. and M. J. E. Golay (1964). Smoothing and differentiation of data by simplified least squares procedures. *Anal. Chem.* **36**(8): 1627-1639.

Sigl, M., T. J. Fudge, M. Winstrup, J. Cole-Dai, D. Ferris, J. R. McConnell, K. C. Taylor, K. C. Welten, T. E. Woodruff, F. Adolphi, M. Bisiaux, E. J. Brook, C. Buizert, M. W. Caffee, N. W. Dunbar, R. Edwards, L. Geng, N. Iverson, B. Koffman, L. Layman, O. J. Maselli, K. McGwire, R. Muscheler, K. Nishiizumi, D. R. Pasteris, R. H. Rhodes and T. A. Sowers (2016). The WAIS

Divide deep ice core WD2014 chronology – Part 2: Annual-layer counting (0–31 ka BP). *Clim. Past* **12**(3): 769-786.

Sijimol, M. R., S. Jyothy, A. P. Pradeepkumar, M. S. S. Chandran, S. S. Ghouse and M. Mohan (2015). Review on fate, toxicity, and remediation of perchlorate. *Environ. Forensics* **16**(2): 125-134.

Silva, M. A. (2003). Perchlorate from Safety Flares. At Threat to Water Quality. Santa Clara Valley Water District Publication, Santa Clara Valley Water District San Jose, CA, USA.

Simonaitis, R. and J. Heicklen (1975). Perchloric acid: A possible sink for stratospheric chlorine. *Planet. Space Sci.* **23**(11): 1567-1569.

Slawinska, J. and A. Robock (2018). Impact of volcanic eruptions on decadal to centennial fluctuations of Arctic sea ice extent during the last millennium and on initiation of the Little Ice Age. *J. Clim.* **31**(6): 2145-2167.

Solomon, S., R. W. Sanders, R. R. Garcia and J. G. Keys (1993). Increased chlorine dioxide over Antarctica caused by volcanic aerosols from Mount Pinatubo. *Nature* **363**(6426): 245.

Song, C. H. and G. R. Carmichael (1999). The aging process of naturally emitted aerosol (sea-salt and mineral aerosol) during long range transport. *Atmos. Environ.* **33**(14): 2203-2218.

Steinier, J., Y. Termonia and J. Deltour (1972). Smoothing and differentiation of data by simplified least square procedure. *Anal. Chem.* **44**(11): 1906-1909.

Steinmaus, C. M. (2016). Perchlorate in water supplies: sources, exposures, and health effects. *Curr. Envir. Health Rpt.* **3**(2): 136-143.

Stephenson, J. B. (2011). *Perchlorate: Occurrence is Widespread but at Varying Levels; Federal Agencies Have Taken Some Actions to Respond to and Lessen Releases*, DIANE Publishing.

Sturchio, N. C., A. Beloso Jr, L. J. Heraty, S. Wheatcraft and R. Schumer (2014). Isotopic tracing of perchlorate sources in groundwater from Pomona, California. *Appl. Geochem.* **43**: 80-87.

Textor, C., H. F. Graf, M. Herzog and J. Oberhuber (2003). Injection of gases into the stratosphere by explosive volcanic eruptions. *J. Geophys. Res.* **108**(D19).

Thouret, J.-C., E. Juvigné, A. Gourgaud, P. Boivin and J. Davila (2002). Reconstruction of the AD 1600 Huaynaputina eruption based on the correlation of geologic evidence with early Spanish chronicles1. *J. Volcanol. Geotherm. Res.* **115**(3-4): 529-570.

Trumpolt, C. W., M. Crain, G. D. Cullison, S. J. P. Flanagan, L. Siegel and S. Lathrop (2005). Perchlorate: sources, uses, and occurrences in the environment. *Remediation* **16**(1): 65-89.

Urbansky, E. T. (1998). Perchlorate chemistry: implications for analysis and remediation. *Bioremediat. J.* **2**(2): 81-95.

Urbansky, E. T. (2002). Perchlorate as an environmental contaminant. *Environ. Sci. Pollut. R.* **9**(3): 187-192.

Urbansky, E. T., S. K. Brown, M. L. Magnuson and C. A. Kelty (2001). Perchlorate levels in samples of sodium nitrate fertilizer derived from Chilean caliche. *Environ. Pullut.* **112**(3): 299-302.

Volz, F. E. (1975). Distribution of turbidity after the 1912 Katmai eruption in Alaska. *J. Geophys. Res.* **80**(18): 2643-2648.

von Glasow, R. (2010). Atmospheric chemistry in volcanic plumes. *Proceedings of the National Academy of Sciences* **107**(15): 6594-6599.

von Glasow, R., N. Bobrowski and C. Kern (2009). The effects of volcanic eruptions on atmospheric chemistry. *Chem. Geol.* **263**(1-4): 131-142.

Winski, D., E. Osterberg, D. Ferris, K. Kreutz, C. Wake, S. Campbell, R. Hawley, S. Roy, S. Birkel and D. Introne (2017). Industrial-age doubling of snow accumulation in the Alaska Range linked to tropical ocean warming. *Sci. Rep.* **7**(1): 17869.

Winski, D. A., T. J. Fudge, D. G. Ferris, E. C. Osterberg, J. M. Fegyveresi, J. Cole-Dai, Z. Thundercloud, T. S. Cox, K. J. Kreutz and N. Ortman (2019). The SP19 chronology for the South Pole Ice Core–Part 1: volcanic matching and annual layer counting. *Clim. Past* **15**(5): 1793-1808.

Zelenski, M. and Y. Taran (2012). Volcanic emissions of molecular chlorine. *Geochem. Cosmochim. Acta* **87**: 210-226.

Zhang, T., Q. Wu, H. W. Sun, J. Rao and K. Kannan (2010). Perchlorate and iodide in whole blood samples from infants, children, and adults in Nanchang, China. *Environ. Sci. Technol.* **44**(18): 6947-6953.